N° d'ordre : 2012ISAL0140 Année 2012

Thèse

Investigation on the Control of Supercritical Centrifugal Compressors supported by Active Magnetic Bearings:

Toward a new Control Strategy?

Présentée devant
L'institut national des sciences appliquées de Lyon

Pour obtenir
Le grade de docteur

Formation doctorale : Mécanique
École doctorale Mécanique, Energétique, Génie civil, Acoustique

Par

Benjamin D. DEFOY
(Ingénieur INSA de Lyon)

Soutenue le 14 décembre 2012 devant la Commission d'examen

Jury MM.

Codirecteur	T. ALBAN	Responsable conception mécanique (GE Oil & Gas)
Rapporteur	P. KEOGH	Professeur (Université de Bath - UK)
Directeur	J. MAHFOUD	Maître de conférences HDR (INSA de Lyon)
Rapporteur	E. MASLEN	Professeur (Université James Madison – USA)
Président	F. THOUVEREZ	Professeur (Ecole Centrale de Lyon)

Laboratoire de recherche : Laboratoire de Mécanique des Contacts et des Structures
(LaMCoS, INSA de Lyon, CNRS UMR5259)

INSA Direction de la Recherche - Ecoles Doctorales – Quinquennal 2011-2015

SIGLE	ECOLE DOCTORALE	NOM ET COORDONNEES DU RESPONSABLE
CHIMIE	**CHIMIE DE LYON** http://www.edchimie-lyon.fr Insa : R. GOURDON	M. Jean Marc LANCELIN Université de Lyon – Collège Doctoral Bât ESCPE 43 bd du 11 novembre 1918 69622 VILLEURBANNE Cedex Tél : 04.72.43 13 95 directeur@edchimie-lyon.fr
E.E.A.	**ELECTRONIQUE, ELECTROTECHNIQUE, AUTOMATIQUE** http://edeea.ec-lyon.fr Secrétariat : M.C. HAVGOUDOUKIAN eea@ec-lyon.fr	M. Gérard SCORLETTI Ecole Centrale de Lyon 36 avenue Guy de Collongue 69134 ECULLY Tél : 04.72.18 60 97 Fax : 04 78 43 37 17 Gerard.scorletti@ec-lyon.fr
E2M2	**EVOLUTION, ECOSYSTEME, MICROBIOLOGIE, MODELISATION** http://e2m2.universite-lyon.fr Insa : H. CHARLES	Mme Gudrun BORNETTE CNRS UMR 5023 LEHNA Université Claude Bernard Lyon 1 Bât Forel 43 bd du 11 novembre 1918 69622 VILLEURBANNE Cédex Tél : 04.72.43.12.94 e2m2@biomserv.univ-lyon1.fr
EDISS	**INTERDISCIPLINAIRE SCIENCES-SANTE** http://ww2.ibcp.fr/ediss Sec : Safia AIT CHALAL Insa : M. LAGARDE	M. Didier REVEL Hôpital Louis Pradel Bâtiment Central 28 Avenue Doyen Lépine 69677 BRON Tél : 04.72.68 49 09 Fax :04 72 35 49 16 Didier.revel@creatis.uni-lyon1.fr
INFOMATHS	**INFORMATIQUE ET MATHEMATIQUES** http://infomaths.univ-lyon1.fr	M. Johannes KELLENDONK Université Claude Bernard Lyon 1 INFOMATHS Bâtiment Braconnier 43 bd du 11 novembre 1918 69622 VILLEURBANNE Cedex Tél : 04.72. 44.82.94 Fax 04 72 43 16 87 infomaths@univ-lyon1.fr
Matériaux	**MATERIAUX DE LYON** Secrétariat : M. LABOUNE PM : 71.70 –Fax : 87.12 Bat. Saint Exupéry Ed.materiaux@insa-lyon.fr	M. Jean-Yves BUFFIERE INSA de Lyon MATEIS Bâtiment Saint Exupéry 7 avenue Jean Capelle 69621 VILLEURBANNE Cédex Tél : 04.72.43 83 18 Fax 04 72 43 85 28 Jean-yves.buffiere@insa-lyon.fr
MEGA	**MECANIQUE, ENERGETIQUE, GENIE CIVIL, ACOUSTIQUE** Secrétariat : M. LABOUNE PM : 71.70 –Fax : 87.12 Bat. Saint Exupéry mega@insa-lyon.fr	M. Philippe BOISSE INSA de Lyon Laboratoire LAMCOS Bâtiment Jacquard 25 bis avenue Jean Capelle 69621 VILLEURBANNE Cedex Tél :04.72.43.71.70 Fax : 04 72 43 72 37 Philippe.boisse@insa-lyon.fr
ScSo	**ScSo*** M. OBADIA Lionel Sec : Viviane POLSINELLI Insa : J.Y. TOUSSAINT	M. OBADIA Lionel Université Lyon 2 86 rue Pasteur 69365 LYON Cedex 07 Tél : 04.78.69.72.76 Fax : 04.37.28.04.48 Lionel.Obadia@univ-lyon2.fr

*ScSo : Histoire, Geographie, Aménagement, Urbanisme, Archéologie, Science politique, Sociologie, Anthropologie

Abstract

Investigation on the Control of Supercritical Centrifugal Compressors supported by Active Magnetic Bearings:

Toward a new Control Strategy?

The dynamic behaviour of large turbomachinery should satisfy stringent requirements dictated by international standards and final users. Their flexible rotor is sensitive to the unbalance distribution and subjected to particular excitations coming from the industrial process. Usually, the performance margins between the requirements and the classical controller capabilities are small. Consequently, the magnetic bearing characteristics depend on the rotor geometry. Designing such controllers is difficult and time consuming. The objective of this thesis is to investigate the dynamic behaviour of supercritical centrifugal compressors in order to propose a new control strategy.

First, each bearing is considered as one entity by coupling its two axes of action. The introduction of polar quantities permits a better observation of the rotor dynamic behaviour. In addition, by using logic close to human being reasoning, the fuzzy logic modulates the action forces as a function of the global dynamic behaviour. The coupling of the two approaches is an efficient way to apply targeted corrective actions. This controller attenuates the unbalance vibration when crossing critical speeds by applying damping forces, or increases the stiffness during transient or asynchronous excitations in order to limit the maximum displacement reached.

As their structural damping is low, flexible rotors are very sensitive to spillover effect, which cannot be managed by fuzzy controllers. Consequently, an underlying PID is necessary. This hand-synthesized controller has high frequency characteristics tuned in order to ensure stability and robustness for each rotor. Compared to a classical approach, the polar fuzzy controller enables to increase the performance margins. These margins are used to fulfil three objectives: the achievement of standards requirements, the improvement of the subsynchronous behaviour, and the simplification and the standardization of the PID controller that we called SPID. This SPID is designed for a given application, such that the bearing characteristics on the operating frequency range are always the same.

The control strategy is assessed numerically and experimentally. First, the numerical model is validated with experimental tests. Then, the controller developed is applied to an academic test rig. The controller is stable and robust. It exhibits performance superior to the augmented PID supplied with the test rig for both unbalance response and response to subsynchronous excitations. Finally, the control of an industrial compressor is assessed numerically. The results obtained are close to the standards requirements used for classical bearings. The optimization of the approach and the utilization of an automatic tuning algorithm for high frequency characteristics could lead to the standardization of Active Magnetic Bearings.

Keywords: Active Magnetic Bearings, Centrifugal Compressors, Fuzzy logic, Flexible rotor, Rotordynamics, Control, MIMO.

Résumé (en français)

Recherches sur le Contrôle des Compresseurs Centrifuges Supercritiques supportés par des Paliers Magnétiques Actifs :

Vers une nouvelle stratégie de contrôle ?

Le comportement dynamique des turbomachines industrielles doit respecter des critères émis par les normes internationales et les utilisateurs. Les rotors flexibles sont sensibles à la distribution de balourd, et sont soumis aux excitations aérodynamiques de leur environnement. Usuellement, les contrôleurs utilisés peinent à délivrer le niveau d'exigence demandé, par conséquent les propriétés mécaniques des paliers magnétiques sont fortement dépendantes de celles des rotors. L'objectif de ce mémoire est d'analyser le comportement dynamique des compresseurs centrifuges afin de proposer une stratégie de contrôle innovante.

D'abord, chaque palier est considéré comme une entité a part entière en couplant ses deux axes d'action. Le comportement dynamique du rotor est exprimé dans le repère polaire. Par ailleurs, la logique floue, qui utilise un modèle de pensée proche du raisonnement humain, applique des actions correctives en fonction du comportement dynamique global du rotor. Ainsi, l'utilisation couplée de ces deux approches créé une synergie permettant d'agir sur le système de manière ciblée. Le contrôleur dissipe l'énergie cinétique du rotor lors du franchissement de vitesses critiques afin d'atténuer la réponse au balourd, ou augmente la raideur du palier lors de vibrations transitoires ou asynchrones afin de réduire la trajectoire du rotor.

Le faible amortissement structurel du rotor le rend sensible au phénomène de « spillover » (l'énergie de contrôle affecte les modes de fréquence élevée). Or, la logique floue ne peut pas gérer ce phénomène. Ainsi, un contrôleur PID sous-jacent est utilisé pour maîtriser la stabilité des modes hautes fréquences. Au final, le contrôleur flou polaire permet d'obtenir des marges de performances entre les capacités de cet asservissement et le cahier des charges. Ces marges sont utilisées pour trois objectifs : le respect des spécifications, l'amélioration du comportement subsynchrone, et enfin la simplification et la standardisation du contrôleur sous-jacent nommé ici SPID. Ce contrôleur est tel que ses caractéristiques, dans la plage de fréquence utile, sont indépendantes du rotor pour une application donnée.

Enfin, la stratégie développée est évaluée avec des simulations numériques et des essais expérimentaux. D'abord, le modèle numérique est validé, puis le contrôleur est appliqué à un banc d'essais académique. Le comportement est stable et robuste. Il présente des performances supérieures au PID augmenté fourni avec le banc, que ce soit pour la réponse au balourd, ou pour la réponse à des excitations subsynchrones. Finalement, la démarche est appliquée à un compresseur industriel. Les simulations montrent que le comportement est proche de celui exigé pour des machines sur paliers classiques. L'optimisation de l'approche et l'automatisation de la conception pourraient conduire à la standardisation des paliers magnétiques actifs.

Mots-clés : Paliers Magnétiques Actifs, Compresseurs Centrifuges, Logique floue, Rotor flexible, Dynamique des machines tournantes, Contrôle, MIMO.

« Il semble que la perfection soit atteinte non quand il n'y a plus rien à ajouter, mais quand il n'y a plus rien à retrancher. »

Antoine de Saint-Exupéry – Terre des hommes (1939)

Acknowledgements

I was born in Nîmes in 1986. I grew up in a little town of Bourgogne, studied at the "University" of Bourg en Bresse, and then in Lyon. This thesis is the result of a research work I have carried out between 2010 and 2012 at the Laboratory of Mechanic of Contacts and Structures (LaMCoS) in cooperation with GE Oil & Gas.

First, I would like to thank my supervisors Jarir Mahfoud and Thomas Alban for their support, their useful comments and for having placed their trust in me. We have exchanged so many interesting discussions.

I would like to express my sincere gratitude to Patrick Keogh, Eric Maslen and Fabrice Thouverez for reviewing my dissertation and for paying attention to my work as co-examiners.

I thank all the persons that have contributed to this work, in many different manners: Amélie Tarnier, Danielle Trusau, Dominique Fayard, Johan Der Hagopian, Laurence Genty, Marie-Ange Andrianoely, Matthieu Gerbet, Pascal Gaudez, Pierre Laboube, Régis Dufour and Rémi Falcand.

A special thanks for all of my friends that are present in the laboratory Catherine Chochol, Florian Mora, Hafedh Bouassida, Hugo Boffy, Mathieu Garcia, Romain Fargère, Sophie Baudin, Vincent Bruyère and many others. They have allowed me to enjoy coffee breaks, lunches and so many other pleasant times. I hope continuing to see you regularly.

I wish to thank my colleagues from the laboratory and GE Oil & Gas for their warm welcoming and making work a pleasant time. I would also like to thank the members of the University of Uberlândia (Brazil) for their welcoming, and the SKF Company for supplying the test rig and supporting me during its commissioning.

Several students have contributed to enlarge the scope of this thesis. I wish to thank them for their involvement and their contribution: Alberto Lauriero, Lihan Xie and Roger Montes Parra.

Last, but not least a very special thanks to my wife Céline for her love, her support and for giving me so many reasons to be happy.

A Céline,

Table of Contents

Résumé étendu

Introduction

Les premiers Paliers Magnétiques Actifs sont apparus au début des années 70 simultanément en France et aux Etats-Unis. Cette technologie fit son apparition tardivement car les PMAs sont intrinsèquement instables et nécessitent donc une boucle d'asservissement. Lorsque le concept de PMA a été créé, les performances des systèmes électroniques étaient insuffisantes pour obtenir un palier compétitif. De plus, la compréhension de ces paliers nécessite une expertise multi-physique (mécanique, contrôle, magnétisme, électricité…). Ainsi même s'ils ont de nombreux avantages, leur temps d'adoption par le marché est relativement lent. La société General Electric n'avait produit que trois compresseurs centrifuges sur PMAs (1987, 1994, 1997), avant de lancer l'ICL en 2006 présenté en Figure 1. 1. Ce nouveau concept de compresseur intégré figure aujourd'hui dans le catalogue des machines disponibles. Cette thèse vise à développer une nouvelle stratégie de contrôle dédiée à ces machines.

Concept de Paliers Magnétiques Actifs

Les PMAs sont de purs produits mécatroniques. Ils utilisent les propriétés ferromagnétiques pour appliquer des forces sans contact. Plusieurs électroaimants sont nécessaires afin d'assurer une lévitation complète et stable. Mais, un seul suffit pour comprendre les principes de base, comme montré en Figure 1. 2. Un PMA est constitué d'un capteur de déplacement qui produit un signal électrique u_x proportionnel au déplacement x du rotor. En fonction de ce déplacement et des déplacements précédents, le contrôleur calcule une réponse du palier qui stabilise le système. Ensuite, il produit une tension de commande u_i. Cette tension est transformée en un courant proportionnel par l'amplificateur, puis en une force par l'électroaimant. Comme un électroaimant ne peut appliquer que des forces d'attraction, deux électroaimants positionnés de part et d'autre du rotor sont nécessaires (par ligne d'action) afin d'appliquer des forces dans les deux sens. Finalement, des paliers atterrisseurs (généralement des roulements à billes) sont placés à proximité des PMAs avec des jeux inférieurs afin de protéger les PMAs, et de supporter le rotor lors de l'arrêt complet de la machine.

Les PMAs ont de nombreux avantages, ils permettent de supprimer le frottement entre rotor et stator. Ainsi, les pertes d'énergie sont minimisées, le rotor

peut évoluer à des vitesses de rotation élevées avec une usure quasi inexistante. Les opérations de maintenance s'en trouvent réduites. Le lubrifiant est supprimé, il n'y a donc plus de contamination avec le fluide traité par la machine. Néanmoins, les PMAs présentent aussi des inconvénients. Bien qu'ils réduisent le coût d'utilisation, ils sont plus chers que des paliers classiques et représentent donc un investissement initial important. Ils nécessitent un dimensionnement soigné, puisqu'ils ne tolèrent aucune surcharge même passagère. Ils nécessitent une boucle d'asservissement. Finalement, ils sont généralement plus volumineux que des paliers classiques à charge équivalente.

Introduction aux compresseurs centrifuges

Les compresseurs centrifuges permettent de couvrir la quasi-totalité des besoins en compression de l'industrie pétrolière. La carte permettant le choix de la technologie de compresseur en fonction de ces besoins est donnée en Figure 1. 3. Dans le cadre de notre étude, certains effets aérodynamiques sont à considérer. Les joints d'étanchéité dynamiques, permettant de limiter les recirculations internes de gaz, doivent être pris en compte. En effet, ils peuvent être vus comme des paliers gaz qui apporteraient une raideur et un amortissement effectifs négatifs à basses fréquences. La structure d'un ICL est disponible en Figure 1. 6. Le carter est entièrement pressurisé dans le gaz de procédé. Ainsi, les étanchéités de bouts d'arbre sont supprimées empêchant totalement les fuites atmosphériques. Ce compresseur permet d'éviter l'utilisation de 30 000L d'huile et le rejet de 600 tonnes de CO_2 par an pour chaque compresseur.

Pugnet [2010] présente le développement du projet ICL. Du point de vu compressoriste, les deux principaux inconvénients des PMAs sont :

- La conception des contrôleurs prend beaucoup de temps, et
- Les caractéristiques mécaniques des paliers sont trop dépendantes des propriétés mécaniques du rotor. Comme les propriétés finales du rotor dépendent des tolérances de fabrication, il y a parfois des écarts entre le contrôleur prévu et celui adapté aux caractéristiques réelles.

Motivations

Les composants mécatroniques sont de plus en plus présents sur les turbomachines industrielles. Cependant, l'optimisation globale de la machine n'est possible que si le fabricant maîtrise toutes ces technologies. De plus, chaque composant doit être amélioré et optimisé vis-à-vis de l'application considérée. Concernant les PMAs, les principales voies de recherche sont le contrôle de rotors flexibles, l'analyse du comportement dynamique du rotor lors d'un défaut de sustentation, l'approfondissement du concept de machine intelligente et enfin la résistance à des environnements chimiques agressifs ou des températures élevées. L'essentiel de ce

mémoire porte sur le contrôle de rotors flexibles, même si les autres voies sont considérées de manière implicite.

Objectifs et contributions

Ce travail a pour ambition de développer une nouvelle stratégie de contrôle dédiée aux compresseurs centrifuges permettant d'améliorer le comportement des machines ainsi que leur processus de conception. Les objectifs sont :

- Comprendre et analyser le comportement d'un rotor sur PMA,
- Comprendre la conception des contrôleurs industriels existants,
- Développer une nouvelle stratégie de contrôle permettant une optimisation du comportement dynamique tout en respectant les normes et les spécifications industrielles, et
- Mettre en place une démarche de conception globale optimisée pour une ligne de produits.

Pour ces machines, le respect des normes internationales, tel que l'ISO 14839 [2002][2004][2006][2012] et l'API 617 [2002], est primordial. Les exigences des utilisateurs finaux doivent aussi être prises en compte. Une nouvelle stratégie de contrôle est recherchée dans le but d'obtenir de meilleures performances avec une robustesse équivalente à celle des PID augmentés utilisés auparavant. Les PID augmentés sont des contrôleurs linéaires et généralement utilisés en mode SISO (Single-Input Single-Output), ainsi il y a au moins deux voies d'amélioration exploitables en utilisant des contrôleurs MIMO (Multiple-Input Multiple-Output) et non-linéaires. La logique floue produit des contrôleurs non-linéaires adaptés aux systèmes complexes. De plus, en tenant compte de l'incertitude des données d'entrée (déplacements), elle conduit à un comportement robuste. D'autre part, au lieu de contrôler séparément les différentes lignes d'action, l'utilisation des coordonnées polaires permet de concevoir un contrôleur unique pilotant les deux lignes d'actions de chaque palier radial. Ainsi, le contrôleur est capable de corriger le comportement global de la machine en plus du comportement local.

Dans le cadre d'une première approche, la stratégie de contrôle est développée pour des excitations qui concernent uniquement le comportement normal, à savoir un faible déplacement par rapport aux jeux rotor-stator et un comportement quasi linéaire de l'actionneur.

Chaque compresseur centrifuge est unique ou presque. Ainsi, comme les caractéristiques mécaniques des paliers peuvent influencer la conception du rotor, il est intéressant de développer un contrôleur avec des propriétés partiellement figées pour une ligne de produit. De plus, nous avons la conviction qu'un contrôleur plus simple pourrait avoir des propriétés plus constantes entre la phase de conception et la mise en marche de la machine sur site. Ce contrôleur devra avoir un nombre maximum de paramètres standard pour être facilement ajusté à chaque machine, et

ainsi permettre une conception des machines plus aisée. Le but d'une telle approche de contrôle serait aussi d'augmenter le niveau de confiance des clients finaux dans cette technologie en permettant de réaliser des analyses dynamiques préliminaires très en amont dans le projet.

Les contrôleurs PID augmentés sont parfois insuffisants pour obtenir une réponse au balourd acceptable. Des filtres synchrones à bande étroite permettent de satisfaire largement les spécifications. Ces filtres paramétriques utilisent la vitesse de rotation du rotor obtenue à partir d'un tachymètre. Ces filtres sont très répandus dans l'industrie, cependant ils nécessitent des capteurs de vitesse dédiés qui réduisent la fiabilité globale du système. Ainsi, si les performances obtenues sans ces filtres étaient suffisantes, le système serait plus simple et plus robuste.

Le processus de validation d'un nouveau contrôleur est relativement long et complexe. Il passe par des étapes qui permettent d'atteindre de proche en proche le système industriel final. Par conséquent l'objectif de ce travail de recherche était de valider les premières étapes permettant de quantifier les améliorations escomptées, en procédant à la validation expérimentale sur un banc d'essais de dimension académique, ainsi que la simulation numérique du comportement dynamique d'un compresseur industriel.

Les principales contributions de ce travail peuvent être résumées par :

- Une nouvelle approche de contrôle. D'abord, un PID Standardisé (SPID) est conçu puis un contrôleur flou module les gains de celui-ci. Le SPID est réalisé de manière à obtenir des propriétés basses fréquences (i.e. pour la plage de fréquence de rotation) indépendantes de la géométrie du rotor. Seul le gain général de la fonction de transfert doit être modifié pour adapter le contrôleur à la taille des différentes machines. Ensuite, les propriétés hautes fréquences sont personnalisées pour chaque palier afin d'assurer la stabilité et la robustesse du système.
- L'utilisation des grandeurs physiques exprimées dans les coordonnées polaires est introduite. L'originalité de la méthode développée est d'exploiter les vitesses radiale et tangentielle respectivement associées au comportement transitoire et permanent. De plus, les coordonnées polaires permettent d'appliquer des actions ciblées. La force de commande est calculée dans les coordonnées polaires puis convertie en courants de contrôle qui actionnent simultanément les deux lignes d'actions du palier. Le contrôleur considère alors le palier magnétique comme un unique système MIMO, les données d'entrée étant les déplacements dans deux directions orthogonales (prises dans le plan du palier).
- Un contrôleur flou utilisant des entrées exprimées dans les coordonnées polaires fut développé. La logique floue qui est un outil d'aide à la décision est adaptée pour traiter les informations obtenues dans le repère polaire. Cette formulation permet d'éviter l'anisotropie produite normalement par

l'utilisation de contrôleurs non-linéaires dans le repère Cartésien. Le contrôleur flou est basé sur un algorithme de forme Sugeno utilisé avec des règles simples. Par ailleurs, le module flou ne nécessite pas d'adaptation fine aux propriétés mécaniques du rotor puisqu'il est défini comme fonction du comportement dynamique des machines tournantes. Ce comportement est presque constant pour une ligne de produits, puisque les variations géométriques peuvent modifier les amplitudes des réponses, mais pas les phénomènes considérés.

Détermination de la stratégie de contrôle adaptée au problème

Ce travail de recherche est dédié au contrôle de rotors flexibles supportés par deux PMAs radiaux. Les rotors considérés ont peu d'effet gyroscopique, et les conditions nominales d'utilisation sont considérées. Pour les machines visées plusieurs types de contrôleurs furent considérés. La stratégie de contrôle développée a été choisie suite à une recherche bibliographique.

Nonami [1995] a montré que les contrôleurs du type LQ, LQG, « disturbance cancellation » et H_2 n'avaient pas la robustesse nécessaire, alors que les contrôleurs μ-synthesis et H_∞ permettent d'obtenir de bons résultats. Maslen et Montie [2001] discutent l'application du « sliding mode control », ils en concluent que ce type de contrôleur n'est pas plus performant qu'un PID augmenté.

Après plus de vingt ans de recherche, trois stratégies de contrôle sont encore étudiées : μ- synthesis, modale et floue. Pour l'instant, aucune des trois n'est arrivée à prendre l'ascendant sur les stratégies conventionnelles. Pour chaque application, il faut considérer les avantages et les inconvénients pour déterminer quelle stratégie est susceptible de répondre au problème posé de manière pertinente.

Les trois méthodes sont comparées (à titre indicatif et en essayant d'être le plus objectif possible) à un contrôleur PID dans la Table 2. 1. Aucune de ces trois méthodes n'est complètement prête pour l'industrialisation, mais seul le contrôle modal nécessiterait d'importants travaux de recherche. La complexité de la théorie utilisée doit être considérée puisqu'elle pourrait limiter la mise en place, l'évolution et la diffusion de l'approche utilisée. Une utilisation industrielle requiert qu'un grand nombre de personnes comprenne cette théorie. Sur ce point, la logique floue semble plus abordable que les autres alternatives. Ensuite, il faut évaluer la difficulté liée à l'application de l'approche pour la conception du contrôleur de chaque nouvelle machine. Ici, ce sont les techniques modales et μ-synthesis qui prennent l'avantage en éliminant presque complètement l'intervention humaine. Finalement en ce qui concerne la qualité du résultat obtenu (pouvant être vu comme l'équilibre entre stabilité, performance et robustesse), les méthodes peuvent être classées dans cet ordre en partant de la meilleure : modale, floue et enfin μ-synthesis.

Nous avons choisi de développer une stratégie basée sur la logique floue puisqu'elle présente des facilités pour l'industrialisation, ses non linéarités sont

maîtrisables et elle peut être couplée avec une des deux autres stratégies afin de combiner leurs avantages.

Modélisation

Les différents éléments constituant le palier ont été étudiés en vu de créer un modèle précis du palier. On peut voir l'agencement de ces différents éléments sur la Figure 3. 1, il s'agit des capteurs de déplacement, des câbles électriques, du contrôleur numérique, des amplificateurs et des électroaimants. Par ailleurs, le rotor a lui aussi été traité.

Après l'étude détaillée des différents composants, seuls les paramètres principaux ont été conservés afin d'obtenir un modèle simple et efficace en simulation numérique. Ainsi, les courants de Foucault sont négligés, tout comme l'hysteresis magnétique et la saturation magnétique. Les phénomènes très haute fréquence, tel que le résidu de la porteuse alimentant le pont de Wheatstone du capteur ou les commutations de l'amplificateur ne sont pas considérés non plus. Enfin, tous les composants sont linéarisés autour de leur point de fonctionnement.

De cette manière, on obtient un capteur de déplacement modélisé par sa sensibilité mesurée en $mV/\mu m$, et un filtre passe bas. Pour le contrôleur numérique, seul le convertisseur numérique analogique est considéré. Il est représenté par une approximation de Padé d'ordre un (du bloqueur d'ordre zéro), visible dans l'équation (3.7). Les électroaimants sont modélisés grâce à une représentation linéaire classique avec une raideur négative et une raideur en courant comme écrit dans l'équation (3.18). L'amplificateur est considéré uniquement comme un filtre passe bas dû à son asservissement. Les câbles ne sont pas pris en compte puisque leurs effets peuvent être efficacement gérés par des circuits électroniques. Enfin, le rotor est modélisé par ses énergies potentielles et de déformation. La méthode des éléments finis est utilisée, avec des éléments de poutre de Timoshenko pour l'arbre, et des disques considérés rigides. Le modèle est réduit pour ne garder que les modes pertinents et un amortissement modal équivalent à un facteur d'amplification égal à 100 est introduit.

Les équations du mouvement sont écrites dans l'espace d'état. Les paliers, les joints d'étanchéité et les effets gyroscopiques sont écrits comme forces de restitution, comme montré en Figure 3. 14. Les équations sont résolues dans le domaine temporel. L'approche utilisée a l'avantage d'être très modulable et de permettre l'ajout d'autres composants.

Développement de l'approche de contrôle

Spécifications

Le système doit satisfaire les exigences élémentaires de performances, stabilité et robustesse. Des critères édités par les normes internationales permettent de vérifier que ces exigences sont remplies. Différents cas sont considérés pour couvrir l'ensemble des conditions d'opération. Ces cas peuvent êtres liés à des distributions de balourd différentes, des vitesses de rotation ou des perturbations particulières.

Deux normes sont principalement utilisées : l'API 617 dédiée aux compresseurs centrifuges supportés par des paliers hydrodynamiques, et l'ISO 14839 dédiée aux rotors sur PMAs. Aucune des deux n'est parfaitement adaptée aux compresseurs industriels sur PMAs. Ainsi, la réponse au balourd sera qualifiée à partir des recommandations de l'API 617, tout comme l'amortissement des modes contenus dans la plage de vitesse de la machine. L'ISO 14839 sera, quand à elle, utilisée pour vérifier la robustesse et la stabilité du système avec la fonction de sensibilité, et pour juger le niveau vibratoire global de la machine. Dans ce mémoire, les spécifications suivantes sont prises en compte :

- Le déplacement dû au balourd doit satisfaire l'exigence de l'API 617 pour les paliers classiques (pris à $25\mu m$ pour des raisons de confidentialité),
- Le facteur d'amplification calculé pour la réponse au balourd devra être inférieur à 2.5,
- Le déplacement global devra être classé A selon l'ISO 14839 ($60\mu mpp$ pour le banc d'essais), et
- Le gain maximum de la fonction de sensibilité devra être inférieur à 3.

Limitations théoriques et technologiques

Certaines règles physiques ou propriétés des paliers magnétiques doivent être considérées quelque soit la stratégie de contrôle choisie.

Le capteur de déplacement n'est pas collocalisé avec l'actionneur. Il y a donc toujours au moins un mode flexible présentant un nœud entre le capteur et l'actionneur. Il faut donc pour ce mode que l'action consécutive à un déplacement soit opposée par rapport à celle appliquée normalement.

L'énergie des forces de contrôle est physiquement limitée. Ainsi, et afin d'avoir un modèle le plus proche possible du domaine expérimental, le contrôleur doit contenir un filtre passe bas.

Le convertisseur numérique analogique introduit un retard proportionnel au temps d'échantillonnage. Ainsi, l'amortissement fourni par le palier est atténué. Il en découle que la fréquence d'échantillonnage doit être aussi élevée que possible. Cependant, le microprocesseur doit être capable de calculer la réponse du palier

entre deux pas consécutifs. Donc, l'algorithme de contrôle doit être adapté au calcul en temps réel.

La limite des capacités dynamiques du palier peut être atteinte (incluant une saturation en tension des amplificateurs). Ceci est souvent le cas pour le franchissement de vitesses critiques de modes élevés. Dans ce cas, le contrôle du rotor est parfois impossible.

Pour un PMA de conception classique, les autres limites sont presque négligeables et des tests de vérifications à la fin du processus de conception sont normalement suffisants.

Pour minimiser le retard entre la mesure et l'action, les contrôleurs linéaires utilisés sont le plus souvent à phase minimale. Pour ces contrôleurs et selon le théorème de Bode, la phase de ces contrôleurs est proportionnelle à la dérivée de leur gain. Or, pour obtenir de l'amortissement, une phase positive est nécessaire, par conséquent le gain du contrôleur augmente en fonction de la fréquence. Cette loi mène à un conflit entre les objectifs de performance, stabilité et robustesse. La performance nécessiterait un gain élevé pour les basses fréquences, la robustesse un faible gain à haute fréquence et enfin la stabilité une importante augmentation du gain entre les basses et les hautes fréquences. De plus, le filtre passe bas utilisé pour limiter la bande passante du contrôleur produit nécessairement un amortissement négatif sur une plage de fréquences.

L'étude des PID augmentés permet de souligner les avantages et les inconvénients de cette stratégie de contrôle. Les principaux avantages sont : la pertinence des outils utilisés pour analyser le système (commun à tous les contrôleurs linéaires), la facilité d'implémentation du contrôleur dans un microprocesseur et enfin le domaine fréquentiel permet d'ajuster les caractéristiques du contrôleur à chaque mode. Les inconvénients sont, d'une part les propriétés hautes fréquences du rotor impactent trop fortement les performances globales du système. D'autre part, la raideur basse fréquence est trop faible tout comme l'amortissement des modes flexibles par rapport aux exigences.

La conception du contrôleur pourrait être améliorée en utilisant une approche automatisée. Cependant, l'équilibre performance / stabilité / robustesse ne serait pas pour autant amélioré. Nous voyons quatre possibilités permettant d'optimiser le comportement du système : le contrôle MIMO, le contrôle non-linéaire, les observateurs d'état et l'ajout de composants (capteurs et/ou actionneurs). L'approche développée considère uniquement les deux premières possibilités. Les autres pourraient être développées dans des études futures.

Coordonnées polaires

Usuellement, le comportement vibratoire des machines est observé à l'aide de capteurs de déplacements. Le signal temporel est alors soit traité directement pour contrôler le système, soit transposé dans le domaine fréquentiel afin d'analyser le comportement. Les analyses fréquentielles sont très utiles mais ne peuvent pas être utilisées à des fins de contrôle, puisqu'elles se font sur une fenêtre de temps. Ainsi, elles introduisent un retard inacceptable. Au contraire, nous pensons que les variables exprimées dans le repère polaire introduisent des possibilités intéressantes pour l'analyse et le contrôle de machines tournantes.

L'utilisation des variables polaires est rendue possible par deux changements de repère, entre le repère Cartésien des capteurs et actionneurs et le repère polaire du contrôleur. Il est montré au travers des équations (5.5) et (5.6), qu'il est possible de réaliser les changements de repère sans dispositif additionnel. Les capteurs de déplacement intégrés aux PMAs suffisent.

Les PMAs sont normalement des paliers symétriques. De plus, la distribution de balourd est l'excitation principale. De ce fait, la trajectoire du rotor dans le palier est très proche d'un cercle. Cette trajectoire, en régime permanent et stable, est définie par un rayon constant, une vitesse radiale nulle et une vitesse tangentielle constante, comme illustré en Figure 5. 2. Ainsi à chaque instant les variables polaires donnent des informations précises sur le comportement du système, alors que les variables Cartésiennes ne cessent d'osciller. Par ailleurs, une vibration subsynchrone apparaîtra principalement par des oscillations des variables polaires radiales à une fréquence égale à celle de rotation du rotor moins celle de la perturbation. La vitesse tangentielle est quand à elle peu affectée. Au contraire, il est difficile dans le repère Cartésien de différencier les deux vibrations (synchrone et asynchrone) comme montré par la Figure 5. 4.

Les coordonnées polaires peuvent aussi être utilisées pour appliquer des forces ciblées. La maîtrise du balourd lors du franchissement de vitesses critiques associées aux modes flexibles requiert de l'amortissement. L'amortissement généré directement par le palier est limité pour des questions de robustesse. Cependant, il serait préférable d'avoir une capacité d'amortissement supérieure. Cet amortissement pouvait être produit jusqu'alors par l'utilisation de filtres synchrones ou des raideurs croisées. Les premiers nécessitent un capteur de vitesse et les deuxièmes sont peu robustes vis-à-vis des conditions de fonctionnement. L'amortissement tangentiel utilise une formulation plus complexe qui combine les déplacements mesurés par les deux capteurs de chaque palier. Ainsi, la sensibilité au bruit de mesure est réduite. D'autre part, l'utilisation de deux vitesses (radiale et tangentielle) permet de séparer en partie les différentes composantes de la vibration. Si l'on compare par rapport à l'utilisation de raideurs croisées, l'amortissement tangentiel mesure par lui même le sens de la précession principale, et applique une force proportionnelle à la vitesse, ce qui en fait un dispositif adapté à toutes les

vitesses de rotation. En particulier, lors d'une montée en vitesse les modes inverses et directs sont successivement stabilisés de manière automatique. Il partage néanmoins un inconvénient avec les raideurs croisées, même si celui-ci est plus contenu dans le cas de l'amortissement tangentiel. Il applique des forces stabilisatrices seulement pour les précessions communes avec la précession principale. Généralement, en fonctionnement continu la précession directe est excitée par le balourd, donc les précessions inverses peuvent être perturbées.

Contrôle flou

Ce contrôleur MIMO non-linéaire permet d'obtenir des marges de performances par rapport aux exigences. Ces marges sont utilisées afin de simplifier la mise au point des contrôleurs et d'améliorer le comportement dynamique des machines.

Le contrôle flou se compose de trois étapes principales. D'abord, la fuzzification des entrées numériques en valeurs linguistiques. La vitesse sera alors considérée grande, petite, positive, négative… Chaque valeur linguistique est associée à une fonction d'appartenance de sorte que le signal soit considéré, par exemple, grand à 70%.

Le moteur d'inférence intègre les règles. Celles-ci sont conditionnelles et se présentent sous la forme « si… alors… ». Ces règles doivent correspondre au comportement dynamique du système contrôlé de sorte à optimiser la réponse du contrôleur aux différentes configurations envisagées.

Enfin, la commande est obtenue après défuzzification. Cette étape consiste en l'agrégation des différentes conclusions linguistiques, afin d'obtenir une réponse quantifiée.

Le contrôle non-linéaire SISO engendre une anisotropie qui nuit au bon fonctionnement du palier. Nous avons opté pour le développement du contrôleur flou dans le repère polaire. De plus, ce repère est bien adapté à la logique floue puisque les quantités instantanées des variables révèlent le comportement dynamique du système. En effet, dans le repère Cartésien, un couple déplacement-vitesse peut être dû à plusieurs comportements différents. Ici, l'association des trois variables polaires permet d'identifier et séparer la contribution due au balourd, des autres contributions.

La logique floue n'est pas capable de maîtriser complètement le phénomène de « spillover ». Un PID sous-jacent est alors utilisé pour assurer la stabilité des modes haute fréquence du système. Ce PID a des caractéristiques standardisés dans la plage de fréquence utile pour le comportement mécanique (jusqu'au 2ème flexible), puis des caractéristiques personnalisées en hautes fréquences pour assurer la stabilité du système. Ce contrôleur sera alors nommé SPID dans la suite.

Le contrôleur flou est utilisé pour moduler les gains du SPID. L'amortissement tangentiel pourrait atténuer les performances basses fréquences du système. Ainsi, il

est intéressant de l'appliquer seulement lorsqu'il est vraiment nécessaire. Une vitesse tangentielle élevée reflète le passage d'une vitesse critique, et permet d'appliquer un amortissement tangentiel utile. Par ailleurs, il existe un compromis entre la raideur et l'amortissement, de sorte que la raideur maximale du palier est limitée. Un comportement anormal peut être détecté par une vitesse radiale. Ainsi, une augmentation de la raideur durant un court instant permet le retour au comportement normal sans réduire l'amortissement du palier. Le contrôleur flou utilise des fonctions d'appartenance trapézoïdale. Les règles sont :

- Pour le comportement permanent, lorsque la vitesse tangentielle est élevée, l'amortissement tangentiel augmente de 50%.
- Pour le comportement transitoire, lorsque la vitesse radiale est positive, la raideur radiale augmente de 50%.

Ces règles semblent bien adaptées au système en fonctionnement normal, même si elles pourraient être complétées par des règles considérant des défauts temporaires.

SPID

Le contrôleur flou polaire permet d'obtenir des marges de performance non atteignables avec un contrôleur linéaire. Pour cette étude nous avons choisi d'utiliser ces marges pour remplir trois objectifs : d'abord, pour simplifier la mise au point du contrôleur, ensuite pour satisfaire les spécifications sans filtre synchrones et finalement pour améliorer le comportement en basse fréquence. Bien entendu, d'autres choix de compromis auraient été possibles. Nous pensons que celui-ci représente un équilibre intéressant entre performance du système et simplicité d'utilisation.

Usuellement, les propriétés d'un PID augmenté sont choisies en fonction du comportement dynamique, du nombre de modes inclus dans la plage d'opération et de leur fréquence. Ainsi, la raideur est choisie relativement faible et l'amortissement est concentré autour des fréquences des modes. Pour notre SPID, les caractéristiques ont été choisies de manière à obtenir un comportement robuste en basse fréquence ou les effets de la raideur négative du palier et des joints d'étanchéités sont le plus visible. De plus, comme la fréquence du mode de flexion est supposée inconnue, l'amortissement est réparti sur toute la plage de fréquence. Ainsi, le palier possède de bonnes propriétés pour les modes rigides et des performances moyennes pour le mode flexible. Le contrôleur est alors globalement moins performant mais plus multifonctionnel, d'autant plus que les caractéristiques mécaniques du palier sont presque indépendantes de la géométrie du rotor. Il peut être supposé que l'ajustement du gain global du contrôleur permettra d'adapter le contrôleur à différentes tailles de paliers et de rotors pour une application donnée.

Validation

Banc d'essais expérimental

Les différentes stratégies de contrôle ont été testées sur un banc d'essais académique ayant un comportement proche d'un compresseur centrifuge du point de vu de la dynamique d'arbre. L'objectif de ce banc a été d'évaluer les performances, la stabilité, la robustesse ainsi que les limites des différentes stratégies.

Le banc est composé d'un rotor flexible supporté par deux paliers magnétiques radiaux, comme visible sur la Figure 6. 1. Le rotor est entraîné, via un accouplement flexible, par un moteur électrique pouvant atteindre 12 600*rpm*.

Un modèle numérique du banc est développé sur la base des caractéristiques des différents éléments. Ce modèle est alors comparé avec les résultats obtenus sur le banc. L'analyse des caractéristiques statiques des paliers a montrée une importante dissymétrie due aux tolérances de montage des paliers. Par ailleurs, la réponse au balourd montre que la raideur en courant est 30% inférieure à celle prévu. La cause n'est pas parfaitement identifiée, même si les tolérances de fabrication et de montage semblent responsables d'une partie importante de l'erreur.

Finalement la démarche de validation suggérée par l'API 617 est appliquée. La raideur en courant est considérée comme un paramètre à calibrer, et le gain général du contrôleur est ajusté sur le banc d'essais en conséquence. Les résultats montrent qu'en utilisant cette méthode, il est possible d'obtenir des résultats expérimentaux en accord avec les prévisions des simulations numériques (voir Figure 6. 13). Dans ce cas, le modèle numérique est validé, permettant d'avoir confiance dans les résultats obtenus uniquement par simulations numériques.

Evaluation expérimentale du contrôleur flou polaire

Le contrôleur développé est évalué à travers différents tests et par comparaison avec le PID augmenté fourni avec le banc d'essais. Les tests concernent : la fonction de sensibilité, la fonction de transfert en boucle fermée, la raideur dynamique, la réponse au balourd et la réponse à des excitations subsynchrones similaires à celle rencontrées sur les machines. Ces tests ont pour but d'évaluer la stabilité, la performance et la robustesse de la stratégie de contrôle développée. Même si ces outils (particulièrement la sensibilité, la fonction de transfert en boucle fermée et la raideur dynamique) ne sont normalement pas utilisables avec des contrôleurs non-linéaires, ils sont appliqués ici car les non-linéarités apparaissent principalement dans les phases transitoires. L'analyse linéaire est donc valable pour de petits déplacements. Il faut aussi mentionner que la réponse au balourd est proportionnelle au balourd (comme pour les contrôleurs linéaires) à proximité des vitesses critiques i.e. lorsque l'amortissement tangentiel est totalement activé.

Les résultats numériques et expérimentaux concordent. Ils montrent que par rapport à un PID augmenté la solution développée est tout aussi robuste et stable. Par ailleurs, au niveau des performances, le contrôleur flou permet une réduction de l'ordre de 40% des vibrations dues au balourd, comme montré par la Figure 7. 4. Il permet aussi de réduire notablement les facteurs d'amplification et la puissance des forces de contrôle, comme révélé par la Table 7. 6.

D'autre part, pour la maîtrise des vibrations subsynchrones, la stratégie développée permet une réduction de l'ordre de 25% des déplacements générés par les excitations subsynchrones (voir Figure 7. 9).

Les résultats montrent que le SPID est suffisant pour répondre aux exigences de stabilité et robustesse. De plus, le contrôle flou polaire permet non seulement de combler les carences du SPID dues à la standardisation, mais aussi d'améliorer le comportement dynamique en réduisant sensiblement les vibrations.

Application industrielle – Evaluation par simulations numériques

Suite à la validation de la démarche sur un banc d'essais de dimension académique, elle fut appliquée pour le contrôle d'un compresseur industriel. Le rotor est supporté par des PMAs. L'objectif est de démontrer la facilité de mise au point du contrôleur, son efficacité et la robustesse de l'approche développée.

Le modèle numérique du compresseur est très proche de celui du banc d'essais. Les différents éléments (rotor et paliers) sont adaptés pour correspondre à la machine industrielle puis les effets dynamiques des joints d'étanchéité sont ajoutés. Le comportement du système est évalué pour différentes configurations qui correspondent aux normes et aux exigences des utilisateurs finaux. Le contrôleur flou polaire est comparé au SPID seul. Les cas d'étude concernent : la fonction de sensibilité, la fonction de transfert en boucle fermé, la raideur dynamique, la réponse au balourd, la réponse à des excitations aérodynamiques subsynchrones et la réponse à un impact.

Le SPID seul permet d'obtenir un comportement sain avec de bonnes marges de stabilité, une faible susceptibilité au bruit de mesure, une raideur dynamique minimale relativement élevée et des facteurs d'amplification satisfaisant pour tous les modes contenus dans l'intervalle 0–2kHz. Seule la réponse au balourd ne satisfait pas les spécifications des normes. Le contrôleur flou polaire permet alors de réduire les déplacements de 27% et le maximum du facteur d'amplification de 20%, comme montré par la Table 8. 8. Le comportement du système est alors tout près du comportement requis pour des paliers hydrodynamiques. L'ajout d'un simple filtre synchrone réduisant la raideur synchrone du palier permet alors de respecter toutes les spécifications. Ce filtre a pour principale vocation de réduire les forces de contrôle pour permettre l'utilisation de paliers magnétiques plus petits. Par ailleurs, la réponse à des excitations aérodynamiques subsynchrones est étudiée. Le contrôleur

flou polaire permet de réduire de 30% les déplacements du rotor, comme montré en Figure 8. 9.

Une étude regroupant plusieurs machines pourrait conduire à la définition d'un contrôleur flou polaire respectant systématiquement toutes les spécifications. Ainsi, deux avantages seraient obtenus : la standardisation du contrôleur, et la suppression du capteur de vitesse et des filtres synchrones adaptés à chaque machine. Finalement, le système serait alors plus simple et plus robuste.

Conclusions

Le comportement dynamique des compresseurs centrifuges supportés par paliers magnétiques actifs a été examiné. La distribution de balourd, les joints d'étanchéité et les excitations aérodynamiques subsynchrones constituent les principales sources de perturbations et doivent être considérés afin d'évaluer les performances vibratoires de chaque machine. De plus, le comportement dynamique doit satisfaire des critères exigeants édités par des normes internationales et les utilisateurs finaux. Ces spécifications visent à la sécurité et à la fiabilité des équipements.

Les stratégies de contrôle industriel usuelles des PMAs ne sont pas pleinement adaptées aux besoins des turbomachines. Une nouvelle stratégie de contrôle est développée. Celle-ci tient compte des possibilités et des limitations de la technologie existante.

Comme l'amortissement structurel des rotors flexibles est faible, ils sont très sensibles au phénomène de « spillover ». Pour répondre à cette problématique, la bande passante du contrôleur est divisée en deux régions, la transition étant au voisinage du deuxième mode flexible. Pour les basses fréquences, les caractéristiques du contrôleur sont standardisées pour chaque ligne de produit. Ces caractéristiques sont celles du contrôleur flou polaire développé. Pour les hautes fréquences, le PID sous-jacent est adapté pour assurer la stabilité et la robustesse de chaque machine.

Le contrôleur développé est constitué de trois éléments : le PID sous-jacent standardisé que nous avons nommé SPID, le contrôleur flou et le calcul des variables polaires. Le SPID est conçu de manière à simplifier la fonction de transfert du contrôleur, alors que le l'approche complète est conçue pour satisfaire le cahier des charges et améliorer le comportement très basse fréquence (0-50Hz). Par l'utilisation de variable exprimées dans les coordonnées polaires couplant les deux axes d'action, chaque palier est considéré comme une entité à par entière. L'introduction des variables polaires permet une meilleure observation du comportement dynamique du rotor. De plus, comme les variables polaires utilisent les deux capteurs de déplacement simultanément, il est possible de calculer des forces de contrôle moins sensibles au bruit de mesure. Enfin, la logique floue permet d'appliquer des forces de commande basées sur le comportement dynamique global. Comme les variables polaires permettent l'observation de ce comportement et la dissociation des sources de perturbation, le couplage des deux approches est efficace pour l'application d'actions correctives.

Nous avons montré que ce contrôleur était capable d'atténuer la réponse au balourd en utilisant des forces d'amortissement qui n'affectent pas de manière significative la robustesse du système. De plus, il peut aussi augmenter la raideur du palier pour faire face à des excitations transitoires ou asynchrones, et réduire ainsi

l'amplitude des déplacements. Si nécessaire les forces de contrôle peuvent être réduites en utilisant un filtre synchrone simple. Ce filtre vise à tolérer l'utilisation de paliers plus petits.

La stratégie de contrôle fut évaluée par des simulations numériques et des essais expérimentaux. Le modèle numérique tient compte de tous les éléments de la ligne d'action (le capteur, l'électroaimant, l'amplificateur, les câbles électriques, le contrôleur numérique) et le rotor. Les résultats numériques furent comparés avec ceux obtenus expérimentalement sur le banc d'essais. La calibration de la raideur en courant nous a permis d'obtenir des résultats satisfaisant et les mêmes allures furent constatées. Le contrôleur flou polaire a montré une bonne robustesse, une bonne stabilité et des performances supérieures au PID augmenté fourni avec le banc d'essais, à la fois pour la réponse au balourd et la réponse à des excitations subsynchrones.

Finalement, l'approche fut appliquée pour la simulation numérique du contrôle d'un compresseur industriel. Les résultats des simulations numériques nous donnent d'excellentes perspectives. En utilisant le filtre synchrone toutes les spécifications furent respectées. D'autre part, le comportement obtenu avec le contrôleur flou polaire seul est très proche des spécifications utilisées pour des paliers classiques hydrodynamiques. Dans ce second cas, le palier est plus simple et plus fiable.

Pour finir, les conceptions du contrôleur et de la machine sont plus aisées, pour le contrôleur moins de paramètres doivent être choisis et pour la machine les propriétés mécaniques des paliers sont connues par avance. D'autre part, le comportement dynamique est amélioré. L'optimisation de l'approche et l'utilisation d'un algorithme de conception automatique pour les caractéristiques hautes fréquences pourraient conduire à la standardisation des paliers magnétiques actifs.

List of Figures

List of Tables

Symbols and Nomenclature

Symbols

For more simplicity, the usual symbols are used. As the problem is multi-physic, several letters are used for different meanings and the major part of symbols is defined locally. The main symbols (used in different sections) are defined below.

F_{AMB}	Force applied by a magnetic bearing		N
g	Air gap		m
g_0	Nominal air gap		m
G_{AMB}	Bearing transfer function		-
G_C	Closed loop transfer function		-
G_{Rotor}	Rotor transfer function		-
G_S	Sensitivity transfer function		-
i	Current in coil		A
i_c	Control current		A
I_0	Bias current		A
I_W	Static control current		A
K_i	Magnetic bearing current stiffness		NA^{-1}
K_x	Magnetic bearing negative stiffness		Nm^{-1}
L	Inductance		H
L_R	Average length of magnetic flux lines in rotor		m
L_S	Average length of magnetic flux lines in stator		m
N	Number of turn in coil		
S	Active surface		m^2
x	Rotor position		m
α	Angle between the action line and the line linking the rotor centre to the pole centre		deg
δ	Generalized displacements		m
μ_0	Magnetic permeability of vacuum space	$4\pi.10^{-7}$	Hm^{-1}
μ_r	Relative Magnetic permeability steel		-

Abbreviations

ADC	Analog to Digital Converter
AF	Amplification Factor
AMB	Active Magnetic Bearing
CF	Correction Factor
CLTF	Closed Loop Transfer Function
DAC	Digital to Analog Converter
DSP	Digital Signal Processor
FE	Finite Element
FEM	Finite Elements Method
GE	General Electric Company
ICL	Integrated Compressor Line
MCS	Maximum operating Continuous Speed
MIMO	Multiple Inputs Multiple Outputs
OLTF	Open Loop Transfer Function
PID	Proportional Integral Derivative
PWM	Pulse Width Modulation
RMS	Root-Mean-Square
SF	Synchronous Filter
SISO	Single Input Single Output
SM	Separation Margin
SPID	Standardized Proportional Integral Derivative
ZOH	Zero Order Hold

Chapter 1 – INTRODUCTION

Historical perspective

Since the invention of the wheel, human kind has not stopped researching solutions to reduce friction. In numerous applications, friction is responsible for loss of energy, wear and reduction of the system lifetime. The main solutions used are lubrication and the third-body in dry friction. In both cases, the separation of the moving surfaces reduces the friction forces. Hence, levitation appears as the ultimate solution of this old problem.

Magnetic forces are known since the Antiquity. Magnets permit application of force at a distance (attractive or repulsive). The first engineering utilization of this phenomenon is the compass invented during the Middle Age in China. The utilization of magnets to support a load without friction seems obvious. However, Earnshaw's theorem [1842] shows that it is impossible to master the six degrees of freedom of a body only with passive magnets.

To the author's knowledge, the first description of a complete active magnetic suspension dates from 1957. It appears in a French patent issued by the Hispano-Suiza company. However, at this time the electronic capabilities were not sufficient to realize the bearings. Thus, the first Active Magnetic Bearings (AMBs) appear simultaneously in France and in the USA during the early 70's. Hamilton [1973] presents a magnetically suspended momentum wheel. The study is carried out by the General Electric Company for NASA. In France the researches are conducted by the LRBA (Laboratoire de Recherche de Balistique de l'Armement). This part of the laboratory has now become the S2M company (Société de Mécanique Magnétique), worldwide leader in AMBs production.

AMBs are inherently unstable and require feedback control to ensure stable operation. At the beginning, the electronic technologies were not satisfying. In addition, the range of expertise necessary to develop magnetic bearings is large (mechanics, control theory, magnetism, electricity…). Thus, even if they have numerous advantages, they have had a slow expansion. General Electric has produced three centrifugal compressors on AMBs (1987, 1994, 1997) before launching the Integrated Compressor Line (ICL) in 2006 which is now a classical product presented in Figure 1. 1. Bolusset and Pugnet [1989] relate the commissioning of the

first European oil free compressor. From 1987 to 2004, the number of compressors on AMBs produced worldwide was less than ten per year. The technology is really expanding since 2005. Swann et al. [2008] present a diffusion model of AMBs in large turbomachinery applications. They show that despite the number of new applications on compressors, the penetration of AMBs into industry is rather slow, compared to typical adoption rate time for a new technology.

Due to the progress made in electronics, AMBs are now widely used in different industrial applications and have been successfully implemented in the field of turbomachinery. Masala et al. [2010] present the lateral analysis of a vertical compressor. The magnetic bearings are currently used for:

- Flywheels,
- Turbomolecular pumps,
- Compressors,
- Artificial heart, and
- High speed milling spindle.

Figure 1. 1: Integrated Compressor Line (compressor in green and motor in white)

Concept of Active Magnetic Bearing system

AMBs sum up the definition of mechatronics. They use the unique capability of magnetic attraction. Electromagnets are utilized to apply forces without contact. Several electromagnets are necessary to control a complete rotor. In the following, only one is considered to explain the main principles. The functioning of one quadrant of a radial bearing is described by Figure 1. 2.

Electromagnets can produce only magnetic attraction forces. Besides, with a constant current, as the air gap decreases, the force increases. Consequently, the system is

naturally unstable, since it aims to pull the rotor onto the bearing inner surface. A control is then unavoidable to maintain the rotor in a stable levitation.

An active magnetic bearing is constituted by a sensor that produces an electric signal u_x proportional to the rotor displacement x. A controller then computes from this signal a command u_i intended for the actuator. This signal is transformed to a proportional current i in an electromagnet coils which produces a force on the rotor.

The feedback loop makes it possible to stabilize the rotor in its steady state position. It is responsible for the stiffness and the damping of the bearing. In order to be able to apply forces in the two opposite directions, two electromagnets are positioned on each side of the rotor. Finally, at least two radial magnetic bearings and one magnetic thrust are necessary to master the rotor support.

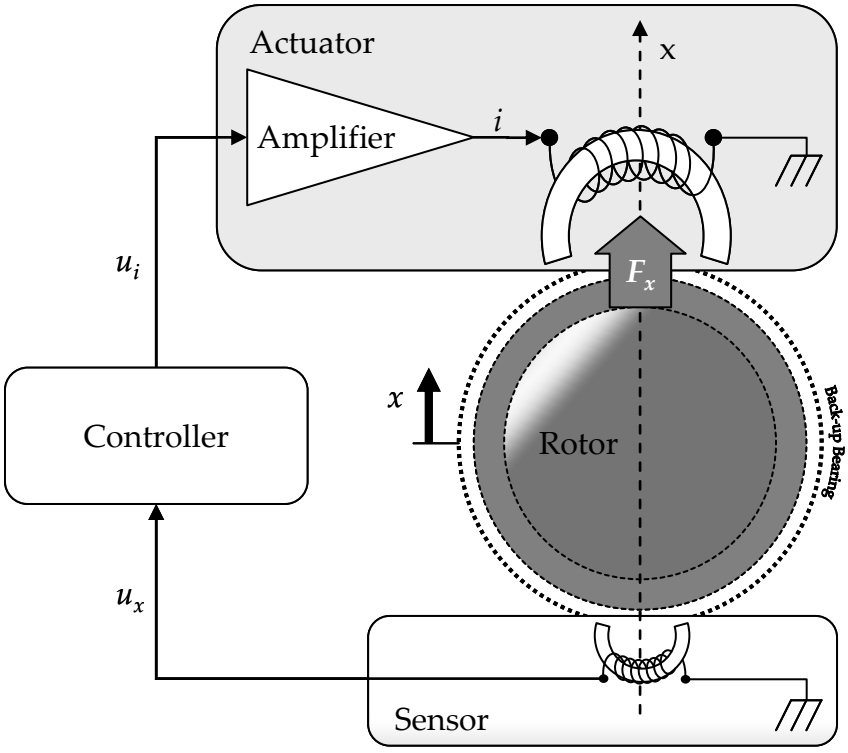

Figure 1. 2: Schema of an AMB device

The displacement sensor technology used depends on the application. Generally, inductive probes are used: variable reluctance or eddy current. For particular needs, optical probes can be used. Because of the structure of actuators, it is impossible to place the sensor at the same location. Thus, the sensors are positioned slightly on the actuator's side. It is the so-called non-collocation. Hence, there is some discrepancy between the measured displacement and the real displacement at actuator location. This error can lead to instability and the reduction of overall system performances. The controller must be adapted accordingly to this property.

Since their introduction, digital controllers have replaced analog ones. Now they are used quite exclusively. They can integrate a large range of control algorithms, and they have the advantage to allow easily the modification of the controller. The controller is an algorithm that takes into account the history of the system and its last position to compute an adapted control force. Generally, the controller is design with a linear transfer function. Several studies have been devoted to the elaboration of new controllers that enable better design and performance in operating situations, with acceptable levels of stability and robustness. However, even the most successful of these controllers has not permitted, for the moment, to replace the PID controller in industrial applications. The augmented PID controller permits designers to master the control process. Nevertheless, the control of flexible rotors remains difficult due to unavoidable spillover effects. This problem is currently overcome by using phase lag and phase lead filters. In this case also, tuning these controllers is a delicate operation and is time consuming. On the other hand, the controller allows unbalance control and diagnostic.

In order to supply bearings with current, linear amplifiers are avoided, as switching amplifiers are much more efficient and limit energy consumption of the bearings. In addition, the cooling of linear amplifier might be a difficult task.

Finally, the contact between rotor and magnetic bearing is avoided by using auxiliary bearings. These secondary bearings are used to support the rotor at rest and during AMBs faults and failures. Usually, roller bearings are used. Angular contact ball bearings enable to support radial and axial loads. These bearings have numerous names in the literature: touch-down, roller, secondary, auxiliary, back-up, catcher, emergency and retainer bearings are the most common.

Magnetic bearings offer numerous advantages. The rotor levitation enables to suppress the friction. Then, less energy is necessary to spin the rotor. The rotor can turn at higher speeds and the wear is reduced. Consequently, the maintenance operations are less frequent and quicker. There is no need for lubricant. Thus, there is no contamination with process and some applications such as vacuum pumps become possible. However, AMBs have also disadvantages, even if they reduce the operating cost, they are much more expensive than classical bearings. They need a high expertise level to be mastered especially because they cannot support an overload even for a short time. Finally, for a given rotor, they are generally bigger.

Introduction to centrifugal compressors

The centrifugal compressor is a turbomachine that can cover the greater part of the oil and gas range of applications in term of flow rate and pressure ratio. The ranges of utilisation of the different types of compressors is provided in Figure 1. 3. It offers

a high level of availability and is used in almost all the oil and gas processes from upstream (exploration and production) to downstream (petrochemical) through the midstream (transportation and storage).

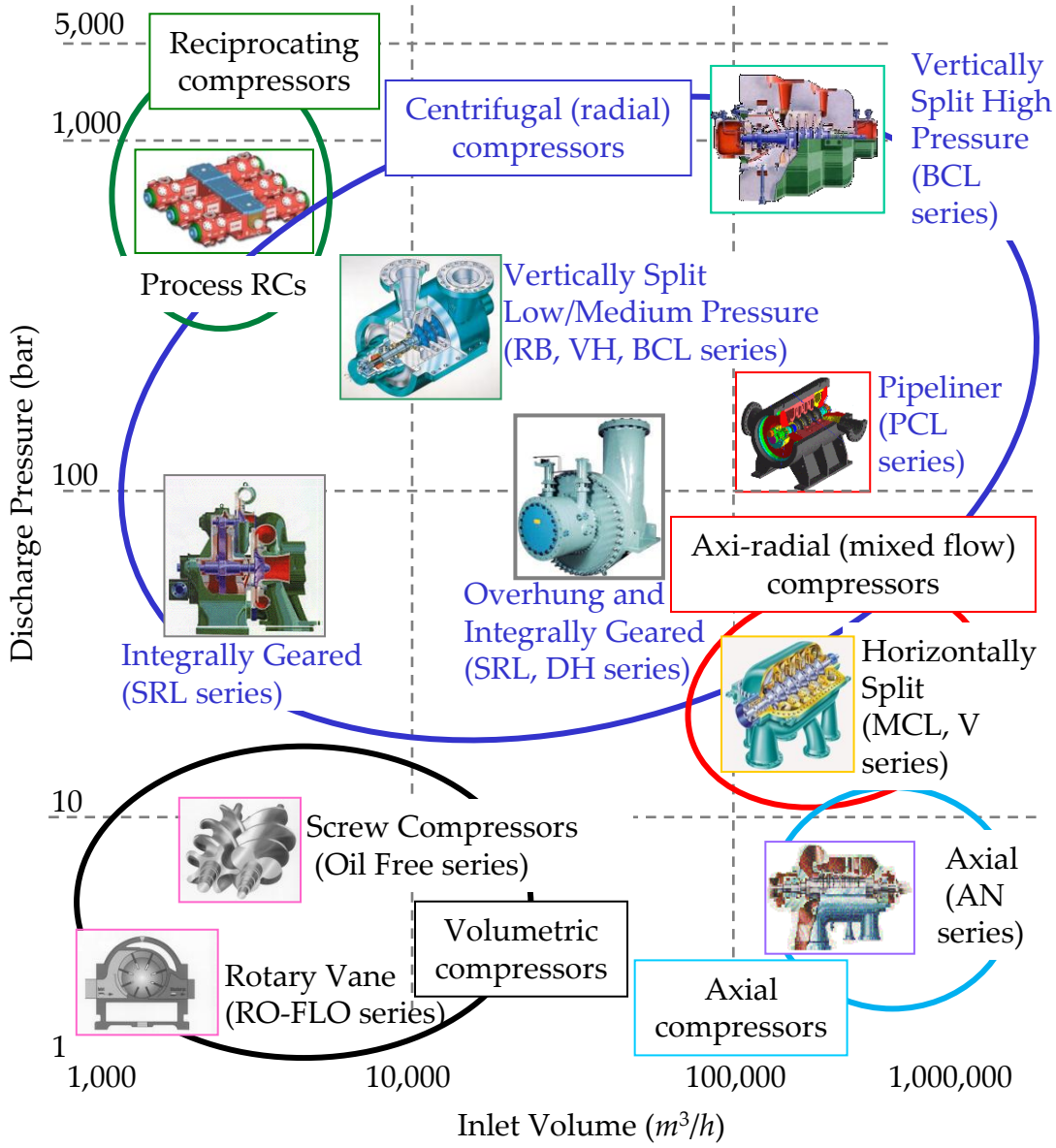

Figure 1. 3: Simplified Compressors map

The main parts of a centrifugal compressor are first, the suction pipe and the IGV (Inlet Guide Vanes) which guides the gas flow. Then, several impellers compress the gas (see Figure 1. 4). Between two consecutive impellers, the gas flow is guided through the stator by the diffuser, the bend and the return channel. A stage of compression is shown in Figure 1. 5. Finally, the gas is collected in the discharge scroll. Labyrinth gas seals are used to avoid internal gas leakages. They are placed on the two sides of each impeller. Naturally, an axial force appears on each impeller due to the flow and the pressure gap between the two faces. The balance drum positioned

on the rotor compensates this force. On one side of the balance drum is applied the suction pressure and on the other the discharge one. The thrust bearing supports the remaining axial force, which depends on the operating conditions.

Figure 1. 4: Photography of a horizontally split compressor

These machines are produced in a very limited number: typically each machine is unique. Generally, the machine is supported by tilting pad bearings. A low speed motor is coupled to the compressor through a gear train.

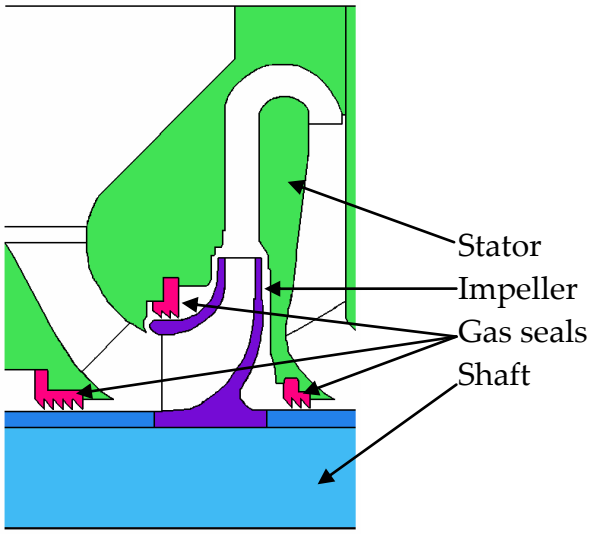

Figure 1. 5: Scheme of a compression stage

Since 2007 GE Oil & Gas manufactures a new compressor supported by magnetic bearings in the range of 3*MW* to 15*MW*. A high speed motor is directly coupled to the compressor through a flexible coupling. The overall is placed in a unique pressurized casing as described by Figure 1. 6. Only the use of magnetic bearings permits to have bearing immerged fully in the process gas, and to avoid the use of any additional external fluid.

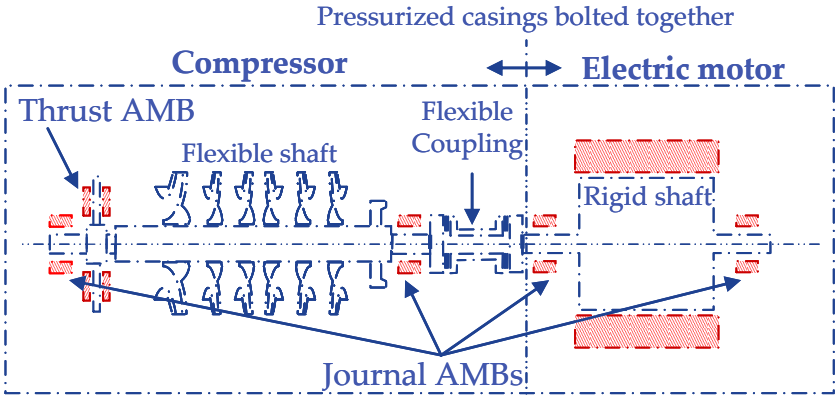

Figure 1. 6: Schema of the ICL structure

Consequently, the advantages of the ICL are that it enables to save 30,000*L* of lubricant per year. The absence of lubricant improves the safety by reducing the risk of fire. The machines are more convenient since there is no need to heat the lubricant several hours before startup. Finally, all gas leakages are suppressed avoiding the emission of 600 tons of CO_2 per year. As oil systems are often more bulky than compressors themselves, the mass and the footprint of the unit are considerably reduced as revealed by Figure 1. 7. Finally, as the time between two maintenance operations is longer the compressor can be placed directly on the oceanic floor. The Blue-C™ compressor of GE dedicated to this operating environment is currently under development.

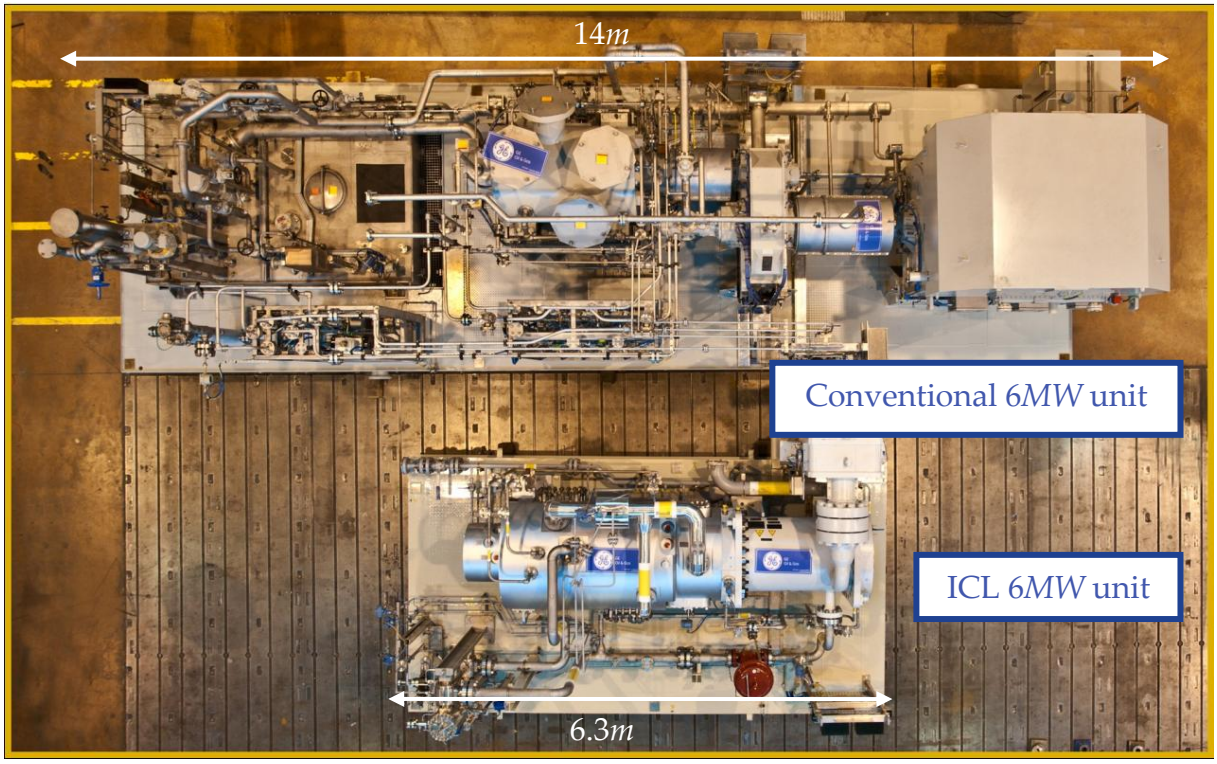

Figure 1. 7: Photography of conventional compressor unit VS ICL unit

Pugnet [2010] presents the development of compressors supported by AMBs starting from the first European compressor on AMBs to the ICL project. From a machinery manufacturer point of view, the AMBs still have two disadvantages:

- The design of controllers is time consuming, and
- The bearing characteristics depend too much on the rotor properties. As the final rotor properties are uncertain due to manufacturing tolerances, there are sometimes discrepancies between numerical predictions and final tunings on the machine.

Motivations

Mechatronics devices become widespread in all industrial areas. Maslen [2008] discusses the utilization of mechatronics in industrial turbomachinery. Several studies have shown the effectiveness of diagnostic for the detection of crack, surge or several other faults. The active systems are more and more used from AMBs to motor through active control of inlet guide vanes for example. However, the function remained separated. It is clear that integration of global control should improve the results obtained. In addition, these highly technological devices are often produced by different subsuppliers. The optimization of the machines is possible, only if the machinery manufacturer masters the design of all these different advanced technologies.

Concerning AMBs, Schweitzer [2009] sees several research axes that need to be deepened. Among them, we consider essential for a turbomachinery the control of flexible rotors, the analysis of rotor behaviour during bearing fault and the concept of smart machines. Even if significant progresses have been made, the control of synchronous forces is still studied. Finally, we think that progress must be realized concerning the susceptibility to chemical aggressions and high temperatures.

AMBs are a key component to design mechatronic systems and to introduce the concept of smart machines. Such a machine is able of high precision, autocalibration, adaptation or diagnostics. It could estimate its capability to operate normally, its remaining lifetime, or compensate faults. Obviously, these faculties should lead to less maintenance and safety issues. The mechatronic structure of AMBs permits to develop these tools and to implement them in the software.

The number of turbomachines supported by AMBs is constantly increasing. However, the possibilities offered by this technology are not completely used. Magnetic bearings are used like simple bearings and not for identification or diagnostics. They are also actuators able to excite the rotor with a defined signal with high precision on forces applied. Aenis et al. [2002] present an assessment of different

methods used to measure the electromagnetic forces. Magnetic bearings can be used for health monitoring. Nordmann and Aenis [2004] show that it is possible to observe a system fault in a centrifugal pump (bearing or hydrodynamic components). Mani et al. [2006] present a method for the detection of cracked shaft. And, Kjølhede [2007] uses the capabilities of AMBs to identify the characteristics of a tilting pad journal bearing. Finally, the AMBs can be used to control a process. Blom and Van den Hof [2008] estimate the cutting forces in micromilling. This project aimed to control the micromilling process.

Even if progress has been realized, it is certainly the research topic where gains are the most expected. There are different solutions for diagnostics or analyses but not yet for auto-corrections. Finally, a smart machine should be able to master all its components at any moment.

In most cases, faults and failures produce contact between rotor and stator. Rotor stator contacts lead to high level of vibrations with potential damage. The risk of damage is reduced by using auxiliary bearings. These bearings support the rotor until the return to normal operating conditions or until complete shut down of the machine. Normally, the auxiliary bearings have the minimum clearance of the machine. Moreover, even during high dynamic loads the rotor must not touch another element.

The contact between auxiliary bearings and rotor exists only at rest or during faults. Gelin [1990] studies the dynamic behaviour of rotor after its drop. On the other hand, Cole et al. [2002] study the dynamic behaviour of a rolling element following rotor impact. Keogh and Woon [2007] present the thermal effect of contact between rotor and auxiliary bearings.

Keogh et al. [2004] show that even with a stable controller a temporary contact can lead to unstable behaviour. They propose a new synchronous controller that enables recovery of stable levitation. Cole et al. [2006] propose to use compact wavelets to design a controller able to return the rotor from a contacting to a non-contacting state. In addition, Na et al. [2000][2001][2002] present methods to maintain operation when coil failure occur.

Large industrial machines have specific behaviour due to rotor inertia, high rotating speeds and high dynamic loads. Ransom et al. [2009] present the numerical and the experimental investigations on vertical rotor drop onto auxiliary bearings. The high speed rotor is medium scale (1/3 of a real motocompressor). Results show good auxiliary bearing performance, providing confidence in a satisfactory lifetime of these bearings. Nevertheless, it exists remaining problems. For example, there is a lack of information on the dynamic behaviour of rotor and roller bearings when radial bearings are operating well, but a thrust bearing failure occurs. Finally, several studies have begun to deal with floating platform or ship-board machines, which are subjected to particular loads produced by stator movements. In addition, for certain machines, the complete failure is not acceptable (e. g. for aircraft engines). It is then

necessary to develop new solutions (redundancy components, algorithms…), to ensure the safety of goods and human beings.

In some applications, faults arise because of the harsh environment. Centrifugal compressors are used in field where the gas can be very aggressive, particularly in upstream. Until now, canned AMBs are utilized for these applications. In this case, a thin sheet of stainless steel protects the bearings. Consequently, the magnetic air gap is increased between stator and rotor and the performance decreased. Moreover, emergency compressor depressurisation produces a differential pressure on each side of the sheet and damage can occur. New solutions could improve the behaviour of these machines.

In addition, there is an important range of applications where thermal considerations limit the utilization of magnetic bearings (steam turbines, gas turbines, aircraft engines…). Burdet [2006] discusses the design of high temperature magnetic bearings. It presents and validates a design operating at temperatures up to 550°C. However, this technology is still far from industrialisation.

Even when the bearings operate in a friendly environment, the control of the dynamic behaviour of the rotor remains a challenge. Modern machines are optimized according to the performances and the production cost. Consequently, they are lighter and operate at higher rotational speeds. When the operating speed is above the first bending critical speed, the machine is considered supercritical. The control of a flexible rotor is much more complicated than that of rigid one. Indeed, a flexible rotor is susceptible to respond to an excitation on a wide range of frequencies. Thus, the high frequency characteristics of the controller are decisive for the system global stability. In addition, when the sensor and the actuator are non-colocalized, there is always at least one flexible mode with a node between sensor and actuator. Then, the misinterpretation can produce instabilities.

Several studies have shown the feasibility of such a control. Lei and Palazzolo [2008] apply an augmented PID controller to a flexible flywheel. The design of synchronous filters and notch filters permits design of a controller robust relative to unbalances, measurement noise and sensor run-out. Spirig et al. [2002] present among other things, the design of a PID controller for an industrial centrifugal compressor. More advanced controllers are discussed in the next chapter.

Each type of machine has its own characteristics. Thus, it is necessary to define which control strategy is the most suitable for each one. Then, different alternatives exist for each strategy: SISO, MIMO, gain scheduling…

An efficient way to improve the performances of the system is to apply special filters in order to control the main disturbances. These disturbances are synchronous, like the unbalance distribution resulting from the misalignment between the geometrical axis and the axis of inertia of the rotor. The so-called sensor run-out produces also

synchronous excitations due to imperfect circularity and non-uniform magnetic properties of the rotor. Several methods are available to treat these excitations depending upon the particular goal. For large turbomachinery they can lead to two problems, first excessive vibrations and second dynamic saturation of the bearing. Thus, they must be considered seriously. The main existing control methods are presented in the next chapter. However, most of these algorithms are adapted to linear controllers, and modifications have to be considered to utilize them with non-linear controllers.

Rotor can be disturbed by non-synchronous excitations, from very common negative stiffness and measurement noise to very particular arising from process. For centrifugal compressor excitations are produced by gas seals and aerodynamic subsynchronous excitations. Of course, as these disturbances depend on the application considered there are few documents in the literature.

Many other studies have been done in these different domains. Obviously, some of the important contributors are forgotten and the author apologizes for this in advance. This study is mainly focused on the control of flexible rotors. Even if the other domains are considered, they are not treated explicitly.

Objectives and contributions

AMB technology has many advantages to argue. This work aims to develop a new control strategy optimized for motocompressor, considering industrial requirements for the development of a new generation of turbomachinery.

The spectrum of applications covered by AMBs is nowadays largely diversified. Each application presents its own operating conditions and excitations in addition to the unbalance distribution. For a centrifugal compressor, inherent disturbances are generated by gas turbulences and lead to undesirable excitations. In addition, annular gas seals utilized to prevent internal gas leakage introduce a negative effective damping at low frequency whatever the technology used (Ertas et al. [2012]). Consequently, a given control strategy could not match all the particular requirements. The lateral dynamic behaviour of these machines must respect rules dictated by international standards such as ISO 14839 [2002][2004][2006][2012] and API 617 [2002]. Industrial requirements involve several constraints regarding performance, robustness, easiness of implementation and final tuning. The specifications of the final users must also be taken into account. New controllers should exhibit better performance with the same level of robustness as classical augmented PID controllers. As known, industrial augmented PID controllers are linear and SISO systems. Thus, there are at least two ways of improvement: non-

linear and MIMO controllers. Fuzzy logic produces a non-linear controller adapted to complex system and leads to robust behaviour since it takes into account uncertainties. On the other hand, instead of controlling separately the different action lines, making use of polar coordinates permits to design one controller for the two action lines of the bearing. Then, the controller applies actions on the global behaviour of the machine and not only on localized behaviour.

For a first approach, the controller is designed to control relatively small disturbances, which concern nominal behaviour (class A ISO 14839 [2002]). Faults and failures are beyond the scope of this document. They lead to special non-linear effects such as momentary contact with catcher bearings or dynamic saturation of AMBs. These effects depend strongly on the controller and the bearings capacities (magnetic and auxiliary). The capacity of the controller to maintain a stable behaviour in these special conditions could be tested later.

A centrifugal compressor is produced in a very limited number. As the bearing characteristics can influence the rotor design, it is interesting to develop a specific controller for a range product. Very often, the AMB dynamic characteristics depend on the rotor and there are discrepancies between numerical simulations and the on site controllers. It is expected that a simpler controller could have more constant characteristics. This controller has to be relatively standard in order to be easily adjusted to each machine. Thus, the rotordynamic analysis can be done easily during the machine design process. The aim of this kind of controller is also to make customers more confident with this technology and to reduce the design and tuning time. In this document, this motivation was considered as a major requirement for the elaboration of the controller.

Generally, PID controllers are not sufficient to obtain acceptable unbalance responses, and the specifications are satisfied by using general notch filters. These filters utilize the tachometer signal provided by rotational speed sensor. Synchronous filters are widespread in industrial applications. However, the implementation of most of these filters requires additional hardware and obviously affects the global system reliability even if speed sensors are robust. Speed sensors are useful for diagnostic and monitoring purpose but with the structure of ICL two speed sensors are necessary for control subject instead of only one for monitoring purpose. Indeed, the flexible coupling between the motor and the compressor serves as a fuse in case of high torque between the two machines. For example, abnormal high torque can appear in case of electrical short circuit inside the motor. This torque can reach 8 times the nominal value and could damage the compressor. Consequently, after such an event the two rotors run-down at different rotating speeds and two speeds sensors are necessary. The suppression of synchronous filters would permit to obtain two advantages: the standardization of the controller and the

suppression of the speed sensor. Thus, the hardware of the bearing would be simpler and more robust.

The controller developed must be validated. Usually, four steps are necessary: first the numerical design and analysis, second the experimental assessment on an academic rotor, third the experimental test on a medium scale rotor having dynamic properties close to a compressor, and finally the validation on a real machine. This process is relatively long. Consequently, the objectives were only the implementation and the experimental assessment on an academic test rig. Then, numerical investigations have allowed analyzing the control of an industrial compressor.

The major contributions of this work can be summarized as:

- A new control approach. First, a Standard PID was tuned (SPID) and then the fuzzy controllers modulated the SPID gains. The SPID is designed in order to have low frequency characteristics independent of rotor geometry.
- The utilisation of polar coordinates is introduced. The originality of the methodology developed is that it manages two significant physical quantities, namely tangential and radial velocities, which are associated with steady state and transient behaviours respectively. Besides, the polar physical quantities are interesting to apply targeted actions. The outputs are the forces computed in the polar coordinates and are converted into currents that drive the action lines at the same time. The controller considers each bearing as a single MIMO system, with the displacements in the two orthogonal directions as inputs. Hawkins et al. [2000] and Park et al. [2008] utilize this type of MIMO control with cross control to compensate flywheel gyroscopic effects. It was also applied by Matsushita et al. [1990] to generate synchronal damping by using general notch filters associated with cross stiffness.
- A fuzzy controller was developed by making use of inputs expressed in polar coordinates. The fuzzy logic, which is a decision support system, is a powerful tool in order to use this information for control issues. This controller enables tackling undesirable anisotropic behaviour of non-linear controllers by using polar coordinates. A Sugeno algorithm with simple rules is used. The fuzzy blocks are easy to tune, as the fuzzy rules are defined as a function of the dynamic behaviour of the rotating machinery. This behaviour is almost the same for a given range of products, the geometrical variations may affect the amplitudes of the response, but not the phenomena considered.

Organization of this thesis

Chapter 2: In this chapter the most advanced control strategy are discussed. The advantages and disadvantages of μ-synthesis, modal control and fuzzy control are highlighted. The motivations for developing fuzzy logic strategy are emphasized.

Chapter 3: This chapter deals with the numerical model of the rotor supported by two magnetic journal bearings. The behaviours of sensors, numerical controllers, amplifiers electromagnets and cables are described. The modelling of the different components of an AMB system is presented. The characteristics and the limitations of each element are shown.

Chapter 4: The standards requirements are discussed. The technical limitations and the physical laws use for the controller design are detailed. Finally, the controller synthesis method is described for an industrial augmented PID.

Chapter 5: The control strategy developed is detailed. The advantages of the utilization of polar quantities for observation and action are highlighted. The principles of the fuzzy logic are presented. The tuning of fuzzy controllers is detailed. Finally, the control strategy developed is described and discussed.

Chapter 6: The experimental test rig is presented. Numerical and experimental results are compared and the differences discussed. The numerical model is calibrated to match with experimental results. Finally, the numerical model is validated according standards requirements.

Chapter 7: The fuzzy logic controller is assessed with numerical and experimental investigations on the academic test rig. The results obtained are compared with those of a classical augmented PID controller.

Chapter 8: The controller is applied to an industrial compressor. Numerical simulations are performed to evaluate the controller. The controller is assessed for different configurations that correspond to the standards and the compressor final user specifications.

Chapter 9: The advantages and disadvantages are highlighted and the conclusions are summarized. Some issues for future research are addressed.

Chapter 2 – LITERATURE REVIEW

Introduction

This literature review is not exhaustive. Obviously, some relevant works are forgotten and the author apologizes for this in advance. There are numerous publications on rotor supported by AMBs. Most of them are certainly dedicated to the control. This work is devoted to the control of flexible rotor supported by two classical radial active magnetic bearings. Rotors considered have low gyroscopic effect, and the nominal conditions are considered i.e. without fault or failure. For this type of machine, several controllers were examined. The control strategy developed was chosen based on the literature review and the application considered.

The controller could be classified in terms of different characteristics (linear, non-linear, adaptive, SISO, MIMO, optimal and robust). Most of these properties are inherent to each controller theory, but adaptive control can be used with all the strategies. Adaptive control is the possibility of the controller to change its properties as a function of the system modifications or environmental conditions. It is different from non-linear control where the properties change as a function of the amplitude of measurements. In adaptive control the system shifts from one controller to another, during a time relatively long from a real time control point of view, e.g.: gain scheduling enables adaptive control.

Nonami [1995] shows that some modern controls such as LQ, LQG, disturbance cancellation and H_2 do not provide appropriate robustness. He comments that for linear systems the μ-synthesis controller gives good results, as well as H_∞ controllers that can be classified among μ-synthesis controllers. Finally, for non-linear systems, the sliding mode control associated with the μ-synthesis seems to be a better solution. Maslen and Montie [2001] discuss the application of sliding mode control to AMBs. They conclude that this type of controller is no more efficient than an augmented PID, but it can be a tool during the controller synthesis.

After more than two decades of research, three control strategies are still developed by researchers: μ-synthesis, modal and fuzzy controls (the augmented PID having reached maturity, it will be developed in Chapter 4). The works dedicated to unbalance control are also discussed in this chapter. Unbalance control is different from classical control theory but it is essential for industrial application. Thus, it is important to have an idea about the different strategies. Finally, a comparative analysis is presented.

μ-synthesis

μ-synthesis provides an encouraging method for automatic tuning. It permits to design multivariable controllers that include both performance specifications and robustness guarantees for a given range of uncertainty that has to be set. Unfortunately, this method is very complex and cannot take into account all the requirements for a rotating machine. In particular, there is no simple formulation available for parametric functions such as gyroscopic effect. In addition, requirements can be conflicting and it is of engineer responsibility's to define the major specifications.

Font et al. [1997] present a H_∞ controller applied to a flexible rotor supported by AMBs. This work is original because weighting functions are applied on each mode. Thus, the disturbance rejection is focused on the first modes and the robustness for the high frequency modes. The order of the SISO controller obtained equals seventeen and can be reduced.

Nonami et al. [1997] present the control of a milling AMB spindle with flexible rotor. Robust control is obtained using μ-synthesis with descriptor form. Experimental results show the effectiveness of the method. Fittro and Knospe [2002] present the application of μ-synthesis for the control of an academic flexible rotor supported by two radial AMBs. The MIMO controller obtained is almost as robust as the handmade optimized PD controller, and has 30% higher performances. Besides, the μ-synthesis controller is obtained relatively automatically. The main difference between the two approaches is that the μ-synthesis controller is MIMO. Thus, the controller uses the displacements (from a same direction) provided by the two bearings. Therefore, there are twice more controllers, than for the decentralized optimized PD controller. Although it is clear that making use of all the inputs available enhances the system performances, this type of global control is precluded for handmade controllers by the design difficulties. Lösch [2002] studies an automated control design based on an identification of the rotor supported by active magnetic bearings. The results are convincing and the tuning quick, but the performance of the controllers obtained seems still too limited for industrialization. This attempt to generalize the design approach is encouraging for the development of the method.

Li et al. [2006] apply a μ-synthesis controller to a rotor supported by AMBs. They use a precise identification of the whole system to quantify the modelling uncertainty. Based on these results they design a robust controller.

Schweitzer and Maslen [2009] apply the μ-synthesis method for the control of a two stages supercritical compressor. The result is interesting because the controller is tuned automatically. The controller is obtained from the description of the plant in the state space and the weighting functions. The weighting functions describe the

different objectives that must be met by the controller (performance, robustness…), and are easily constructed from logic reasoning. The authors highlight the remaining difficulties for this type of controller. First, it is difficult to take into account the parametric effects such as gyroscopic ones. Then, the method provides a controller whose order equals the sum of the plant order plus the order of weighting functions. This is an important limitation for the definition of weighting functions. Moreover, convergence of the design process is not guaranteed. The weighting functions must be sufficiently restrictive but not too. Finally, the order of the controller obtained must be reduced so it could be implemented in a real time process. This operation seems particularly difficult to realize, because during reduction an equivalent controller transfer function must be found with a lower order. Then, the reduced controller must still satisfy the specifications.

Last studies take into account not only the general rotor dynamics, but also the process where are involved the machines. Pesch and Sawicki [2012] use a force cutting model in order to stabilize not only the rotor but also the machining process and to obtain chatter attenuation.

Modal

The modal controller can be considered as an ideal controller where the control energy is concentrated on the targeted modes. Modal control is realized through two stages, first the contribution of each mode is separated and then an optimal controller is constructed for each mode in the operating frequency range. The higher frequency modes are ignored since the effect on these quantities is assumed to be negligible. This type of control has two advantages, first, the controller is easily optimized for each mode and, second, the highest frequency modes can be ignored. However, these properties are guaranteed only for an ideal modal controller, this means for an infinity of displacement sensors and for a perfect modal basis of the structure.

The modal approach was validated on numerous applications. Until now, this strategy has been validated experimentally on rotor with hybrid bearings but not with AMBs. The oil film present in these bearings provides damping for the high frequency modes. Consequently, the hypotheses of modal theory are respected. New solutions to this problem have been tested and validated numerically but not yet experimentally.

Nonami and Fleming [1986] present a quasi-modal method to control rotor vibrations through active bearings. The controller requires almost no tuning, since the controller is designed to provide critical damping on each mode. In addition, the controller avoids the use of a state observer. The results show the possibility to control three modes with only two velocity sensors and two actuators positioned

along the shaft. However, this control can be efficient only if the sensor positions can be chosen and optimized. Moreover, the authors report no indication about how the control forces interact with the higher frequency modes.

Lin and Yu [2004] discuss utilization of modal control for flexible rotor on magnetic suspension. They use a first level control to tackle the problem of rigid body modes such that the rotor modes are defined and properly separated. Then, the modal control is implemented in a second level. This work shows how a significant reduction of the spillover effect can be obtained by using a switching approach, which directs the control to modes with higher vibration contributions. Yu et al. [2007] improve the approach by using a robust modal control designed with H_∞ norm and a modal observer.

Simões et al. [2007] present experimental results on a rotor supported by a hybrid bearing made with piezoelectric stack actuators. The modal control is obtained through an LQE state estimator and an LQG controller. The effectiveness of this control strategy is demonstrated during impulse and step disturbances, and also during unbalance responses. Indirectly, this work emphasizes that the utilization of a hybrid bearing can significantly reduce the problem of spillover.

Modal control is an important challenge for the future, but there is no proof on the possibility to separate sufficiently the modes in order to ignore the high frequency modes during the design of the controller. The application of modal control to rotor supported by AMBs requires an adaptation in order to tackle the spillover stability problem.

Fuzzy

There are different types of non-linear controllers (time-variant, linearization based…). Ponsart [1996] presents a non-linear control based on flatness theory. He proves the effectiveness of this theory for the control of a rigid rotor. Among the range of non-linear controller, the fuzzy logic controllers seem to be one of the most suitable for AMBs. Indeed, they are not based on an identification of the system, but on its global behaviour. An expert is then need for the controller synthesis. Fuzzy logic permits to use uncertain measurements by simulating the human being reasoning during decision making.

Fuzzy logic has been extensively developed on flexible beam. The coupling of fuzzy logic with modal control has enabled to obtain efficient controller. It can be expected that the approach will follow the same progression on rotor. Kwak and Sciulli [1996] discuss the application of fuzzy controller to a flexible beam equipped with piezoelectric actuators. They demonstrate the robustness and the performance of this

type of controller. Mahlis [2002] presents a fuzzy modal controller. Piezoelectric actuators are used for the control of a flexible beam and a rotor. Mahfoud and Der Hagopian [2011] show a comparative study of fuzzy control and modal fuzzy control applied to a flexible beam equipped with an electromagnetic actuator. The two controllers give good results, but the modal controller is more efficient while using less control energy.

In parallel, Koskinen [1993] studies the application of fuzzy controller to AMBs. He uses the displacement and velocity to reduce the controller gain at high frequency and improve its robustness.

It is straightforward to realize a fuzzy PI or fuzzy PD controller but less evident for fuzzy PID controller. Qiao and Mizumoto [1996] present a method to realize easily a fuzzy PID controller. They use the displacement and the velocity as inputs of their fuzzy controller. The output is used to generate two controllers in parallel (a fuzzy PI and a fuzzy PD). Then, the commands computed by the two controllers are added to obtain a fuzzy PID controller.

Fuh and Tung [1997] demonstrate the stability of fuzzy control systems through the Popov-Lyapunov approach. The method is applied on a magnetic bearing experiment. This work is interesting because it permits to guarantee a region of stability. Nevertheless, the developed method is relatively complex and certainly not suitable for all fuzzy controllers.

Lei et al. [2000] make use of an AMB to move and control the rotor of an active stall control test rig. They show that in presence of large motions, a classic PID controller cannot manage the rotor in a stable manner. A simple fuzzy controller is developed in order to deal with this kind of non-linearity. Golob and Tovornik [2003] show a comparative study of PID controller and fuzzy PID controller for the experimental control of a magnetically levitated ball. As expected, the fuzzy controller leads to better results.

Couzon [2003] presents a neuro-fuzzy controller for systematic tuning. A neuronal network is used to identify the actuators and the rigid rotor of a vacuum pump. Then, a fuzzy logic controller is automatically tuned. The controller obtained exhibits a robust dynamic behaviour through different experimental tests. Chen et al. [2009] present a self-tuning fuzzy PID controller for unbalance compensation. An observer is used to identify the structural behaviour and to tune the controller. The observer is also used for unbalance identification and compensation. As the classic observer is not suitable for all operating conditions, a fuzzy observer is developed. The experimental results emphasize the efficiency of the obtained controller.

A fuzzy controller is tuned with heuristic rules. Thus, it could not be considered as an optimal controller. It is designed for robustness and its performance stems from its non-linear properties. Even if some tools exist, the analysis of fuzzy controller is still a challenge. The controller can be optimized by using neural network for

example but the expert analysis of the system cannot be avoided. In fuzzy logic method, the identification of the system is not necessary as the control is based on rules that summarize the system behaviour. Unfortunately, it seems that there is no existing solution to integrate the stability of high frequency modes in the controller with simple and efficient rules. The method proposed by Koskinen [1993] seems not sufficient and it was a major goal of this work to solve this problem.

Unbalance control

There are numerous manners to realize unbalance control in the literature. Schweitzer and Maslen [2009] classify them in function of their main goals, i.e. the attenuation of vibrations or forces or the generation of synchronous damping. There are all sorts of possibilities in order to realize synchronous control. One of them is the utilization of synchronous filters designed with notch filters. The goal is to transform the controller transfer function into a parametric transfer function, which depends on rotating speed. The controller is modified locally around the rotating speed frequency. This modification can produce more damping, less stiffness… The cost of this transformation is generally a reduction of the bearing damping for frequencies just below the rotating frequency. The advantage of this proven method is the direct relationship between the tachometer signal and the action of the synchronous controller (there is no delay). The acceleration phases can be a problem with method requiring a delay. The class of studied machine is regularly subjected to emergency shutdowns (several times a month). This type of shutdown is triggered when the machine behaviour is abnormal or more often because the characteristics of the industrial process are not the expected ones. Then, the gas quickly slows down the rotor. During the first seconds, the deceleration rate is of the order of 2500rpm/s.

Generally, information about rotating speed is necessary. Most of the methods use the signal provided by a rotational speed sensor. It is interesting to avoid this sensor, which needs cables and connections while it decreases the mean lifetime of industrial systems. Nonami et al. [1998] show an adaptive algorithm with identification of disturbance frequency. The estimation is precise, but the convergence time is about 1 second, what seems long during acceleration phases. In addition, the estimation is sensitive to noise. Lee et al. [2003] present an unbalance compensation, where the speed is computed directly from vibrations, and then used to reduce the bearing forces. However, the speed estimation lacks of robustness.

The identification based methods are the most powerful during operating conditions. They require an adaptive algorithm, because even if the unbalance distribution is constant, the corrective unbalances must change as a function of rotational speed.

This can be easily illustrated. If we consider a perfect rigid rotor equipped with a unique unbalance at middle span. For the first critical speed (cylindrical mode), each bearing will compensate half the unbalance. However, the unbalance will have no effect on the tilting mode, and compensation will be not required. Moreover, the unbalance can change due to thermal effects, wear… The problem with adaptive algorithms is the time need to refresh the data. Thus, they are less suitable for important accelerations.

Shi et al. [2004] compare two feedforward adaptive controllers. The first is used for attenuation of vibration and the second for attenuation of forces. The algorithm for reduction of vibration enables to compensate the unbalance forces. In this case, the rotor spins around its geometric axis .This type of algorithm is efficient, but needs an actuator capable of providing the huge required forces without power saturation. In the second case, forces are attenuated and the rotor spins around its inertial axis. The control needs low forces but as the compensation is not exact, the displacements are still important. Therefore, the attenuation of forces is more suitable for turbomachinery in order to avoid the saturation of amplifiers.

Cutting-off the synchronous force permits to never cross the rigid body modes because the synchronous stiffness is nil. The problem is that this strategy cannot be applied when the operating speed is close or above the first flexible natural frequency, because the bending frequency is different from zero when stiffness is nil. One possibility, for crossing flexible critical speeds, is the utilization of notch filters that provide damping forces. The two principal methods to produce synchronous damping are the derivation of the displacement and the geometric damping generated by introducing a cross stiffness. Matsushita et al. [1990] use the cross stiffness effect to stabilizing forward and backward vibration. Notch filters are used to apply this cross stiffness at specific frequencies. Larsonneur [2006] makes use of notch filters to produce only synchronous damping (no stiffness).

In all the cases, generalized synchronous filters are an additional feature which modifies the behaviour of the rotor. They have to be considered carefully. They can greatly improve the system performances, but they reduce the stability of the system at least on a narrow range of frequency. Tamisier et al. [2001] show a method that permits to cross the first critical speed. The identification enables a precise compensation without jeopardizing the system stability.

Particularly, the amplification factor computed from the unbalance response with synchronous filters has not the usual sense for the system stability. Moreover, the actual performances are closely linked to the system capacity to measure the rotor speed.

Summary

It is very difficult and of course subjective to attribute a note to each control strategy. We have attempted to qualify the four main strategies (Table 2. 1) on four criteria:

- The maturity achieved by the strategy,
- The initial difficulty to develop the strategy,
- The difficulty to design a controller, and
- The quality of the final result and the advantages for end users

The maturity indicates the ability of the method to be implemented in industrial application within a short time. The initial difficulty comes from the theory complexity and its easiness to be adapted to a given range of application. The goal is to develop the tools and algorithms that will be used by the engineers and technicians. Finally, the design easiness is assessed by the skills required for the person that design the controller of a new machine and the time necessary to do this work. The quality for the end users could be the balance between the stability, the performances and the robustness.

As expected, the three new strategies are globally equivalents and everyone shall choose the strategy adapted to his specifications. At this stage, no weighting functions were attributed to the different criteria. Modal control is the more promising but also the farthest from industrialisation. It offers important advantages if the use of numerous sensors is possible. μ-synthesis enables systematic tuning for moderate problems. It is definitely the controller researched by industrials, but it seems not adapted to complex problems of rotordynamics. Finally, we choose to develop fuzzy controllers because they have no hindrance for industrial utilization. Their non-linear behaviour can be acceptable, if it is used carefully. Besides, they can be coupled with the other controllers in order to combine their advantages.

	PID (ref.)	μ-synthesis	Modal	Fuzzy
Maturity	0	-1	-3	-1
Theory complexity	0	-2	-2	-1
Design easiness	0	+3	+3	+1
Quality for end users	0	+1	+3	+2
Total	0	+1	+1	+1

Table 2. 1: Comparison of the main controllers

Chapter 3 – AMB SYSTEM AND FLEXIBLE ROTOR MODELING

Introduction – Hypothesis

The work presented hereafter aims to detail the hypotheses that have led to the model establishment. The main phenomena have been studied in order to obtain a reliable model representative of the real behaviour. The internal report, addressed to GE Oil & Gas at the end of the first year, details the different achieved studies (Defoy et al. [2010]). Here, only the main conclusions are reported.

Habermann [1984] describes the technical characteristics of a complete AMB device. He considers the electromagnets, the amplifiers, the sensors and the controllers. Schweitzer and Maslen [2009] present the technologies used nowadays. The different elements studied in this chapter are indicated in Figure 3. 1.

In this chapter, the different models used to represent the AMBs in numerical simulation are discussed. The AMBs used for academic test rig and compressor are sufficiently similar to consider only one model. Of course, the model parameters are adjusted for the two applications.

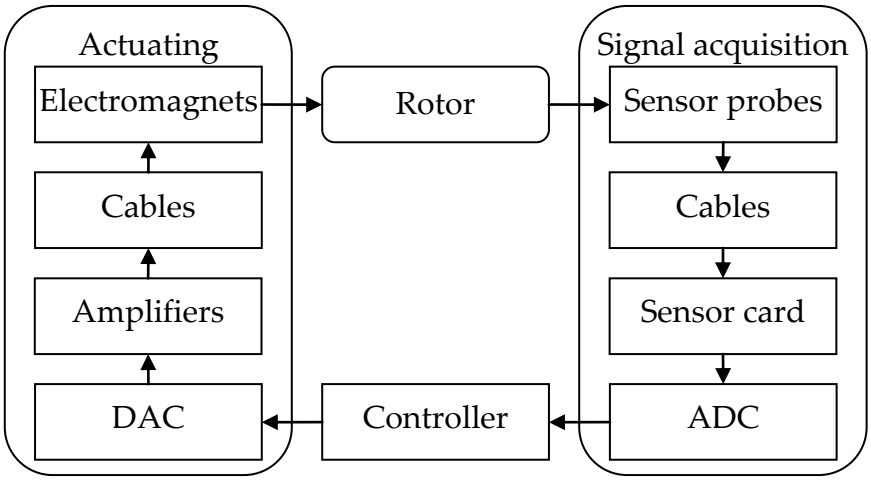

Figure 3. 1: Detail of the different elements of an action line

Modelling of active magnetic bearings can be considered as well known in the case of nominal behaviour. Nominal behaviour is defined by a position close to the bearing centre relatively to the air gap, and force acceptable relatively to the magnetic saturation and amplifier dynamic saturation. The AMBs are normally designed to

accept just slight incursions in the saturation domain. The two reasons are first, the high non-linearity achieved in this domain and second, the desire to limit the magnetic hysteresis effects. Eddy currents slow down the variation of magnetic flux. They depend mainly on two parameters, the electrical resistivity of material and the section of iron core. Thus, whenever possible, in order to reduce the eddy current effects, the iron core of magnetic circuit is made of a stack of laminated sheets of steel insulate each other. Traxler [1985] reports experiments with a radial bearing constructed from sheets, where a constant current stiffness were measured up to a frequency of 1.4 kHz. The eddy currents are neglected in this study.

The hysteresis curve can depend on frequency. This phenomenon appears with high eddy currents. Keith et al. [1993] show that for mild steels, this effect can be neglected. The magnetic hysteresis effects are neglected in this study.

Displacement sensors

The design of the displacement sensors is important for the performance of the magnetic bearing. The sensors must measure the displacement of a rotating surface. Thus, contact-free sensors with low sensitivity to material non-homogeneity are required. The operating conditions inside a compressor (gas, dirt and undesirable residues), coupled with the utilization of electromagnetic actuators with unavoidable flux leakages, make impossible the use of most of the displacement sensors (optical sensors, capacitive sensors and magnetic sensors). Thus, only inductive sensors and eddy current sensor are suitable for this type of application. In some cases, sensors must be protected from gas by a sheet of metal to avoid damages. The sensors are characterized by:

- Their linearity,
- Their sensitivity, indicating the ratio of the output signal voltage variation over the displacement ($mV/\mu m$),
- Their bandwidth of frequency, i.e. the frequency range where the sensitivity is independent of frequency with negligible phase lag,
- Their resolution, the minimum displacement that can be distinguished, and
- Their measuring range, defined by the range of measurable displacements.

In addition, their sensitivity to magnetic external disturbances, non-homogeneity of material (electrical run-out), non-axisymmetry (mechanical run-out) and temperature variations are also taken into account.

Inductive sensors have a smaller frequency bandwidth than eddy current sensors. However, eddy current sensors need a magnetic shield, and the available structures are more sensitive to electrical and mechanical run-out since their surface is small

compared to the typical surface of inductive sensors. On the other hand, Charron [2003] reports that eddy current sensors are more susceptible to material non-homogeneity, leading to electrical run-out for magnetic bearing application. Charron [2004] presents the typical characteristics of contact-free sensors. In the following, only inductive sensors are considered.

Inductive sensors permit to measure the displacement of a ferromagnetic target. Each sensor is formed of two identical probes put on both sides of the target. Each probe is composed of a copper coil wrapped around an iron core. The iron core is made of a stack of laminated sheets of silicon steel (Fe-Si 3% generally). A ring of laminated sheets of steel is placed on the rotor in order to reduce the eddy current effect. This ring must be as homogenous as possible in order to attenuate run-out effects.

The displacement x of the target modifies the air gap g. For the left hand side probe, as shown in Figure 3. 2,

$$g = g_0 + x \qquad \textbf{3. 1}$$

Where, g_0 is the nominal air gap.

Supposing the relative permeability of steel infinite, the reluctance R of the magnetic circuit is mainly function of the air gap, thus

$$R = \frac{2g}{\mu_0 S} \qquad \textbf{3. 2}$$

Where:

- $\mu_0 = 4\pi 10^{-7} Hm^{-1}$ the permeability of vacuum space, and
- S the active surface of one tooth of the probe.

The magnetomotive force equals the number of turn N times the current i (noted I in the Laplace space). Thus, following the law of Hopkinson, the magnetic flux equals

$$\Phi = \frac{Ni}{R} \qquad \textbf{3. 3}$$

The inductance L of the probe detects the total flux Ψ embraced by it. Therefore,

$$L = \frac{d\Psi}{di} = \frac{dN\Phi}{di} = \frac{\mu_0 S N^2}{2g} \qquad \textbf{3. 4}$$

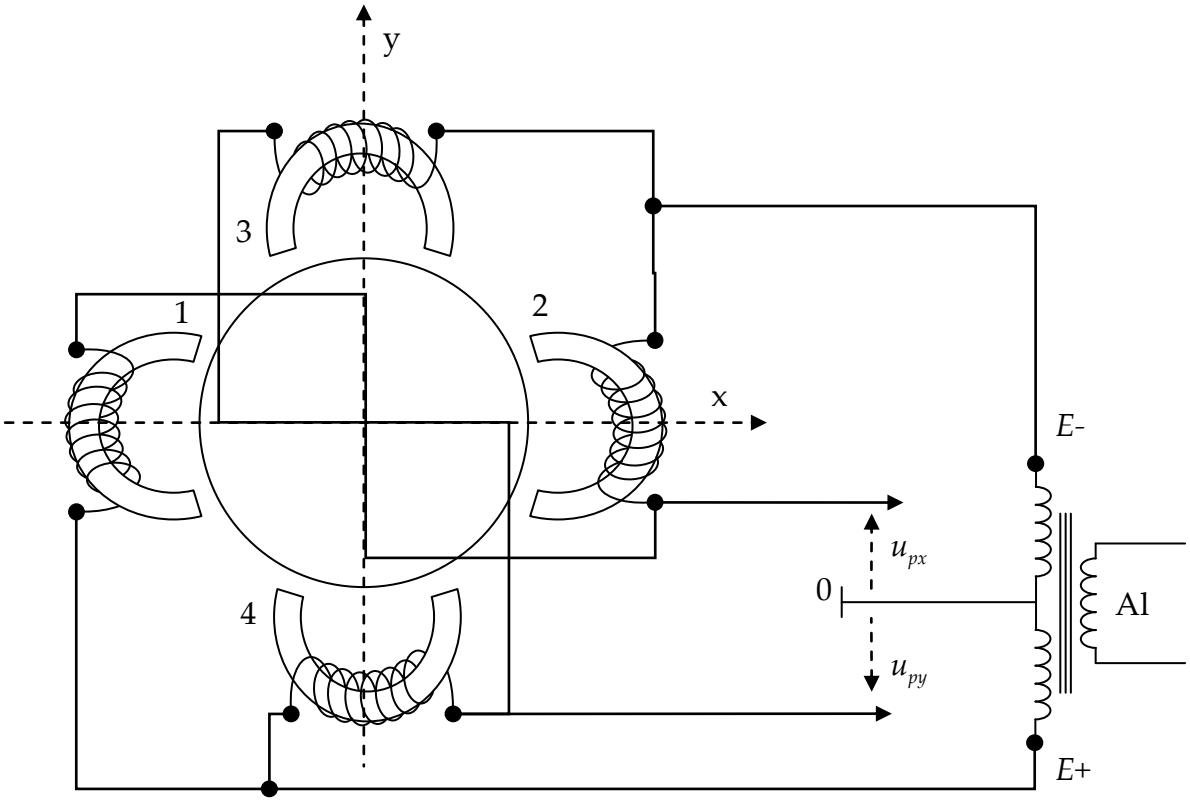

Figure 3. 2: Electric schema of an inductive sensor

The electrical circuit of an inductive sensor is provided in Figure 3. 2. The two probes are arranged in an alternative Wheatstone bridge powered by the excitation E whose frequency equals ω_W. The parts including the derivate of coil inductance and its resistance can be neglected. Thus,

$$2E\left(j\omega_W\right) = j\omega_W L_1 I\left(j\omega_W\right) + j\omega_W L_2 I\left(j\omega_W\right) \qquad \textbf{3. 5}$$

Charron [2003] presents a model with eddy currents and Durand [2002] with parasitic capacitance. However, the parameters of these models are difficult to obtain analytically. After some calculus, the output signal of the Wheatstone bridge is obtained:

$$U_x\left(j\omega_W\right) = \frac{E\left(j\omega_W\right)}{g_0} x \qquad \textbf{3. 6}$$

This signal is sinusoidal with amplitude proportional to displacement. Finally, as shown by Maslen [2000], the displacement is obtained thanks to a classical demodulation circuit. A low pass filter aims to suppress the high frequency

oscillations introduced by the demodulation circuit ($2\omega_W$). Obviously, this low pass filter is a limitation for the AMB system, and its cut-off frequency depends directly on the Wheatstone bridge frequency, which is typically in the range of 10-50kHz. The lower limit is defined by the bandwidth of the sensor and the upper limit by eddy current effects. Therefore, the bandwidth of a well designed inductive sensor is in the interval of 0-5kHz.

Finally, the displacement sensor model is settled from the sensitivity and the final low pass filter, which can be also used as antialiasing filter.

Digital controller

The digital controller permits the utilization of sophisticated control algorithms. It is composed of three parts: the analog-to-digital converter (ADC), the microprocessor (DSP) and the digital-to-analog converter (DAC). Five measures of time are involved in its behaviour:

- The sampling period T_S,
- The time characteristic of the mechanical system. It could be the period of the highest frequency considered. This time should be long relative to the sampling period.
- The time necessary for signal acquisition. It is the time need by the ADC for the conversion. The ADC samples the analog signal at the sampling frequency, and then holds and quantifies it in a very short time. The signal is held by using a Zero Order Hold (ZOH). This time is normally negligible compared to the sampling period.
- The computation time. It is the time used by the DSP to calculate the response of the controller at each sampling step. The controller provides one value for each sampling time. This time is unknown. It depends on the complexity the control algorithm, and in all the cases must be inferior to the sampling period.
- Finally, the conversion time of the DAC. This time depends directly on the sampling time. The DAC holds the computed value during a sampling time by using a second ZOH.

Thus, the only fixed value is the time where the response is held. The other delays are supposed smaller. Therefore, the DAC produces a time delay between the digital signal S_D and the analogical one S_A, whose average equals half the sampling period. The transfer function of this ZOH is approximated by using a first order Padé approximation.

$$S_A = \frac{1-e^{-T_S s}}{T_S s} S_D \approx \frac{1}{1+\frac{T_S}{2}s} S_D \qquad \textbf{3. 7}$$

As shown in Figure 3. 3, for a sampling frequency of 20kHz, the transfer function is correctly approximate up to 1kHz.

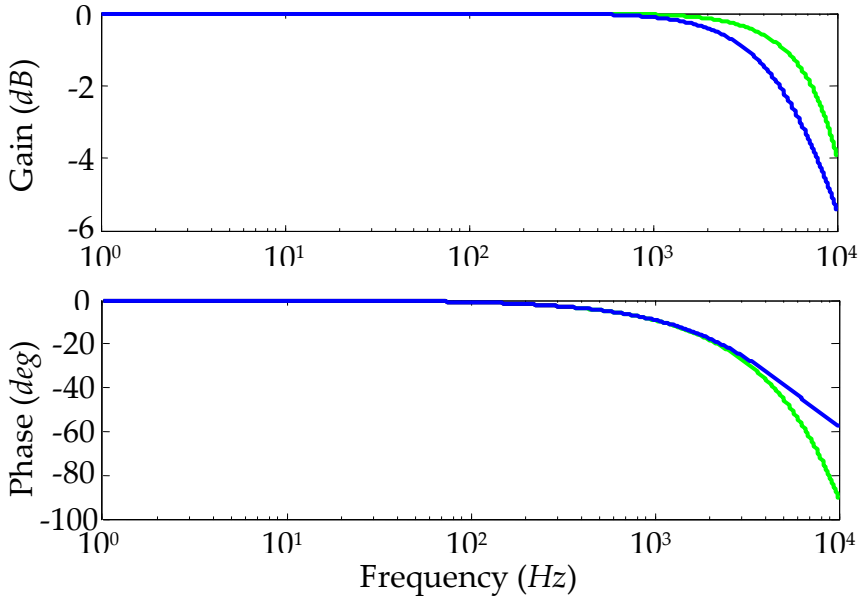

Figure 3. 3: ZOH in black and its approximation in blue (20kHz)

The sampling period must be at least twice the cut-off frequency of the antialiasing filter as depicted by the Shannon theorem. In addition, a low sampling frequency induces a higher time delay (ZOH). Thus, the sampling frequency must be as high as possible, and is limited only by the quality of the ADC and the DAC and the computation time of the DSP.

Electromagnets

The electromagnets are the basis of AMBs. They permit the conversion of electrical energy into mechanical energy. First, a simple horseshoe electromagnet is considered and then the active magnetic bearing is introduced.

The different elements of an electromagnet are presented in Figure 3. 4. The stator iron core is made of laminated sheets of mild steel stacked together. Laminated sheets enable the attenuation of eddy currents. Thus, a ring of laminated sheets is placed on the shaft. Generally, non-oriented silicon steel is used, because it offers a practical compromise between relative permeability, magnetic flux at saturation,

magnetic hysteresis, electrical resistivity and cost. Finally, the coils are wound around the iron core.

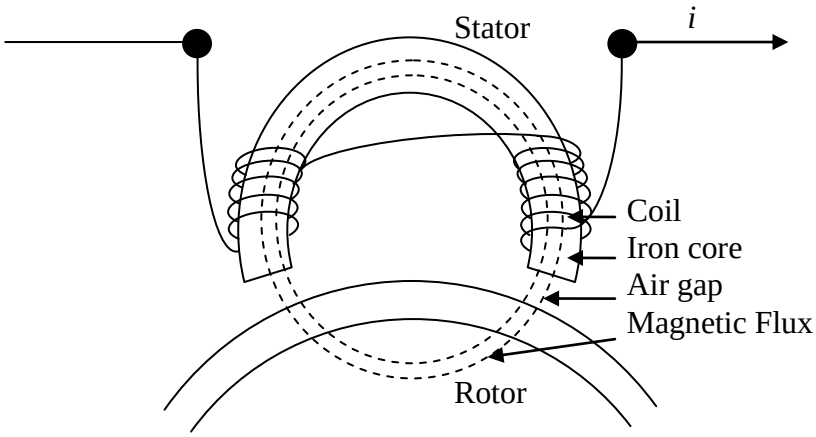

Figure 3. 4: Components of an electromagnet

Several contributions can be found for possible models that relate the current to the force. The models can integrate the leakage fluxes shown in Figure 3. 5. Jufer [1979] presents a reluctance network model that takes into account slot leakages and fringing effects. He validates the electrical behaviour of his model experimentally. Mertens et al. [1996] show the necessity of leakage phenomena modelling. They make use of a reluctance network, besides the Carter factor permits them to establish a model of the fringing effect. Viorel et al. [2007] show the effectiveness of Carter factor representation by a comparison to FEM results.

Based on our studies, for amplifiers controlled with current feedback and for utilizations out of magnetic saturation and dynamic saturation, the model without leakage is sufficient. Thus, a model without magnetic leakage is used in the following.

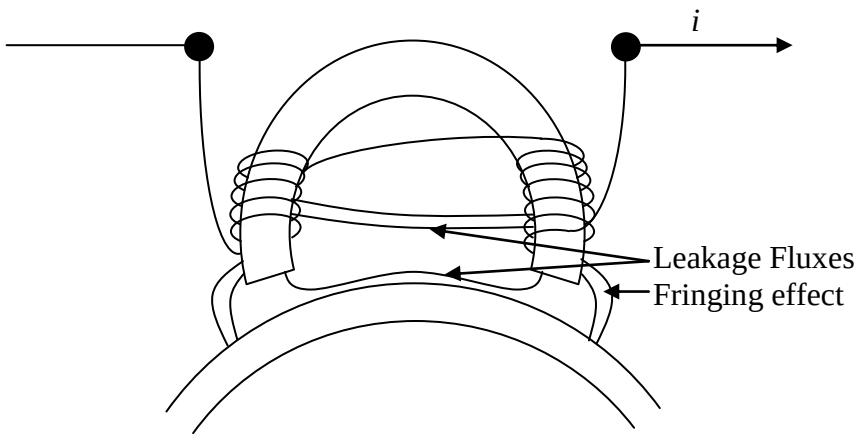

Figure 3. 5: Magnetic leakages

The force applied is calculated with the reluctance network model described by Figure 3. 6. The hypotheses are:

- The magnetic induction is uniform in each section orthogonal to the lines of flux,
- The length of the lines of flux is defined by a middle path, and
- The lines of flux have angles that follow the iron core.

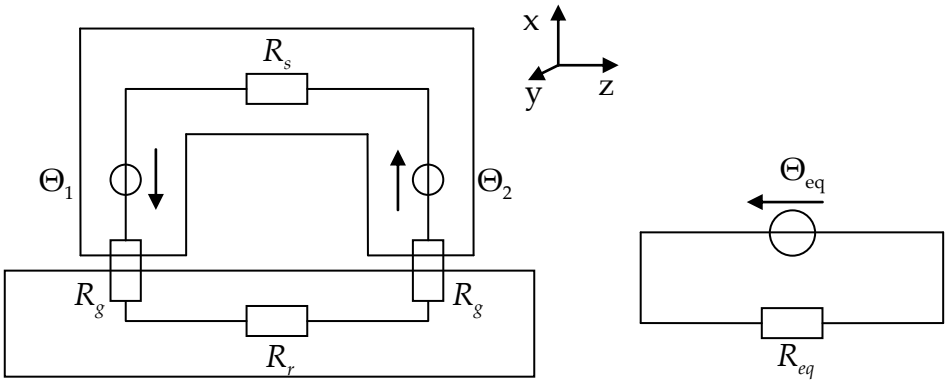

Figure 3. 6: Magnetic circuit

The equivalent circuit is shown in Figure 3. 6. The equivalent magnetic scalar potential is:

$$\Theta_{eq} = 2Ni \qquad \textbf{3. 8}$$

The equivalent reluctance equals:

$$R_{eq} = R_S + R_R + 2R_g = \frac{\frac{L_S + L_R}{\mu_r} + 2g}{\mu_0 S} \qquad \textbf{3. 9}$$

With:

- L_s the average length of the magnetic flux line in the stator,
- L_r the average length of the magnetic flux line in the rotor, and
- μ_r the relative magnetic permeability of steel.

Thus, the magnetic induction is:

$$B = \frac{\Theta_{eq}}{SR_{eq}} \qquad \textbf{3. 10}$$

The Maxwell stress tensor is used to calculate the force applied. The two main air gap surfaces are considered plane and parallel. In addition, the lines of flux are considered perpendicular to the pole surface. Therefore, the magnetizing field in the air gap equals:

$$H = \begin{pmatrix} \frac{\Theta_{eq}}{\mu_0 S R_{eq}} \\ 0 \\ 0 \end{pmatrix} \qquad \textbf{3. 11}$$

Then, the stress tensor is:

$$T = \begin{bmatrix} \frac{1}{2}\mu_0 H_x^2 & 0 & 0 \\ 0 & -\frac{1}{2}\mu_0 H_x^2 & 0 \\ 0 & 0 & -\frac{1}{2}\mu_0 H_x^2 \end{bmatrix} \qquad \textbf{3. 12}$$

Therefore, the force applied by the two poles to the rotor equals:

$$F = 2T_{xx}S \qquad \textbf{3. 13}$$

which can be rewritten as:

$$F = \frac{4\mu_0 S N^2 i^2}{\left(\frac{L_S + L_R}{\mu_r} + 2g\right)^2} \qquad \textbf{3. 14}$$

Hereafter, a complete bearing is considered. The bearing is supposed to be controlled in differential driving mode. This means that each action line is controlled with a constant bias current and a control current, which are added in one electromagnet and subtracted in the opposite electromagnet as shown in Figure 3. 7. Thus, the force applied by the two electromagnets of the x action line is:

$$F = 4\cos(\alpha)\mu_0 S N^2 \left[\frac{\left(I_0 - i_c\right)^2}{\left(\frac{L_S + L_R}{\mu_r} + 2g_0 - 2x\cos(\alpha)\right)^2} - \frac{\left(I_0 + i_c\right)^2}{\left(\frac{L_S + L_R}{\mu_r} + 2g_0 + 2x\cos(\alpha)\right)^2} \right] \qquad \textbf{3. 15}$$

Where α is the angle between the action line and the line linking the rotor centre to the pole centre. Of course, this equation is only valid for eight pole heteropolar bearings in the configuration (NS-SN-NS-SN), and should be adjusted for other types of bearings.

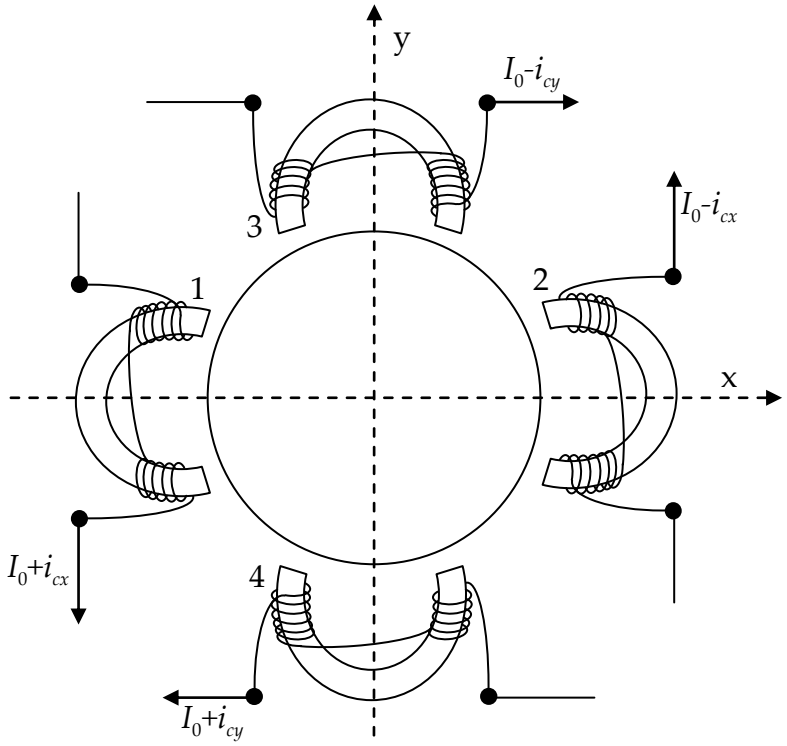

Figure 3. 7: Arrangement of the electromagnets

For nominal behaviour, the expression can be linearized using first order Taylor series. For horizontal rotor, the static control current I_W used to levitate the rotor has to be taken into account. Thus, the current stiffness is:

$$K_i = \left.\frac{\partial F}{\partial i_c}\right|_{i_c=I_W;x=0} = -\frac{16\cos(\alpha)\mu_0 SN^2}{\left(\frac{L_S+L_R}{\mu_r}+2g_0\right)^2} I_0 \qquad \textbf{3. 16}$$

And, the negative stiffness (written as a mechanical stiffness) equals:

$$K_x = -\left.\frac{\partial F}{\partial x}\right|_{i_c=I_W;x=0} = -\frac{32\cos^2(\alpha)\mu_0 SN^2}{\left(\frac{L_S+L_R}{\mu_r}+2g_0\right)^3}\left(I_0^2+I_W^2\right) \qquad \textbf{3. 17}$$

Finally,

$$F = K_i i_c - K_x x \qquad \textbf{3. 18}$$

As long as the displacements and the forces are within the nominal behaviour limits, the linearized model is sufficient to represent the actuator behaviour.

Amplifiers

The amplifier permits the control of the electromagnet. The electromagnet can be controlled either by the feedforward command provided by the controller, or with a feedback control of one of these three physical quantities: the current, the coil voltage or the magnetic flux. If there is no feedback, the amplifier is simple but not precise because one of the particularities of the electromagnets is that it is a variable electric load (the inductance depends on rotor position). Thus, feedback control is a much better solution. Current feedback is the simplest one but has several disadvantages (non-linearity, negative stiffness…). Flux feedback allows tackling almost all these problems, the bearing becomes linear and the negative stiffness disappears at high frequency as explained by Schweitzer and Maslen [2009]. Siegwart [1992] and Maslen [2000] detail the different controls for electromagnets. Voltage feedback is a middle ground solution between current and flux feedbacks for both the difficulties of design and the obtained performances. Hereafter, only current feedbacks are considered.

In this case, amplifiers are transconductance devices. Linear amplifiers must be avoided because they are inefficient. Switching amplifiers give better results with about 90% efficiency for consumed energy. Switching amplifiers supply two different voltages (sometimes three). Thus, when the maximum voltage is applied, the coil current increases. Respectively, with the minimum voltage the current decreases. Therefore, switching amplifiers enable control of the coil current as described by Figure 3. 8.

There are numerous manners to obtain a switching amplifier (Pulse-Density Modulation, comparison with a triangle signal…). In the case of AMBs, Pulse Width Modulation is often discussed in the literature and regroups several methods. Keith et al. [1990] compare two bang-bang control schemas (sample/hold and hysteresis). In the sample/hold design, at each step time the measure current is subtracted to the request current to define the error signal. If the error is positive then the maximum tension is supplied, otherwise it is the minimum one. The sample/hold design exhibits high harmonic distortion and is insensitive to small signals. On the other hand, hysteresis suffers from short-pulse susceptibility, because the switching period is not explicitly defined. With hysteresis design, each time the error achieves the

maximum allowed the amplifier changes its state. Finally, they present a convincing Minimum Pulse Modulation schema as a combination of the two previous algorithms. Thus, this schema has low harmonic distortion, no deadband and no susceptibility to short-pulse.

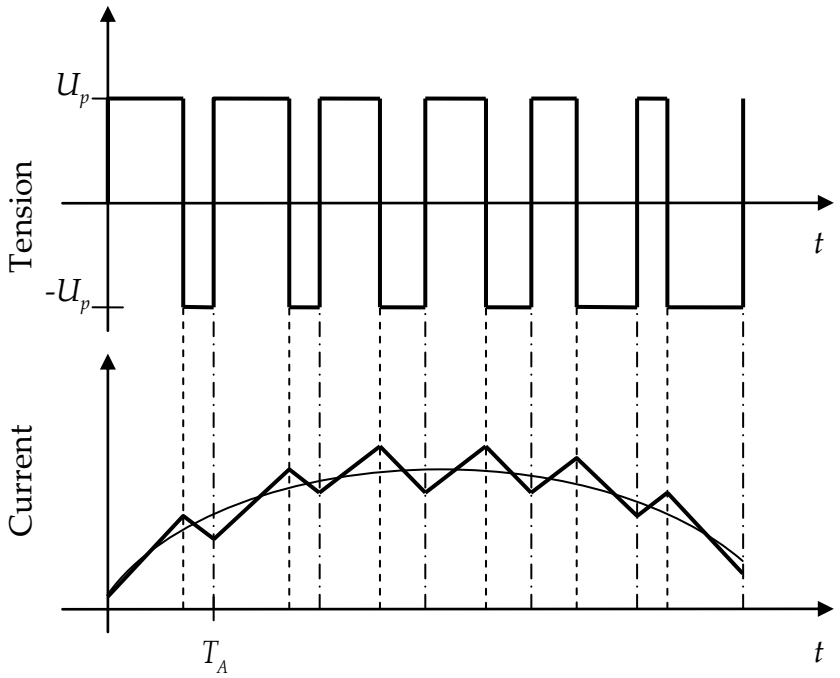

Figure 3. 8: The request current is approximated by the real current (in bold).

The amplifier produces signal distortions. The signal is sampled, thus the Nyquist frequency must be respected and moreover, it is preferable that the switching frequency equals at least four times the maximum frequency included in the signal. Usually, the switching frequency equals at least the digital controller sampling frequency. As for a DAC, the sampling leads to a delay proportional to the sampling frequency. This frequency is not always constant e.g. for hysteresis feedback design. In addition, the current measurement loop can add a transfer function, as the measured current is slightly different from the real one. These distortions are normally small. In addition, they are most of time only known by the amplifier manufacturer. In this work, they are neglected for the compressor and the transfer function supplied by the manufacturer is considered for the test rig.

The main limits imposed by the amplifiers appear when the actuator is considered (i.e. amplifier plus electromagnet). The electrical circuit of the actuator is provided in Figure 3. 9. The maximum supplied current limits the maximum force provided by the bearing. The maximum voltage limits directly the dynamic capabilities of the bearing. In order to assess the maximum capabilities of the actuator, some hypothesis are considered.

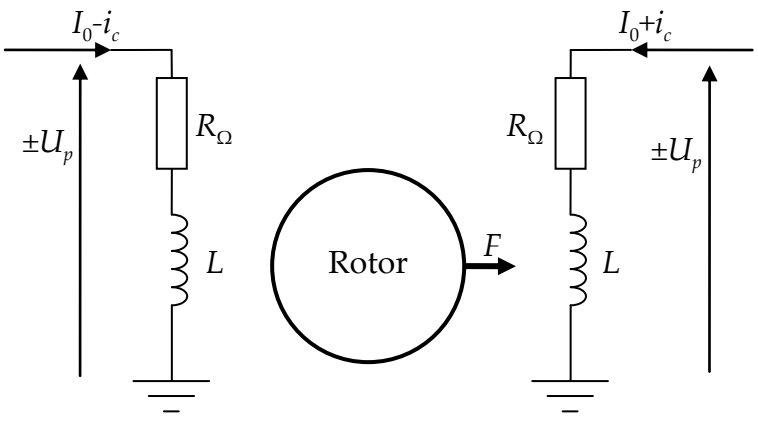

Figure 3. 9: Electrical circuit of the actuators

Supposing an infinite iron relative permeability and a rotor placed at the nominal air gap. Then the force applies by the bearing equals:

$$F = \frac{\mu_0 S N^2}{g_0^2} 4 I_0 i_c \qquad \textbf{3. 19}$$

Thus, the force time derivative is:

$$\frac{dF}{dt} = \frac{\mu_0 S N^2}{g_0^2} 4 I_0 \frac{di_c}{dt} \qquad \textbf{3. 20}$$

The resistance of the coil RΩ can be neglected. And, the inductance of the coil is written as,

$$L = \frac{2\mu_0 S N^2}{g_0} \qquad \textbf{3. 21}$$

Thus, the amplifier voltage is

$$u_A = L \frac{di_c}{dt} \qquad \textbf{3. 22}$$

The amplifier voltage is a binary value and equals $\pm U_p$. Therefore, the combination of the three previous equations leads to the maximum force slew rate:

$$\frac{dF}{dt} \leq \frac{2I_0 U_p}{g_0} \qquad \textbf{3. 23}$$

If the force variation requested is greater than this maximum force slew rate, then the force variation is delayed, and a phase lag appears. Consequently, the damping of the bearing is reduced. Moreover, Maslen et al. [1989] show that this effect is predominant when the current increases. Therefore, this effect generates a dissymmetry, thus the mean current decreases i.e. the bias current, and then the actuator gain (stiffness and damping) is reduced. Bornstein [1991] expresses this limitation as a function of the frequency, if the force can be written as the sum of a constant force and a sinusoidal force:

$$F = F_0 + F_d \sin(\omega t) \qquad \textbf{3. 24}$$

Then, the amplitude of the dynamic force is limited:

$$F_d \leq \frac{2I_0 U_p}{g_0 \omega} \qquad \textbf{3. 25}$$

Consequently, the dynamic capabilities of the actuator depend on the frequency. As for magnetic saturation, this limitation must be considered in the bearing design specifications, but not in the bearing model since the signal is affected with non-linear distortions only if the requested force is beyond the dynamic capability of the actuator.

Cables

For several reasons, the control cabinet can be placed far from the machine. Signal acquisition cards, digital controllers and amplifiers are assembled inside the control cabinet. Then, long electric cables are used in order to connect the bearings. Two type of cable are used. First, power cables (high voltages and heavy currents) are used in order to connect amplifiers to electromagnets. Second, measurement cables (low voltages and low currents) are used in order to connect probes to the sensor card. The problem is that high frequency signals pass through the two types of cables, due to the amplifier commutations for the first one, and the carrier wave for the second one. Thus, physical phenomena can appear and modify the system behaviour.

Elder and Maslen [2008] study the effects of long cables on AMBs. They show that the electrical capacity of the cable implies peak of current after the amplifier switching. They show that, if the feedback of the amplifier is not adapted to capacitive loads, the system could become unstable. They study also the transmission of noise from power cables to sensor cables. They show that this noise can be high, but with a carefully design sensor, there is no relevant problem. Weens [2006] presents analytical models of cables. He validates them with finite element models and experimental results

Measurement cables are made of two insulated conductive copper wires. A magnetic shield is realised with a sheet of aluminium around the two wires. Finally, the whole is covered by an insulator as shown in Figure 3. 10. The model of this cable can be realised with a circuit of inductances L_c, mutual inductance L_K, capacitances C_i and C_s (respectively between the two copper wire and between wire and aluminium) and resistances $R_{\Omega c}$. As the currents are low, the conductances between the conductors can be neglected. This model is sufficient, because the resonance frequency of cables is much higher than the signal frequency. Weens [2006] presents the analytical formula utilized to compute the parameter values of this model.

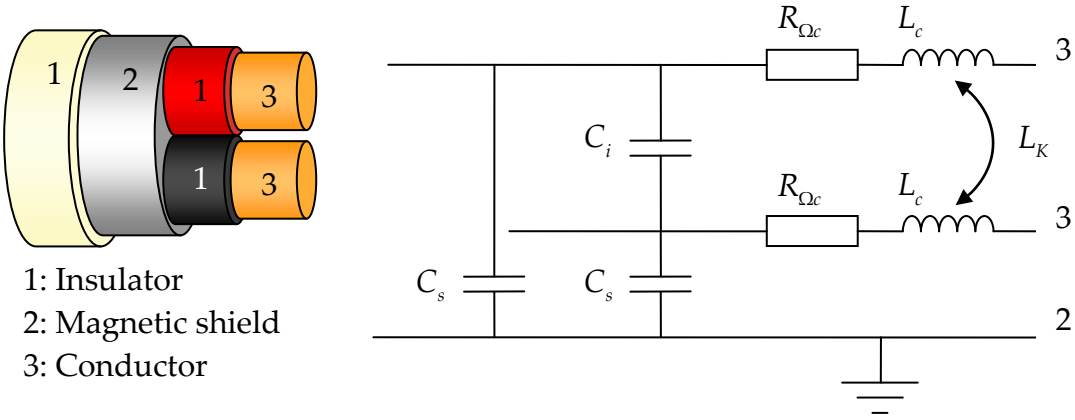

Figure 3. 10: Electrical model of a cable

The model of this cable had been used to show that long cables do not introduce phase lag and keep safe the linearity of the sensors. However, the sensor electronic cards must be design carefully to match the characteristic impedance of the cable and avoid signal reflections. So, cables are not considered in the model.

Rotor

Usually, AMB are studied in frequency domain. However, this method reduces the possibilities for the choice of the control strategy, where only linear (or linearized)

controller can be used. As we intend to develop new control strategies, that could be linear or not, the model of the rotor supported by AMB has been settled in time domain.

Time domain simulations have also the advantage to be close to experimentation. They offer the possibility to reproduce numerically experiments considering transient behaviour. In addition, this approach enables to plan experiments in a reliable and efficient manner. In this study, we choose to perform the numerical simulations under the environment Matlab®/Simulink®. Consequently, the controller is directly implemented on the test rig by using dSpace® tools.

The modelling strategy was chosen to be as flexible as possible. The model of the machine is settled by using "as many as needed" sub-systems. The advantage is to separate the time or speed dependent elements from the linear one as indicated in Figure 3. 11. The sub-systems are built either by using finite elements method or by analytical models or even experimentally identified models. The model is developed for lateral analysis, but could be extended to axial or torsional analysis.

The model of the rotor (shaft with disks) is realised by using Finite Element Method (FEM) with the ROTORINSA® software. The bearings and the gyroscopic matrix are considered as restoring forces and are taken into account in the right hand side of the equation of motion.

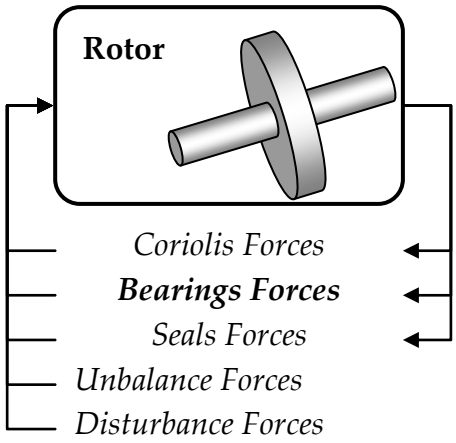

Figure 3. 11: System modelling

Lalanne and Ferraris [1998] detail the method used for rotor modelling. Timoshenko beam elements are used for the shaft. Each element has two nodes and four degrees of freedom per nodes: two displacements and two rotations as shown in Figure 3. 12. Disks are considered rigid. They contribute only to the kinetics energy and are responsible for the gyroscopic effects. In the following, we neglect the effects of the coupling and those due to the acceleration of the rotating speed (Lacroix [1988]). Thus, the dynamic behaviour of the system studied can be described by:

$$M\ddot{\delta} + C\dot{\delta} + K\delta + \Omega G\dot{\delta} = F_{ext} \qquad \textbf{3. 26}$$

With:

- δ the vector containing the degrees of freedom,
- M the mass matrix,
- C the damping matrix,
- K the stiffness matrix,
- G the gyroscopic matrix,
- Ω the rotating speed, and
- F_{ext} the vector of external forces.

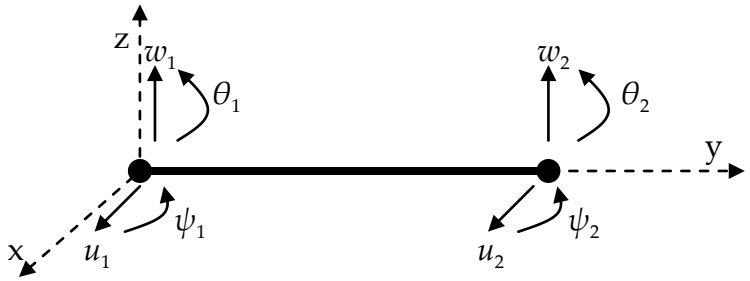

Figure 3. 12: Beam Element

Lacroix [1988] and, Lalanne and Ferraris [1998] discuss the utilization of pseudo modal method. They show that the computation time can be considerably reduced. In addition, this method reduces the number of degrees of freedom without reducing the precision of results. In this study, the pseudo modal method is used. It enables the system size reduction and the utilisation of uncoupled equations. Only the first modes are kept. The number of modes kept has to take into account modes with a relevant contribution relatively to the mechanical energy and the ones in the bandwidth of the controller.

Lalanne et al. [1983] and Ewins [2000] detail the pseudo modal method. In the first step, the system equations are rewritten in the modal space by diagonalizing the matrix $M^{-1}K$. Consequently, the natural frequencies (eigenvalues) and the mode shapes (eigenvectors) are obtained. The rotor was considered suspended by soft stiffness in order to avoid matrix singularity problem. These fictive stiffness are then removed in the modal space. The reduced modal matrixes are obtained by using Ψ, the reduced matrix of system mode shapes.

$$\begin{cases} M_\Psi = \Psi^t M \Psi \\ K_\Psi = \Psi^t K \Psi \\ G_\Psi = \Psi^t G \Psi \end{cases} \qquad \textbf{3. 27}$$

Then, a modal damping is introduced by using a damping factor α_C, which equals to 0.005, as usual for steel structure, which corresponds to an amplification factor of 100.

$$C_\Psi = 2\alpha_C \sqrt{M_\Psi K_\Psi} \qquad \textbf{3. 28}$$

System equations are written in modal space by using q the vector of modal states.

$$M_\Psi \ddot{q} + C_\Psi \dot{q} + K_\Psi q = -\Omega G_\Psi \dot{q} + \Psi^t F_{ext} \qquad \textbf{3. 29}$$

The previous equation is rewritten in its state space form (Figure 3. 13). The input vector U describes the forces applied to the system, and the output vector Y describes the displacements and velocities.

$$\begin{cases} \begin{pmatrix} \dot{q} \\ \ddot{q} \end{pmatrix} = \begin{bmatrix} [0] & I \\ -M_\Psi^{-1} K_\Psi & -M_\Psi^{-1} C_\Psi \end{bmatrix} \begin{pmatrix} q \\ \dot{q} \end{pmatrix} + \begin{bmatrix} [0] \\ M_\Psi^{-1} \end{bmatrix} \left(-\Omega G_\Psi \dot{q} + \Psi^t F_{ext} \right) \\ Y = \begin{pmatrix} q \\ \dot{q} \end{pmatrix} \end{cases} \qquad \textbf{3. 30}$$

X is the state vector constituted of modal displacements and velocities. A is the matrix of the dynamic of the system. B is the input matrix. C is the output matrix. Finally, D is the feedforward matrix, which is null in this study.

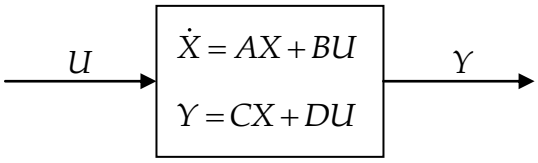

Figure 3. 13: State space equation of the free-free rotor

This sub-model, representing the rotor, is assembled with the other sub-models (sensors, actuators, seals) to constitute the final model of the system.

Conclusions

The equations of motion are expressed in the state space form. The bearings, the seals and the gyroscopic effects are considered as restoring forces and are taken into account on the right hand side of the equation of motion as detailed in Figure 3. 14.

F_{ext} is the vector of external forces that include disturbance forces $F_{disturbances}$, unbalance forces F_b, and seals forces $F_{\Psi seals}$. The physical displacement δ appears only as an input of the AMB. The model retained for modelling each action line of the bearing is provided in Figure 3. 15.

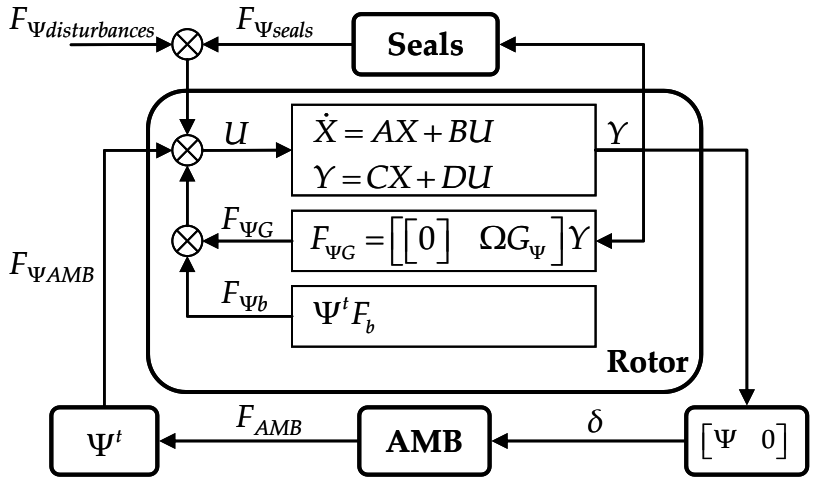

Figure 3. 14: Scheme: Diagram of the numerical model

Finally, a numerical solver is used in order to handle the differential equations in the time domain. Matlab® [2011] proposes several solvers. The Adams-Bashforth-Moulton predictor-corrector method has been chosen. It is a variable step solver that utilizes the solution of several previous steps in order to compute the new solution. Hence, it is not a self-starting method. Usually, Runge-Kutta algorithm is used for the first steps.

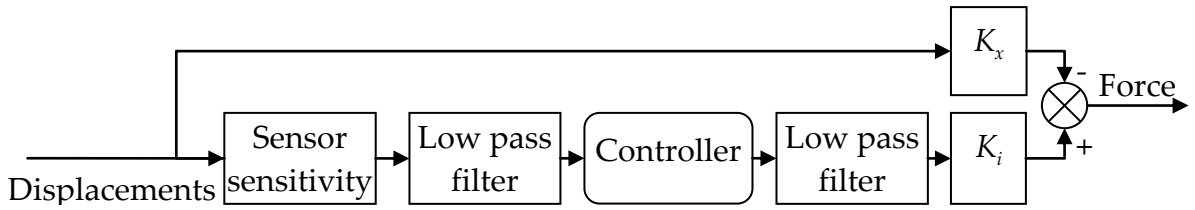

Figure 3. 15: Model of an action line

This modelling approach is flexible and enables to add other subsystems. The settled model represents the main physical phenomena involved in the system studied. Only the control algorithm is still missed. Different control algorithms are developed in the following sections and are implemented successively.

This model has permitted to assess different control strategies. The strategies and the results are discussed in the next chapters.

Chapter 4 – REQUIREMENTS AND LIMITATIONS

The aim of this section is to present the physical limitations of the strategy used nowadays as well as the needs and constraints for the control of turbomachinery vibrations. The system has to satisfy the basic requirements of performance, robustness and stability. The achievement of these requirements shall be measured and evaluated with respect to the standards. Different cases must be considered in order to meet the different operating conditions. This could include the unbalance distribution, the rotating speed or specific disturbances such as the effects of dynamic coefficients of seals for systems such as centrifugal compressors. On the other hand, the specifications of the final users must also be taken into account. It could concern the ease of implementation, the final tuning or the duration of the commissioning.

Industrial requirements are dictated by international standards such as ISO 14839 [2002,2004,2006,2012]. Pugnet [2010] presents the development of the Integrated Compressor Line (ICL) starting from the first European compressor on AMBs. He shows that the requirements of API 617 [2002] can be extended to machinery supported by AMBs. This standard, dedicated to compressors supported by fluid film bearings, is also considered in this study. The first part of the chapter is dedicated to the presentation of these standards.

The designer has to consider basic requirements and physical limitations in order to realize a suitable controller. These elements are discussed in the second part. Finally, the design and tuning of an augmented PID controller is presented in order to illustrate the principle of controller tuning in industry and to point out the limitations that motivate us to develop the new controllers.

Standards specifications

API 617

The main idea is that the unbalance responses enable to determine the acceptable operating speeds range of the machine and are a fundamental test for the compliance of the machine.

The evaluation of critical speeds as well as the mode shapes is a first step in the design process of rotating machinery. The variations of the undamped critical speeds as a function of the bearing stiffness are plot in the undamped critical speed map as presented in Figure 4. 1. Then, the actual characteristics of the bearings are added on this map. Hence, approximate values of the critical speeds are obtained.

The real values of the damped critical speeds are somewhat different and this map is only informative.

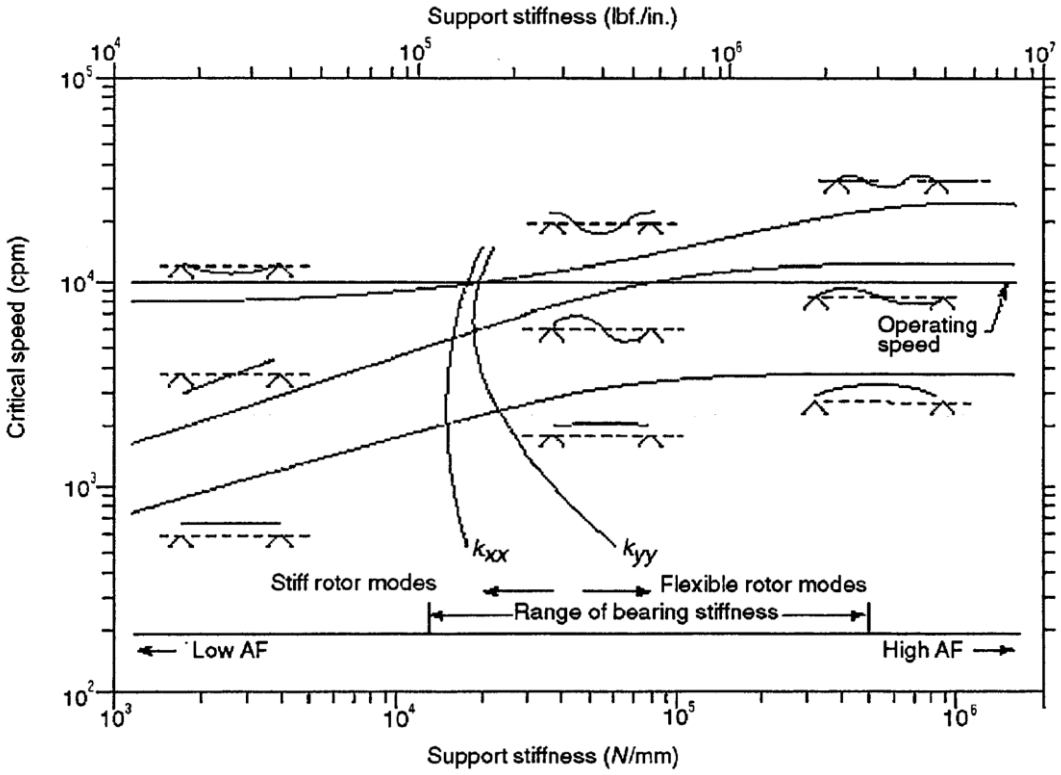

Figure 4. 1: Undamped Critical Speed Map (Figure 1.2-2 of API 617 [2002])

Then, the damped critical speeds are studied with the complete characteristics of the bearings. The amplitude of vibrations, the amplification factor of resonance and the separation margin are determined as described by Figure 4. 2. These studies are carried out for each rotor of the machine separately if flexible coupling are used, otherwise the whole line shafting must be considered.

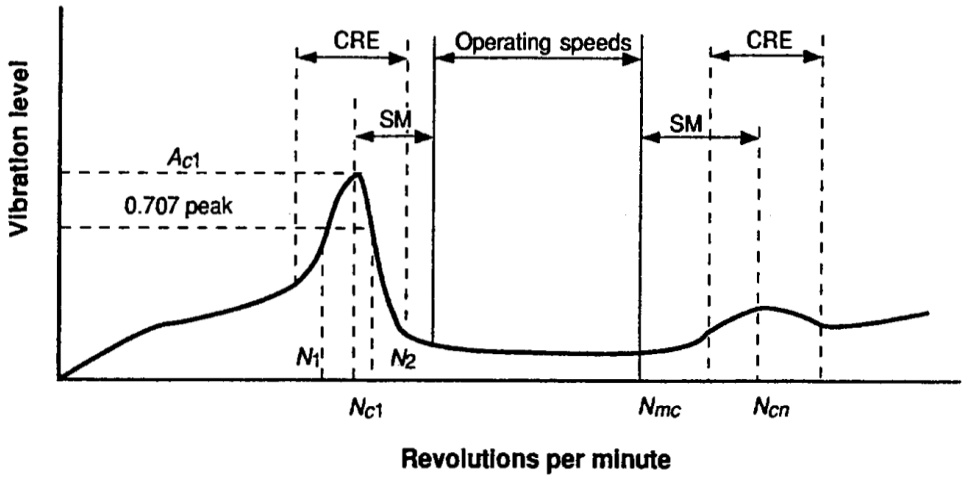

Figure 4. 2: Unbalance response (Figure 1.2-1 of API 617 [2002])

The speed range studied is from 0 to 125% of trip speed (maximum tolerated speed). Several unbalance distributions are studied in order to assess the behaviour of each mode as indicated in Figure 4. 3. The unbalance distributions are determined such that they have the maximum effects on the modes included in the operating speed range. The choice is done as a function of the mode shapes and the position of disks. The unbalance distributions are also specified for rotor with a significant overhung (see API 617 [2002]).

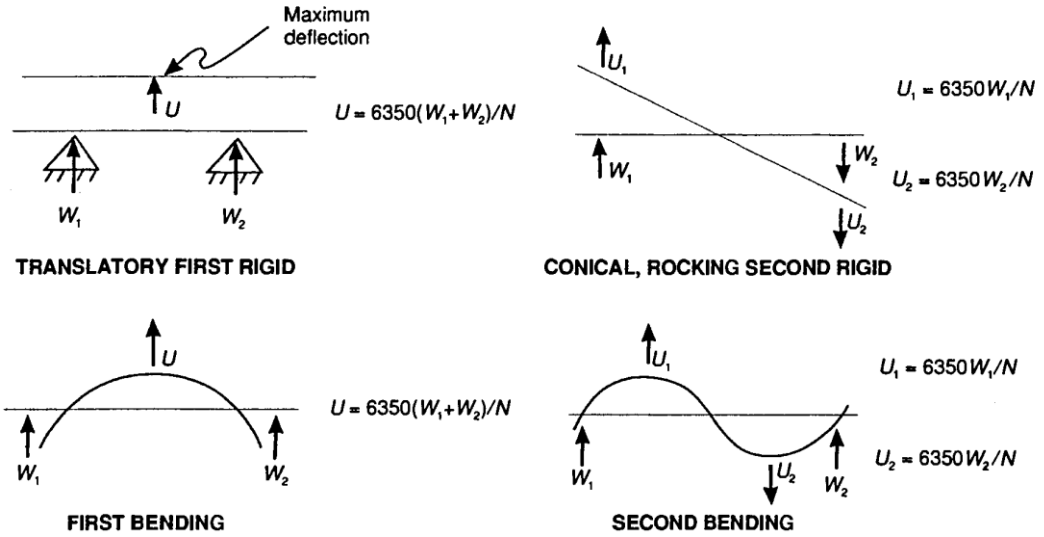

Figure 4. 3: Typical mode shapes and associated testing unbalances (Figure 1.2-3a of API 617 [2002])

The total unbalance uses during computations equals $4U_{API}$, where U_{API} equals (in *g/mm*):

$$U_{API} = \frac{6350m}{N_{MCS}} \qquad \textbf{4. 1}$$

Where:

- m is the mass of the rotor (in *kg*), and
- N_{MCS} is the Maximum operating Continuous Speed (in *rpm*).

Thus, each mode contribution is highlighted by a particular unbalance distribution. Then, an Amplification Factor (AF) and its related Separation Margin (SM) are determined for each mode (see API 617 [2002]).

$$AF = \frac{N_{C1}}{N_2 - N_1} \qquad \textbf{4. 2}$$

If, the AF is less than 2.5 at a particular critical speed, the response is considered critically damped and no separation margin is required. In addition, the critical speed can be included in the operating speed range.

For each unbalance distribution, a Correction Factor (CF) is applied to obtain a maximum peak-peak displacement at the probes location that equals:

$$A = 25\sqrt{\frac{12000}{N_{MCS}}} \qquad \textbf{4. 3}$$

The CF must be greater than 0.5, and the rotor displacement must be checked for each clearance (auxiliary bearing, seals…). At any speed from 0 to 125% of trip speed, the calculated vibrations must be less than 75% of the considered clearances.

These computational results must be verified experimentally. The responses due to test unbalances are assessed as follows. The vibrations are measured for a coastdown with convenient decrement of speed. The synchronous response is measured for residual unbalance and mechanical and electrical run-out. Then, the responses are measured for test unbalances. The data from the two types of response shall be vectorially subtracted in order to access to the contribution of the test unbalances. The numerical model is acceptable if it satisfies the two following conditions:

- The errors are less than 5% for the critical speed values, and
- The amplitudes measured do not exceed the predicted values using the worst computational case (oil temperature…).

In addition, the maximum measured displacement must not exceed the value of equation (4.3).

Finally, an analysis is carried out in order to verify the stability of the first vibration mode, because it is the mode most likely to be unstable. This study is separated into two levels. If the level 1 criteria are not fulfilled then level 2 must be performed. The level 1 uses a simplified model of the system that is more stringent than reality. For the level 2 the models of all components are precisely defined according the worst operating conditions (oil temperature, manufacturing tolerances,…). Then, the log decrement of the first mode is computed and must be greater than 0.1. If after all the design efforts, the log decrement is less, a mutual agreement must be found between vendor and purchaser.

It is clear that some elements are not well adapted to magnetic bearings:

- The limit of vibration amplitude is very restrictive. This value is adapted to AMBs in the annexe 4F of API 617 [2002], which uses the values given by ISO 14839 [2004].

- The AMB characteristics do not depend on operating conditions, thus the error margin on vibration amplitudes is almost nil.
- The stability analysis is not adapted to AMBs, because the level 1 is largely based on field experience with compressors supported by classic bearings.

ISO 14839

ISO 14839 is divided into four parts which describes AMBs, their utilisation and the assessment of a rotor supported by AMBs.

The part 1 of ISO 14839 [2002] defines the vocabulary. For example, three classes of operation are defined for amplifiers. The differential driving mode used in this thesis can be classed A if the bias current equals half the maximum current, or B if less. In all our study, class B was used.

The part 2 of ISO 14839 [2004] considers amplitudes of vibration. The main idea is that a well designed machine should have a minimum clearance at auxiliary bearing locations. In addition, the global vibrations (unbalance plus other excitations) shall not exceed 30% of the auxiliary bearing clearance.

The part 3 of ISO 14839 [2006] deals with system robustness. The stability of a system is its ability to come back to its equilibrium state after an excitation. It is a required condition to operate. However, the robustness is as important, particularly for turbomachinery. The robustness enables to keep the stability over a range of modification of the system. These modifications can be large, even for normal behaviour: gyroscopic effects, seals coefficients… contribute to the characteristics of the system.

The robustness is assessed through the stability margin. The range of frequency studied should be up to the maximum between 2*kHz* and 3 times the MCS.

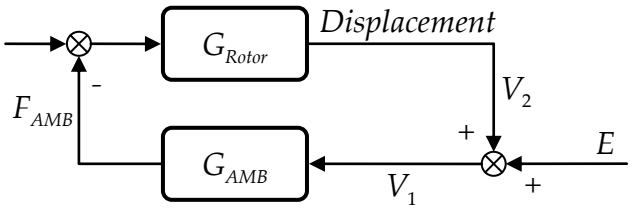

Figure 4. 4: Robustness assessment

The system can be evaluated through the unique diagnostic capabilities offered by AMBs as presented in Figure 4. 4. An excitation signal E permits the measurements of system properties with a simple signal analyser. The open loop transfer function equals:

$$G_O = -\frac{V_2}{V_1} = G_{Rotor} G_{AMB} \qquad \textbf{4. 4}$$

The closed loop transfer function is deduced using Black's formula,

$$G_C = -\frac{V_2}{E} = \frac{G_{Rotor} G_{AMB}}{1 + G_{Rotor} G_{AMB}} \qquad \textbf{4. 5}$$

The closed loop transfer function can be used to evaluate the stability of each mode with an AF. In addition, this transfer function permits the assessment of the effect of the measurement noise (produced by the sensor) on the system. However, the most important transfer function is the sensitivity, which allows the evaluation of the stability margin.

$$G_S = \frac{V_1}{E} = \frac{1}{1 + G_{Rotor} G_{AMB}} \qquad \textbf{4. 6}$$

Usually, the stability margin are defined by the gain margin K_m and the phase margin ϕ_m. The modulus margin is a more stringent criterion because it guarantees a minimum value for the two other criteria as revealed by Figure 4. 5. It can be demonstrated that the modulus margin equals the inverse of the maximum gain M_S of the sensitivity transfer function. Hence, the measurement of sensitivity transfer function enables the assessment of robustness. Consequently, and according to the standard, for new commissioned machine the maximum peak of sensitivity must be less than 3.

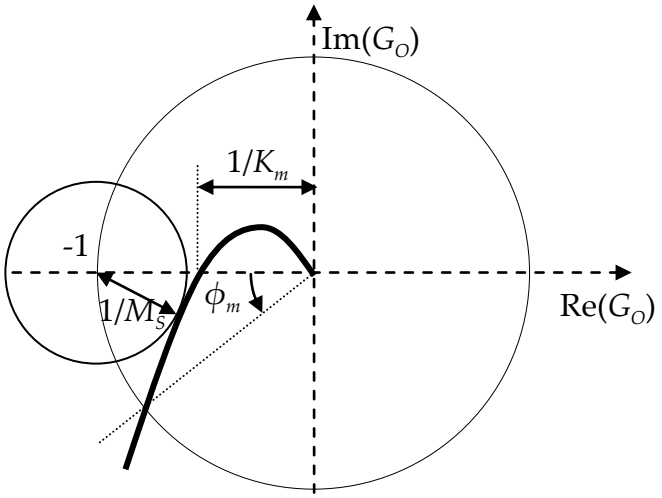

Figure 4. 5: Nyquist plot of the open loop transfer function

This procedure makes it possible to analyze the direct sensitivity functions of the system as if it was composed of uncoupled SISO systems. Nevertheless, a rotor supported by AMBs is a MIMO system. Thus, cross sensitivity functions can be measured, but they are generally useless, and the systematic measurement of the cross sensitivity functions is not required.

The part 4 of ISO 14839 [2012] deals with technical guidelines. This part is focused on the particular characteristics of AMBs. It enables to understand the modifications necessary in order to move on AMB technology. AMBs are compared with other type of bearings. The commissioning and the maintenance of machines equipped with AMBs are discussed.

Conclusions

API 617 should be used to evaluate the system stability and performances through unbalance responses. ISO 14839 should be used to assess the robustness of the system and its vibrations by using the amplitude of displacement. Neither of them is fully adapted to oil and gas compressor supported by AMBs. In this thesis, the following requirements are taken into account:

- The displacement due to unbalance response should satisfy the requirement of API 617 for hydrodynamic bearings (chosen at $25\mu mpp$ for confidentiality reason as this value depends on the rotating speed).
- The amplification factor calculated with the unbalance response should be under 2.5.
- The total displacement should satisfy ISO 14839 ($60\mu mpp$ for the test rig).
- The maximum of the sensitivity function gain should be under 3.

The different displacement limits for the studied compressor are summarized in Figure 4. 6.

API 617 gives practical guidelines for the design of compressor but is not adapted to compressor supported by AMBs. The criteria are too conservative. In addition, the stability analysis is not appropriate. As the level 1 analysis is essentially based on lessons learned from hydrodynamic bearings, it seems that a level 2 analysis is always necessary. All of the modes included in the bandwidth of frequency must be assessed and the level of requirement may be defined and adapted to each of them.

API 617 is convenient for vibration assessment of axial and centrifugal compressors. Indeed, there is a global requirement for the maximum tolerated displacement, but also criteria for displacements resulting from different kind of excitations. Thus, the maximum unfiltered displacement must be less than the value obtained with equation (4.3) or 25µm, whichever is less. Then, the displacement due to unbalance vibration must be less than the value obtained with equation (4.3). Finally, any non-synchronous displacement with a given frequency must have a

displacement less than 20% of the value obtained with equation (4.3) or 6.5µm, whichever is greater. These kind of requirements are missing in ISO 14 839, whereas they would be useful since the lower stiffness of AMBs leads to more non-synchronous vibrations.

ISO 14839 is adapted to AMBs but not to compressor. The requirements are appropriate to experimental assessment but not to numerical one. There is no requirement for the unbalance response, the margins between maximum displacements and machine clearances or the validation of numerical predictions.

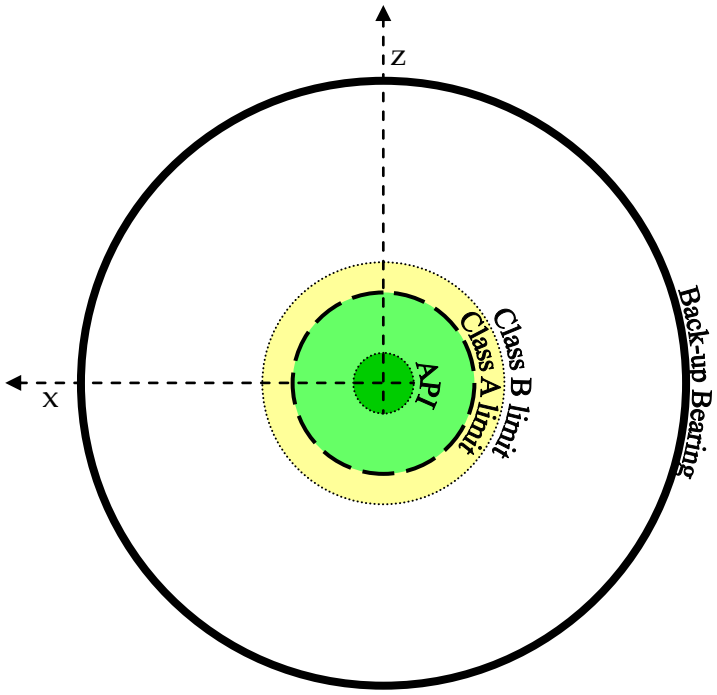

Figure 4. 6: Limits of accepted displacements for the compressor studied

Based on our understanding of the two systems that are centrifugal compressor and AMB, we attempted to highlight the weaknesses and to make some propositions. Neither API 617 nor ISO 14839 takes into account that unlike rotor supported by hydrodynamic bearing the asynchronous vibrations are not negligible relatively to synchronous one for rotor equipped with AMBs. Thus, there is no clear requirement for the amplitude of displacement due to synchronous vibrations. Thus, we think that the assessment of compressor supported by AMBs should be based on API 617 while considering several adjustments.

The unbalance response assessment should be considered without any additional filters (synchronous filters) but the AF limit to consider a mode critically damped should be revised. There are at least four reasons to require a small AF.

- AFs permit a measurement of machine sensitivity to change of unbalance. The unbalance distribution could change due to wear, deposits or corrosion.

Small AFs ensure that the machine response is not sensitive to this kind of modification.

- A small AF enables to observe progressively the apparition of the critical speed vibrations during run up and avoid sudden change in vibration amplitude.
- AF measures the system capacity to dissipate energy.
- Errors on computed damping or modifications of damping have less effect on the response. Considering a same relative error in percent on damping value, the effect is as high as the AF is high.

Nevertheless, an AF of 2.5 seems too low, not because it is not achievable but because it impedes the general optimization of bearing performances e.g in our case the improvement of subsynchronous behaviour is precluded.

- Thus, a value between 2.5 and 3.5 would be more suitable.
- The limit of displacement given by API 617 for unbalance response on classical bearings should be requested only for synchronous displacement with all the filters activated.
- The stability margin should be assessed as required by ISO 14839-3.
- A value should be advised for taking into account internal damping of the rotor in numerical computation in order to assess the severity of resonances. The amplification factor of each mode included in the controller bandwidth should be assessed and a minimum value required with a distinction between modes included in the operating speed range and the other one.

Finally, most of time, the main controller is not sufficient to obtain acceptable unbalance responses. Thus, the specifications are achieved by using general notch filters. Neither of these two standards has a clear position on this topic. There is at least a need of specification considering that these filters affect the sensitivity function.

Basics for controller design

Before considering any design strategy there are a few physical properties that have to be considered. The system must be stable and robust with acceptable performances. The controller must take into account the architecture of the machine, the technical limitations and the physical limitations.

Performances The performances are mainly dictated by the international standards and the final users. The main issue is the reduction of the vibrations. Generally, the performances can be improved by increasing the gain of the controller.

Stability The AMBs are naturally unstable. Two elements permit to stabilize the system. First, the stiffness obtained from controller must at least counteract the negative stiffness of bearings and seals. Second, the controller must increase the damping of all the vibration modes included in its bandwidth of frequencies.

Robustness It is a property of turbomachines to have different characteristics as a function of operating conditions. The natural frequencies depend upon rotational speed (gyroscopic effects) and industrial process (seals dynamic coefficients)… The controller must be adapted to an infinity of systems, due to operating conditions and the unavoidable uncertainties of these conditions. The robustness is obtained by a limited gain of the controller and a limited controller bandwidth of frequency, i.e.: the controller gain tends to zero at high frequencies.

System architecture

In most AMBs systems, the position sensors cannot be collocated with the actuators. The main hindrance of non-collocation is the fact that there is always at least one vibration node between sensor and actuator as shown in Figure 4. 7. Thus, the force applied must be 180° out of phase with the signal provided by the sensor.

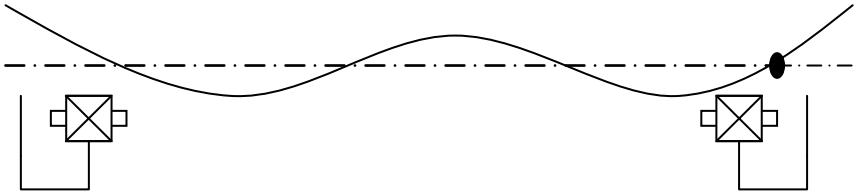

Figure 4. 7: Non-collocation issue

Several studies have shown that a self-sensing bearing is possible e.g. Schweitzer and Maslen [2009]. Nevertheless, there are still some limitations, for example, the measured displacement is less precise (or more affected by noise) and the magnetic saturation must be avoided. Thus, the force capabilities of bearing are reduced.

Either for a collocated or non-collocated system, the position of sensors and actuators must be appropriately considered. The vibration nodes of the free-free modes included in the operating speed range should be as far as possible from the sensors and the actuators, and these nodes should never be between a sensor and its related actuator. On the other hand, for higher frequency modes a node between sensor and actuator leads to an easier tuning of the controller.

Technical limitations

The energy of control forces is physically limited. This property is represented by a low pass filter, which limits the bandwidth of actuators. Moreover, the sampling frequency limits the bandwidth of numerical controllers. An analog low pass filter is used, with a cut-off frequency below the Nyquist frequency, to avoid spectral aliasing.

The DAC introduces a delay (or phase lag) proportional to the sampling time. Consequently, the damping of the bearing is attenuated. Thus, the sampling frequency must be as high as possible (usually between 10-20kHz). However, the DSP must be able to compute the response of the controller between two samplings. Therefore, the controller algorithm should be adapted to real time computation.

The limits of the bearing dynamic capabilities can be reached (see amplifiers in Chapter 3). In this case, the control is sometimes impossible. This event arrives particularly for high rotational speeds, when a flexible mode is crossed. The unbalance control forces lead to amplifier saturation.
Considering a bearing designed with a classical approach (geometry and materials), the other technical limitations are almost negligible and verification tests at the end of the design process are normally sufficient.

The Bode's theorem

According Bode's definition (1945), minimum-phase systems have all their poles and zeros in the left half s-plane. For these systems, there is a direct relationship between the phase and the gain i.e. the phase can be completely determined from the gain curve. This relation can be summed up by the fact that the phase is almost proportional to the slope of the gain curve in the Bode diagram.

In most AMB systems, the controller is a minimum-phase system, because this induces a minimum delay between measurement and action. Then, the system is easier to control. Thus, in order to obtain damping the gain of controller must necessarily increase (versus frequency) and reciprocally, a reduction of gain implies a negative damping for a given frequency range.

Augmented PID controller

The general architecture of the system is presented in Figure 4. 8. The augmented PID or hand-synthesis controller is still the more widespread controller in industry. It permits designers to master the control process. However, the control of flexible

rotors remains difficult due to unavoidable spillover effects. This problem is currently overcome by using phase lag and phase lead filters. Tuning these controllers is difficult and time consuming. Gähler [1998] explains the general approach to design the controller of a flexible rotor.

In this section, we have attempted to summarize the process for augmented PID synthesis. First, the assumptions are detailed. Then, the process is depicted and finally the limitations are highlighted. It was considered as the starting point for the strategy developed

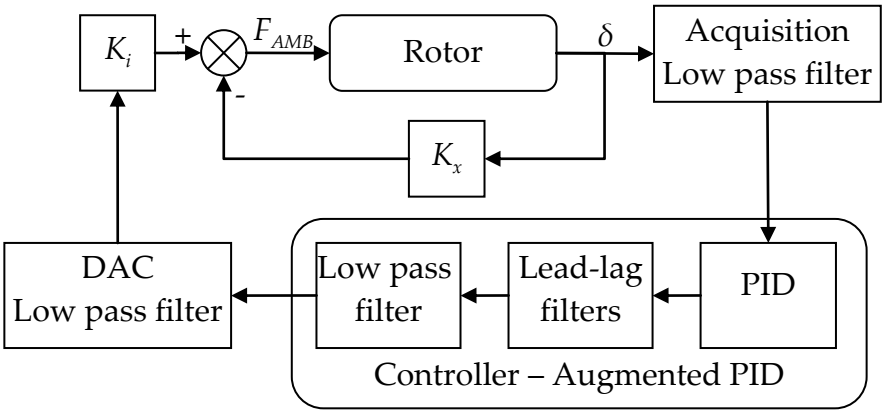

Figure 4. 8: Detail of the feedback loop transfer functions

Basics of PID

A physical PID controller is strictly proper. It is composed of three parts that can be written:

$$G(s) = \frac{K_P}{1+\tau_1 s} + \frac{K_I}{s} + \frac{sK_D}{(1+\tau_2 s)(1+\tau_3 s)} \qquad \textbf{4. 7}$$

The proportional gain K_P is equivalent to the stiffness. It permits to maintain the rotor. If this parameter were high, then the disturbances would need more energy in order to produce large vibrations.

The integral gain K_I enables to keep the rotor centred in the bearing. This function is exclusive to AMBs and, is necessary because the lower stiffness of AMBs typically allows higher displacements. Thus, there is always an optimum clearance between rotor and stator, which avoids rotor-stator contact. In addition, for heavy industrial rotor, considering only the bearing stiffness the deflection due to the rotor weight would be almost equal to auxiliary bearing clearance. If this parameter were increased, the rotor would go faster to its centred position, but also with more kinetic energy. Thus, a high integrator gain leads to a loss of stability.

The derivative gain K_D permits to bring damping to the system. With this element, the bearing dissipates the vibration energy of the system. High damping is necessary to dissipate quickly the energy.

Finally, proportional and derivative terms are not strictly proper alone and consequently cannot be realize in a real physical system. Thus, they are always associated with a low pass filter. Consequently, theirs effects are limited to a defined frequency range.

Usually, an "augmented decentralized SISO PID controller" is used. First, the vocabulary used must be clarified. The PID controller is very common and applies in a wide range of industrial applications. It is composed of three elements Proportional Integral and Derivative that respectively enable a quick response with a nil error on the setting value and stable operation.

SISO or Single Input Single Output is relative to the arrangement where each controller makes use of only one sensor displacement in order to compute the force applied by one actuator. As a complete AMB system possesses five actuators, five independent controllers are need. This is opposed to a MIMO (Multiple Inputs Multiple Outputs) system where several sensors are used in order to compute the force applied by several actuators.

A decentralized controller assumes that there are multiple independent controllers, which do not share information when making control decisions. Decentralized control is more efficient with decentralized structures i.e. when the structure can be decomposed in subsystems.

The PID alone is too poor to control a complex system such as a structure with a high modal density. Thus, several filters are added to obtain the desired behaviour. These filters are mainly first order lead or lag filters or second order lead-lag filters. These filters permit to master the phase of the controller, which is very important as explained in the next sections. In this case, the controller is named augmented PID.

PID synthesis

Remark: in this section, for more simplicity the phase and the gain of the controller are confused with the ones of the action line transfer function (sensor, controller, actuator,…). In reality, it is this second one that should be considered

Considering a classic bearing (ball, fluid film…) the characteristics of damping C and stiffness K can be computed from several parameters which can be tuned (oil viscosity…). Thus, the global action of the bearing can be written:

$$F = -Kx - C\dot{x} \qquad \textbf{4. 8}$$

This force can be written in the Laplace domain:

$$F(\omega) = -\left[K(\omega) + j\omega C(\omega)\right]X \qquad \textbf{4. 9}$$

The bearing characteristics are a transfer function with displacement as input. These properties can be either frequency dependent as for AMBs or speed dependent as for lubricated bearings or even both.

Stiffness and damping are not explicitly chosen during controller synthesis. In Figure 4. 9, the relation between the stiffness and damping and imaginary and real parts of controller transfer function are shown. Moreover, the relation to controller gain and phase are shown. It is more convenient to design a transfer function with gain and phase than with damping and stiffness. Thus, considering the design process, it can be noted that for a given gain the phase determines completely the proportion of damping and stiffness. Consequently, the requirements regarding the phase are much more important than those on amplitude:

- A phase nil imply a pure stiffness,
- A phase of 90° imply a pure damping,
- A phase from 90° to 360° imply negative damping or stiffness or both, and
- A phase from 0° to 90° is suitable for bearings and ensures stiffness and damping.

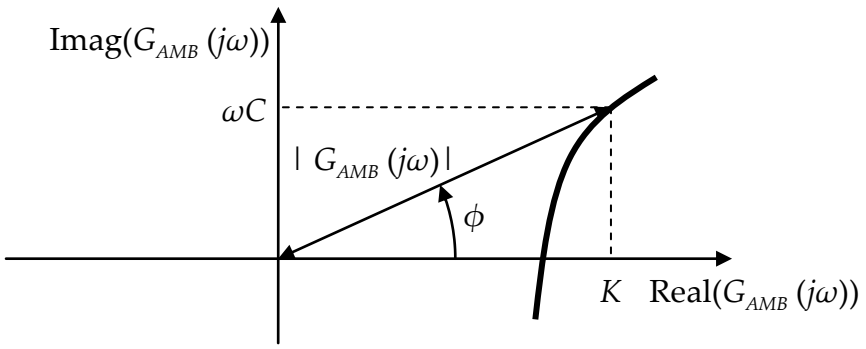

Figure 4. 9: Relation between transfer function and stiffness and damping

Notice that for the configuration with a node between sensor and actuator the controller must have a phase between 180° and 360° for the vibration mode considered to ensure at least damping. Since, it is related to high frequency modes with a high structural stiffness.

Nevertheless, the stiffness that enables an acceptable behaviour can be determined at the first stage of the controller design process as indicated in Figure 4. 10. Schweitzer and Maslen [2009] explain that stiffness value must be chosen in the range where the variation of the stiffness leads to a significant change for the critical speed included

in the operating speed range. The final effective stiffness is chosen in this range since this value enables significant action on the system strain energy and damping. Higher stiffness would produce vibration modes with nodes close from the bearing location. Consequently, the vibrations would be not observable and then not controllable.

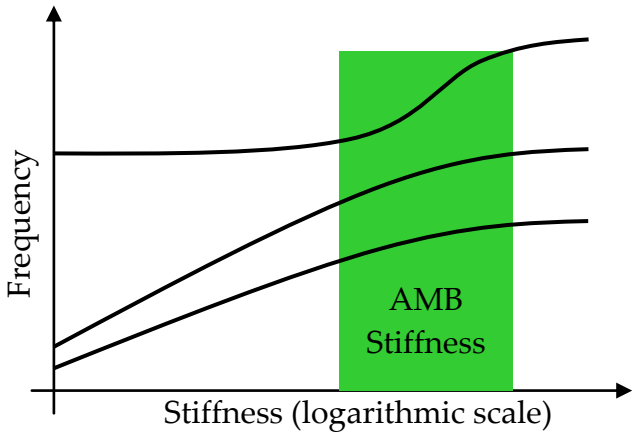

Figure 4. 10: Critical Speed Map

Once the proportional gain of the PID is tuned, the other part can be chosen. On the operating speed range, the controller must generated damping. The damping gain is increased until the phase of the controller is near to 90° for the modes included in the operating speed range. At very low frequencies, the integral gain leads to negative phase, but as there is no vibration modes this negative damping is not important. Generally, the integral gain is increased until instability appears then it is reduced according to a correction factor. The instability is due to the negative damping that grows until achieve the frequency of the first rigid body mode.

This controller could be sufficient for a rigid rotor, but in order to ensure robustness the increase of gain due to derivative part must be limited. A low positive phase enables to obtain damping and to avoid high gain at high frequency. Thus, the phase on the operating speed range is reduced by using a first order lag filter applied on the range of the natural frequencies included in it (typically 50-150Hz).

If the damping induced is not sufficient to reach unbalance response specifications, a second order lead-lag compensator can be used to add damping on a narrow range of frequency e.g. to pass through a flexible critical speed.

The high frequency mode should be either controlled with damping or not influenced. Thus, a low pass filter is used to cut-off the controller gain. This produces a negative damping for a given range of frequency.

Only filters with complex poles enable a modification of the phase on a narrow range of frequency. However, this property is linked to a Q-factor. In Figure

4. 11 the relation between phase lag and Q-factor is presented for a second order filter. The phase transition is as fast as the Q-factor is high.

When using a low pass filter, a phase rotation greater than 180° is necessary between two consecutive modes in order to ensure the system stability (high frequency modes needs only damping since the structural stiffness is high). The modes are relatively close, thus an important Q-factor is unavoidable. Obviously, this high gain, even local, reduces the system robustness. Therefore, the phase rotation must be displayed on the wider band of frequencies possible.

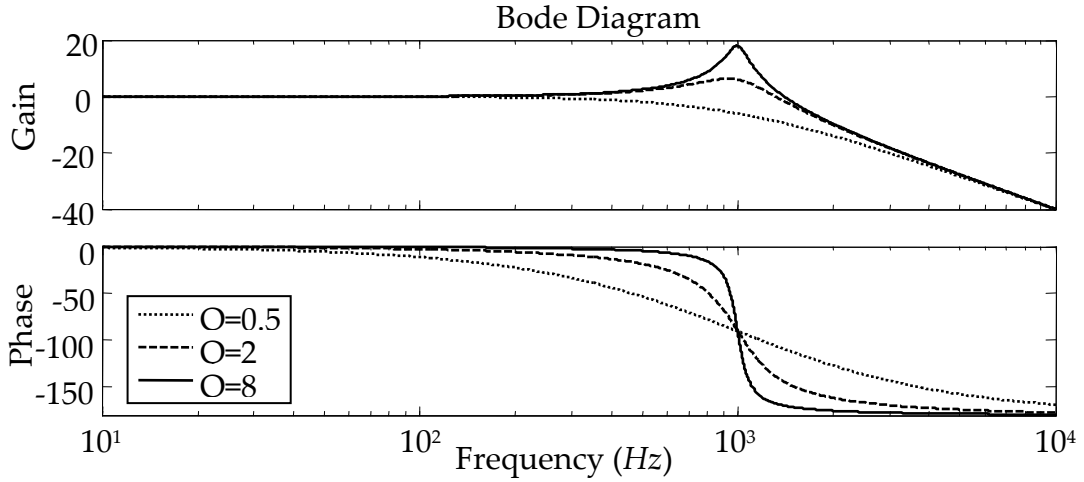

Figure 4. 11: Relation between Q-factor and phase transition

If a mode has a node between sensor and actuator, it is easier to make rotate the phase from positive values to values below -180°. Generally, the rotation must be realized for the lowest frequency, because the vibration modes are closer when the frequency increases (in the useful logarithmic scale).

The Campbell diagram enables to forecast the natural frequencies of the system, not only at rest but also for the complete range of rotational speeds used. A security margin on the computed frequencies can also be taken into account in order to anticipate modelling errors.

Previously, the requirements on the phase value for the system resonant frequencies have been detailed. By using both (Campbell diagram and phase requirements), it is possible to define a path of phase in the AMB Bode diagram (controller plus sensor and actuator). An example of this path is presented in Figure 4. 12. The dark green zones should be crossed from left to right sides. The light green zones are suitable for the mode stability but could be unsatisfying considering the whole system stability. For example, the zone inside the operating speed range induces a high frequency gain too high in order to obtain a robust controller.

It is worth mentioning that there is not always a mode with a node between sensor and actuator in the controller bandwidth of frequency. In this case, the design

is more difficult and often a structural damping must be introduced in the model in order to find a solution. The controller could slightly disturb one or two successive modes without destabilizing them.

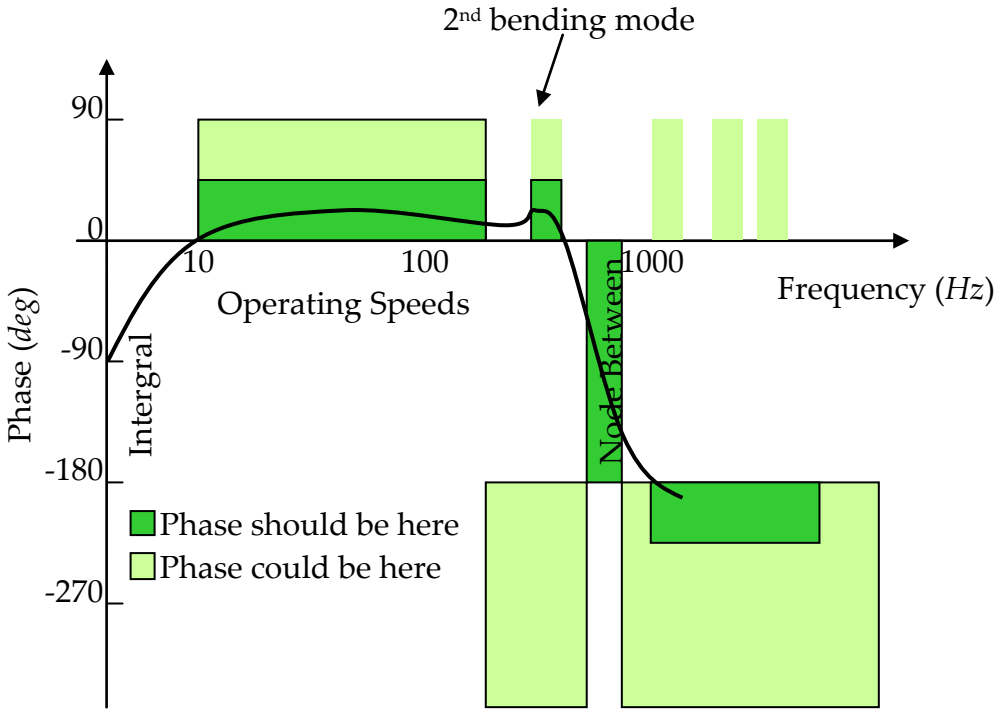

Figure 4. 12: Controller phase

Summary

The objectives of performance, stability and robustness are often conflicting, and the designer has the responsibility to manage each of them to reach the suitable trade-off.

Robustness and performance are directly opposed (performances imply a high gain and robustness a low one). A high stiffness at low frequencies permits to obtain good performances (low vibrations). The rotor is constrained then large forces are necessary to make vibrate it.

A low gain at high frequencies enables to have small effects on high frequencies modes and to ensure system robustness. Moreover, on the frequency bandwidth of the controller, it is preferable to have a moderate gain for modes out of the operating speed range. Even if it is not the target, the controller provides mainly stiffness on these modes. The maximum gain must be low enough to avoid effects on frequency of flexible modes. Indeed, the flexible modes included in the controller frequency range but out of the operating speed range must be stabilized. This can be realized only with damping on a narrow range of frequency. If the gain of controller is high, the strain energy introduced by the bearing modifies the mode frequency. Thus, it becomes very difficult to find a solution to the control problem.

The stability of the rotor on the operating speed range requires a high damping. Hence, according to the Bode's theorem, the stability implies a high increase of gain on this range of frequencies.

Consequently, the ideal controller should have a high gain at low frequency for performances, an increase of gain from low frequency to high frequency for stability and finally a low gain at high frequency for robustness. As this controller does not exist, the real controller must be designed carefully.

The gain at low frequency must be the smallest that compensates the negative stiffness and stabilizes the rigid body modes with an acceptable level of performance. The damping must be applied appropriately, only where it is necessary to ensure damping on each mode i.e. on narrow ranges of frequencies. Thus, the controller gain is not too high in high frequencies, and a good robustness is obtained. Finally, the gain must be cut-off while avoiding undesirable high Q-factor.

For a rotor supported by AMBs, the general gain of the controller can be used to tune the controller as shown in Figure 4. 13. This figure is extracted from the study of compressors (Chapter 8). When this gain becomes small, the bearing stiffness is not sufficient to compensate the bearing negative stiffness and the maximum peak of the sensitivity function increase to indicate a lack of robustness. When the controller gain increases the system performance are improved, but when the gain is too high, the system changes (the natural frequency are different). Thus, the controller is no longer suitable and the maximum peak of sensitivity increases. Consequently, there is a specific gain that optimizes the robustness of the system. As this gain is rarely sufficient from a performance point of view, the gain is increased until the sensitivity reaches the limit value required by international standards.

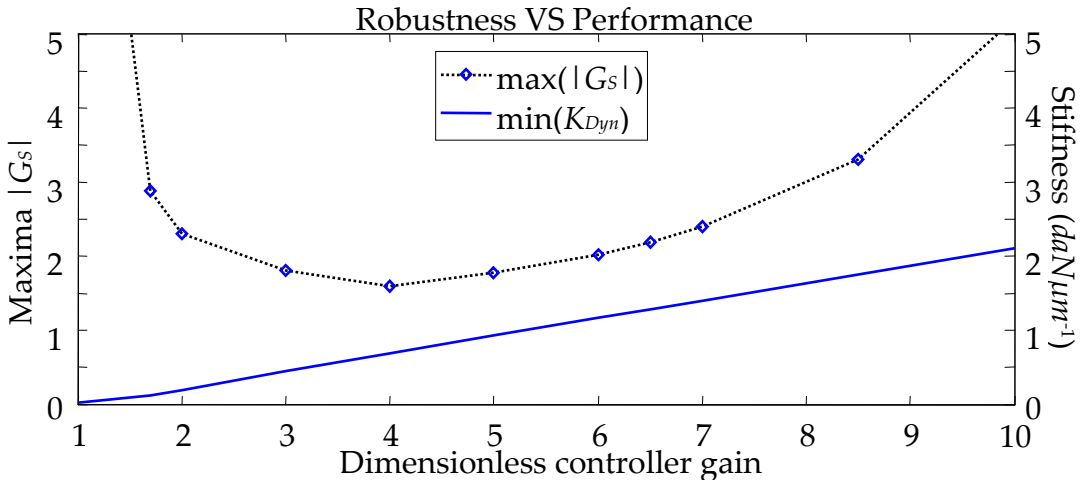

Figure 4. 13: Trade-off between robustness and performance

Finally, the difficulties to cut-off the controller gain at high frequencies influence directly the performances of the controller. Indeed, if the gain can be cut-off only

with a high Q-factor, the gain of the controller should be reduced according to the robustness requirements and consequently poor performances are expected. The issues of the gain curve are summarized in Figure 4. 14.

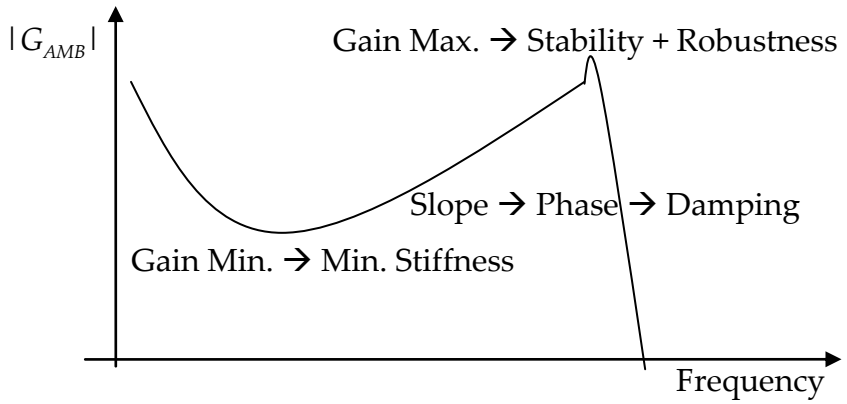

Figure 4. 14: Impact of the gain evolution on the system

Conclusions

The study of PID controllers enabled to emphasize the advantages and disadvantages of this control strategy. The three main advantages are first the power of the tools used for the analysis (common to all linear SISO controllers). Second, the controller is easily implemented in a simple DSP. Finally, the frequency domain permits to tune the stiffness and the damping for each vibration modes.

The disadvantages are first the influence of high frequency characteristics of the rotor on the performances of the controller. Second, the stiffness on the cylindrical mode seems low relative to the specifications. Finally, the damping of flexible modes is low compare to what might be expected of an active system.

The design of the controller could be enhanced by using a systematic approach. However, the performances issue would be not solved. We see four solutions in order to tackle these problems.

MIMO control: by using several sensors and actuators in the same way, improvements are expected. The more promising is modal control, but it requires at least observers or additional hardware. The other solutions using the action lines of two bearings in the same direction, as mixed PID, can lead to optimization of performances and robustness but the gain is mitigated. We have chosen to use each bearing as one entity by coupling their two axes.

Non-linear control: they give more possibilities for the design and the tuning.

Observers: they take into account a model of the structure in order to improve the system behaviour. The controller obtains information that it cannot measured.

The objective is to anticipate the dynamic behaviour of the system in order to apply corrective forces as soon as possible.

Hardware: the utilisation of additional hardware (sensors or/and actuators) could enable modal control. This solution needs additional place on the rotor, which could be difficult to obtain.

The approach develop considers only the two first elements. The last two could be included in the perspectives of this study.

Chapter 5 – POLAR FUZZY CONTROLLER DESIGN

The aim of this section is to present the selected control strategy as well as the improvement expected by using this one. The method developed permits to gain performance margins that could not be obtained with a linear SISO controller. The choices made to utilize these margins in order to enhance the system are detailed. Other possibilities are discussed in the Chapter 9.

In order to satisfy all the specifications, fuzzy based control strategies are developed and assessed. Even if nowadays, fuzzy logic is well known in the field of control, the particularity is that the selected strategy makes use of physical quantities that are not usual which are radial displacement and velocity or tangential velocity. These "polar quantities" are obtained through a usual Cartesian to polar coordinates transformation. The first part of this chapter is dedicated to the illustration of polar quantities advantages for the control, and even for the observation, of rotating machinery.

Before presenting the developed strategy, the design and tuning of an SISO PID fuzzy controller is presented in order to illustrate the principle of fuzzy logic; and to point out the limitations that motivate us to develop the new controllers in polar coordinates.

Polar Quantities

Usually, the displacement (a measurable quantity) is used. For each bearing, two sensors placed in a plane along two perpendicular axes permit to estimate the rotor position and vibration. The phenomena could be studied by processing the measurements either in time or frequency domains. Frequency analyses give precise and useful information on the system, but are not suitable for real time control. These analyses are based on a window of time. Consequently, there would be an important delay between measurement and action. Frequency analyses could be used for updating the controllers' parameters but not directly as inputs of the controllers.

Also, and for control purposes, time domain inputs stemming from the sensors are used. In the case of rotating machinery, we believe that the observation (and the actuating) of these phenomena in polar coordinates will provide a supplementary interesting way for analysis and control.

Cartesian to polar transformation

The controller was developed in the polar coordinate system presented in Figure 5. 1, but measurements and actuating are realized in the Cartesian coordinate system. Hence, two transformations are necessary, first from Cartesian displacements to polar displacements and velocities and, second from polar forces to Cartesian forces.

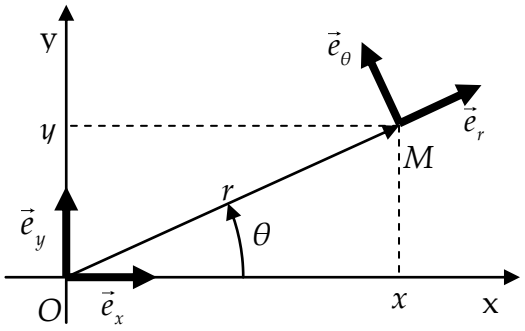

Figure 5. 1: Transformation of coordinates

Let us consider a point M on the plane. The Cartesian coordinates of M can be measured with sensors and are written in (5.1). In the same coordinate system, the velocity of M can be compute from its positions, and is expressed by (5.2).

$$\overrightarrow{OM} = \begin{pmatrix} x \\ y \end{pmatrix} = x\vec{e}_x + y\vec{e}_y \qquad \textbf{5. 1}$$

$$\frac{d\overrightarrow{OM}}{dt} = \begin{pmatrix} \frac{dx}{dt} \\ \frac{dy}{dt} \end{pmatrix} = \begin{pmatrix} \dot{x} \\ \dot{y} \end{pmatrix} \qquad \textbf{5. 2}$$

On the other hand, the polar coordinates of M are described by (5.3), and the velocity by (5.4).

$$\overrightarrow{OM} = \begin{pmatrix} r \\ \theta \end{pmatrix} = r\vec{e}_r \qquad \textbf{5. 3}$$

$$\frac{d\overrightarrow{OM}}{dt} = \begin{pmatrix} \dot{r} \\ r\dot{\theta} \end{pmatrix} = \dot{r}\vec{e}_r + r\dot{\theta}\vec{e}_\theta \qquad \textbf{5. 4}$$

The transformation from Cartesian to polar coordinates can be realized as indicated in (5.5), and the reverse transformation as shown in (5.6). Therefore, the two displacement sensors of each bearing are sufficient in order to establish the controller in polar coordinates.

$$\begin{cases} r = \sqrt{x^2 + y^2} \\ \tan\theta = \dfrac{y}{x} \end{cases} \qquad \textbf{5. 5}$$

$$\begin{cases} F_x = F_r \cos\theta - F_\theta \sin\theta \\ F_y = F_r \sin\theta + F_\theta \cos\theta \end{cases} \qquad \textbf{5. 6}$$

Observation

AMBs are normally symmetric bearings. With this property, the trajectory of the rotor inside the bearing is almost circular. This is due to the fact that the unbalance distribution is the main excitation applied on the rotor, and the others are normally considered negligible or as an ambient noise. In this case, a constant radius, a constant tangential velocity and a nil radial velocity define the orbital properties of the rotor. These quantities describe closely the dynamic behaviour of the system, and lead to a better interpretation of the information by the controllers. They enable the controller to distinguish between a disturbance produced by an unbalance (permanent), and that stemming from a radial disturbance (transient). The following simulations illustrate these two configurations:

Let us consider a rotor running at a constant speed of 6,000*rpm*:

- In the case of circular orbit (observed in polar coordinates), the radial displacement is constant and tangential velocity is constant, while the radial velocity is nil as shown in Figure 5. 2.

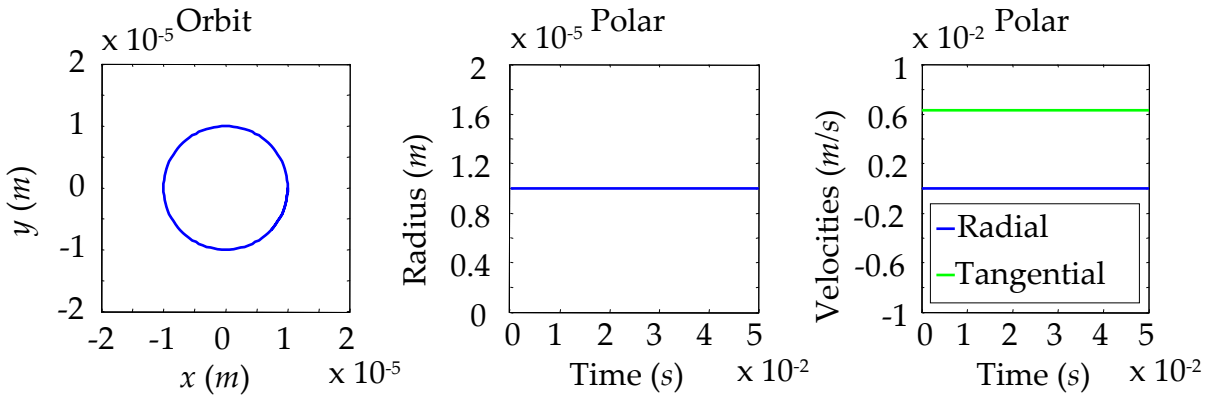

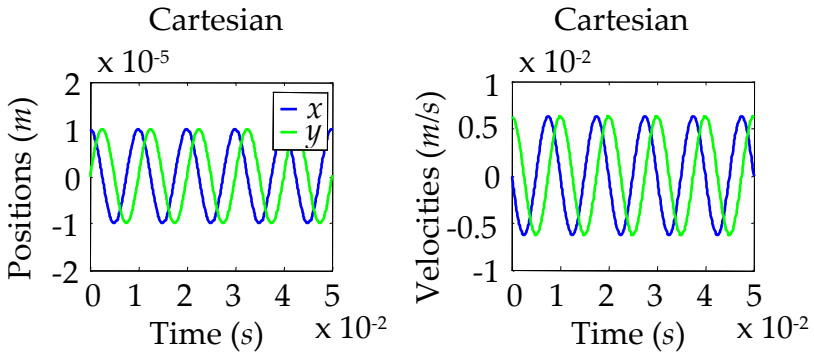

Figure 5. 2: Positions and velocities with a circular orbit

- In the case of elliptical orbit due to the system dissymmetry, radial velocity and position as well as tangential velocity have a harmonic variation that corresponds to the second harmonic of the rotating speed as indicated in Figure 5. 3. This phenomenon is not visible to a SISO controller. Therefore, this controller is unable to apply correcting forces in order to drive the rotor to a circular orbit.

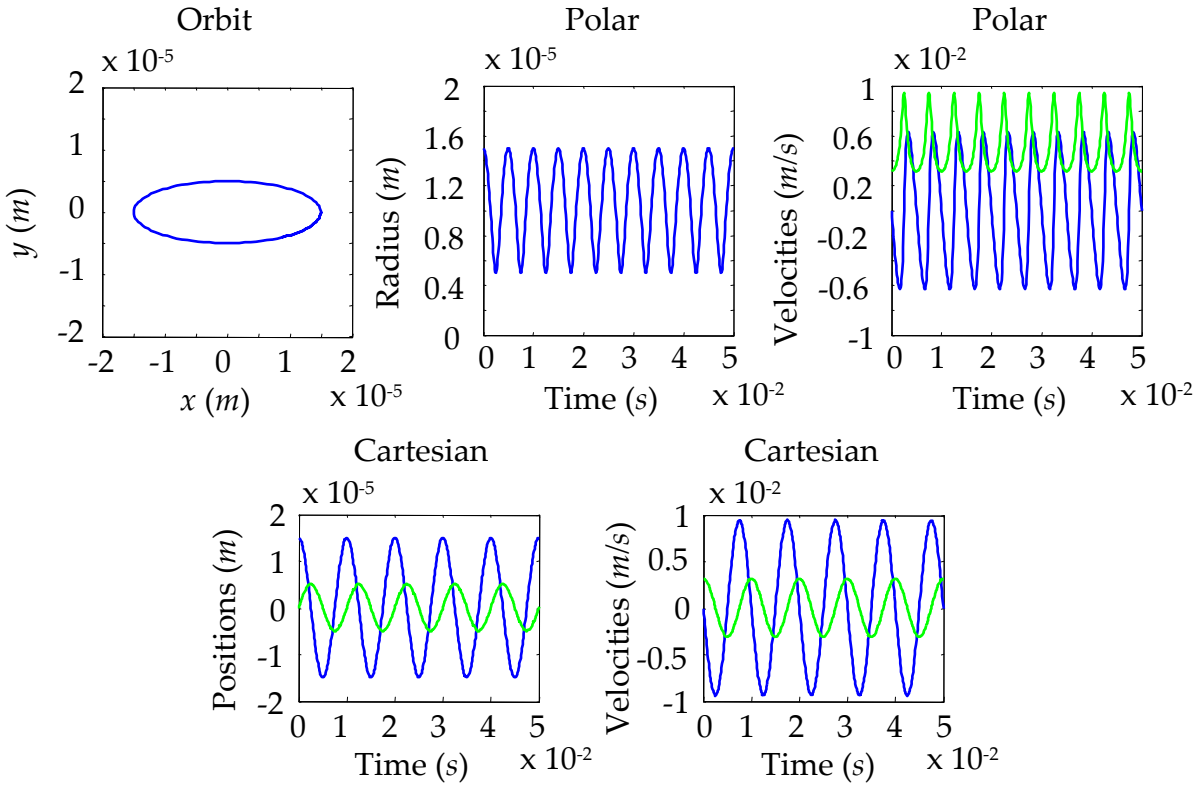

Figure 5. 3: Displacements and velocities with an elliptical orbit

- In the case of low frequency excitation (or impact), the effects can be seen with the presence of excitations close to the first harmonic of the rotating speed as revealed by Figure 5. 4.

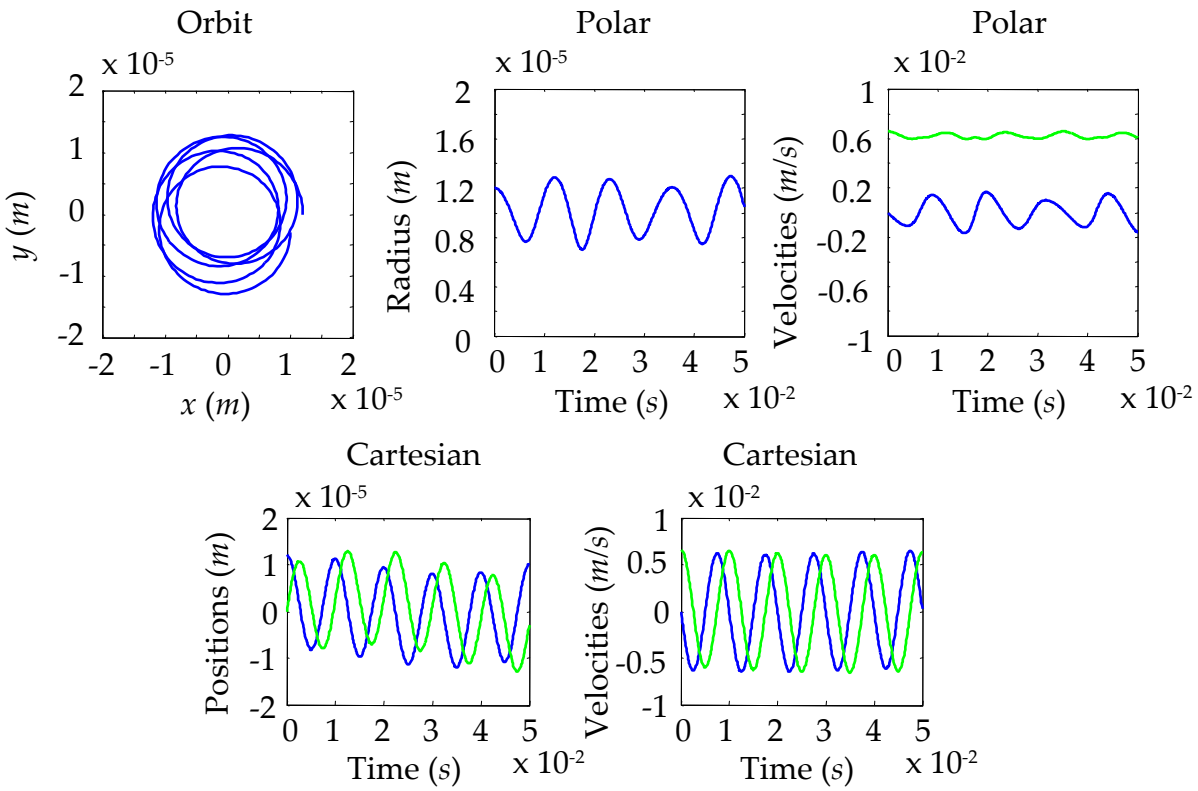

Figure 5. 4: Displacements and velocitiess with a low frequency excitation

For human beings, it is easier to interpret the trajectory in a "Lissajous graph". In this case, the dynamic behaviour is understandable, but this graph is difficult to handle for a digital controller. Even if these different behaviours are visible (or can be deduced) in Cartesian domain, theirs effects are emphasized in polar domain.

It is worth mentioning that the polar coordinates have an effect on the frequencies. A synchronous vibration appears at nil frequency, subsynchronous at a frequency that equals the rotating frequency minus the subsynchronous frequency and dissymmetry at twice the synchronous frequency.

Finally, polar quantities are well adapted to fuzzy logic control, since instantaneous values characterize the system behaviour.

Actuating

Polar coordinates have also advantages in order to apply control forces. This property is illustrated through the comparison of the damping used for unbalance control. The vibrations due to unbalance distribution can be attenuated by applying damping forces. As the trajectory is known (a circle), there are different manners to apply damping forces. Three different possibilities are described by Figure 5. 5.

- A/ Direct damping: The velocities are obtained from the derivates of displacements. Then, damping forces are obtained by multiplying the

velocities by a damping coefficient. In the following, it is considered as the reference case.

- B/ Geometric damping (or cross stiffness): Damping force is a force that anticipates the trajectory of the system. It is applied 90° out of phase of the measured displacement. It can be noticed that for a circular trajectory the velocity along one direction is proportional to the displacement along the perpendicular direction. Consequently, cross stiffness are equivalent to damping forces.
- C/ Tangential damping: Due to conversions of coordinate, the force applied in each direction (x and y), is a function of the two displacements.

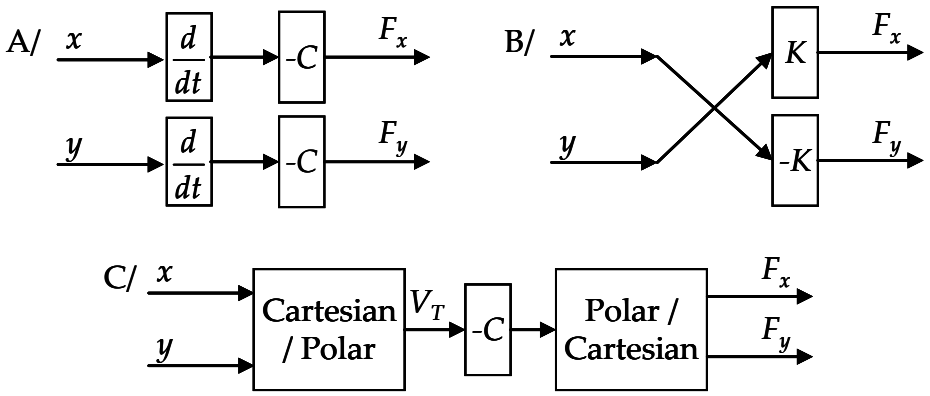

Figure 5. 5: Three different damping circuits

These three methods are compared for the case study presented in Figure 5. 6. The study is carried out with a speed relatively high (12,000*rpm*), since the disadvantages of cross stiffness and tangential damping increase with the rotating speed. Uncorrelated random noise is added to each measured displacement in order to assess the capacity of each method to apply targeted forces.

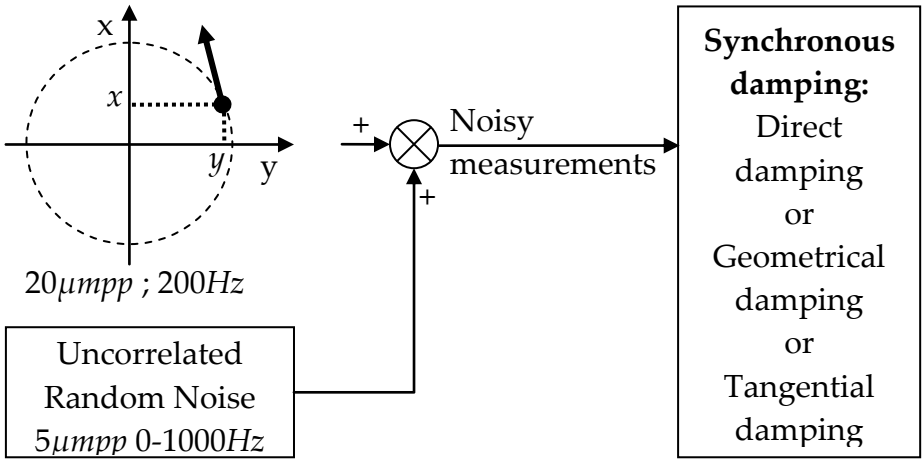

Figure 5. 6: Studied cases

Direct damping is the more stable. It is essential for the system, since damping is provided to every vibration without hypothesis on the trajectory. It is not affected by low frequency disturbances. However, it amplifies the noise produced by the sensor. Usually, the direct damping is optimized and cannot be increased for robustness reasons. Thus, other methods must be found in order to apply additional synchronous damping.

Geometrical damping is not very sensitive to noise. Nevertheless, as the gain is not directly a function of the rotating speed, the resulting damping varies substantially over the speed range (high damping for low speed and vice versa). Moreover, it stabilizes only one of the two precessions (forward or backward) and destabilizes the other one. Hence, the cross stiffness has a limited gain, since it can reduce the performance and the stability to low frequency excitations.

Tangential damping is suitable for all speeds and for the two precessions. It is not affected by measurement noise. As expected, by using two sensors, the disturbance signal is attenuated by almost -3dB compared to geometrical damping as revealed by Figure 5. 7. In addition, the same trends are obtained by applying the same noise on the two axes (x and y). Therefore, tangential damping permits to increase the gain of the controller by 3dB. Nevertheless, it is affected by low frequency disturbances. In addition, tangential damping adapts its own gain as a function of the rotational speed. Hence, the sensitivity to low frequency disturbances increases with the rotational speed. Thus, tangential damping should be tuned accordingly to the maximum rotational speed of the machine.

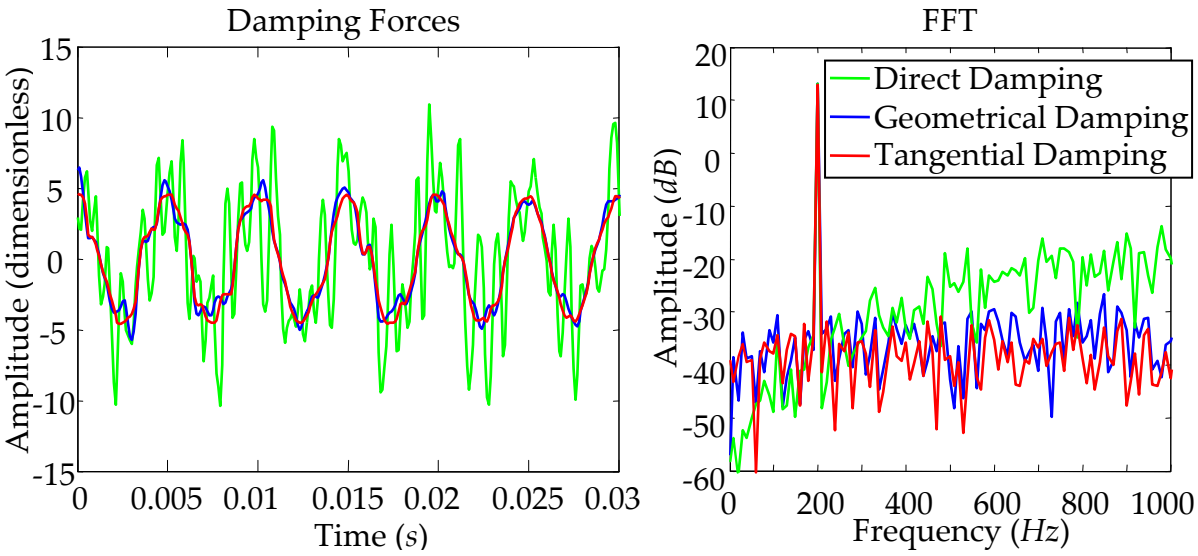

Figure 5. 7: Comparison of noise sensitivity

The main concern with cross stiffness is the disturbance of the backward cylindrical rigid body mode. As cross stiffness and tangential damping have the same trends in the low frequency range, the effects of the three methods on subsynchronous

backward modes are assessed. The direct damping is considered as the reference case. For this study, the trajectory of a rotor running at 12,000*rpm* is considered. The rotor is supposed to have a cylindrical backward mode at 60*Hz*, for this rotating speed. The amplitude of the synchronous vibration is 20*µmpp*, and the one of asynchronous backward vibration equals 10*µmpp*. The FFTs of the force signals enable to compute the damping value (from the amplitude) and its sign (from the phase) for each method as summarized in Table 5. 1.

Method	Subsynchronous damping	Synchronous damping
Direct damping (ref.)	1	1
Cross stiffness	-3.33	1
Tangential damping	-1.58	0.88

Table 5. 1: Normalized damping

Considering this particular case, the destabilizing effect of cross stiffness is twice more important than the one obtained with tangential damping. This implies that cross stiffness must have a limited gain.

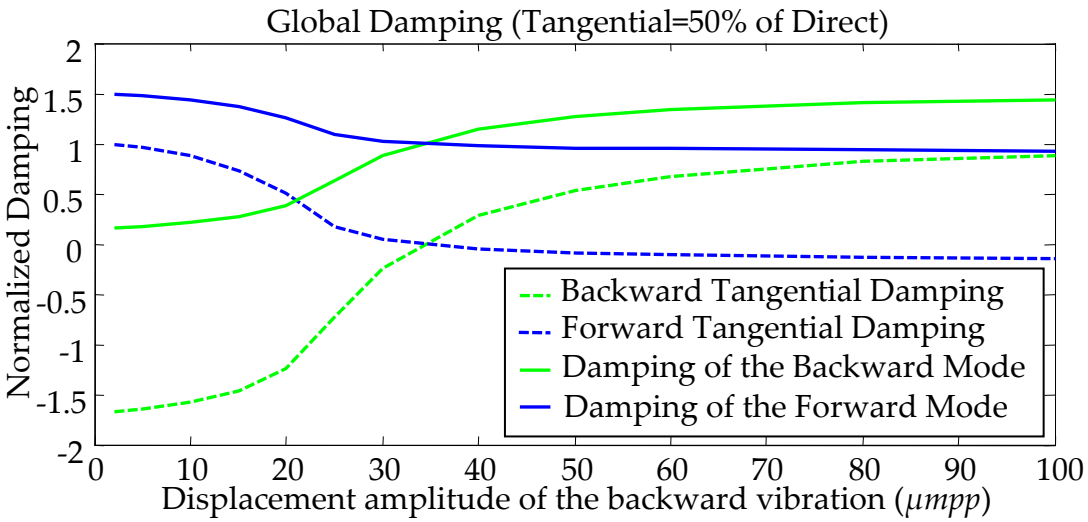

Figure 5. 8: Damping concentration toward the main contributor mode

In the following, the effects of the subsynchronous backward vibration amplitude on the bearing properties are assessed. Based on the previous example, the amplitude of the backward vibration is tested in the range of 0-100*µmpp*. For each amplitude, the synchronous and the subsynchronous damping values are computed. Then, the global damping that is the sum of tangential and direct is plotted.

Tangential damping produces particular effects when two important disturbances coexist. This behaviour results from the fact that the calculation of

tangential damping is valid when the orbit is circular but not for an unknown trajectory. Thus, the synchronous damping is attenuated when the subsynchronous vibration increases, as shown in Figure 5. 8. The subsynchronous damping is negative for low subsynchronous vibrations, and it increases progressively, until becomes positive for high subsynchronous vibrations. This means that the tangential damping is efficient only where there is a prevalent vibration.

The best way in order to apply damping is the classical method using displacement time derivative. However, this method is limited for robustness reason. Thus, tangential damping is an interesting method in order to apply additional damping forces for unbalance control purpose. The tangential damping stabilizes systematically the main precession and the other disturbances have low effect on the force applied. However, it could destabilize the precession opposed to the main one. Regarding the previous example, when the amplitude of displacements related to the backward mode increases, the tangential damping is directed to this mode, as shown in Figure 5. 8. Let us consider that the tangential damping gain is half the direct damping gain (Figure 5. 8), then the normalized global damping of the backward mode start from 0.15 and increases progressively and until it achieves a limit value close to 1.5. On the other hand, the normalized global damping of the mode at 200*Hz* with a forward precession is reduced progressively from 1.5 to 0.9. Consequently, the negative effect of the tangential damping on this mode when the backward precession is the principal contributor is limited as the direct damping alone has a normalized gain that equals 1. In all cases, the gain of the tangential damping is chosen in order that all of the modes are well damped (tangential plus direct), and the system behaviour is expected to be better with tangential damping than without.

Finally, tangential damping is a robust method that permits to apply additional damping forces for unbalance control. In addition, compared to classical unbalance control methods, tangential damping does not make use of the signal provided by a rotating speed sensor. Thus, the hardware of the bearing is simpler and more robust.

Fuzzy controller

Fuzzy logic was first introduced by Zadeh [1965]. Born in the USA, the fuzzy logic has first gained acceptance in Asia and its successful applications have permitted it to be now widespread in the world.

It is an extension of the conventional (Boolean) logic to handle the concept of partial true-false values between completely true and completely false. Fuzzy logic is interesting because it takes into account the fact that most modes of human reasoning

are approximate rather than exact. Fuzzy logic is a decision support system. It allows taking actions with uncertain or imprecise measurements.
Borne et al. [1998] discuss on the theory of fuzzy logic and its main characteristics. Fuzzy control has the advantages of being able to be used in complex systems, non-linear, time-variant, or including uncertainties. In addition, it is less sensitive to parameter variations of the system and it allows use of membership functions adapted to the dynamic behaviour of the subject system. In addition, it enables the calculation of nuanced actions and the consideration of some data variations that leads to robust behaviour. On the other hand, fuzzy controllers handle generally parameters in time domain consequently; the approach is different from the usual approaches utilized in industrial applications, which are frequency domain based.

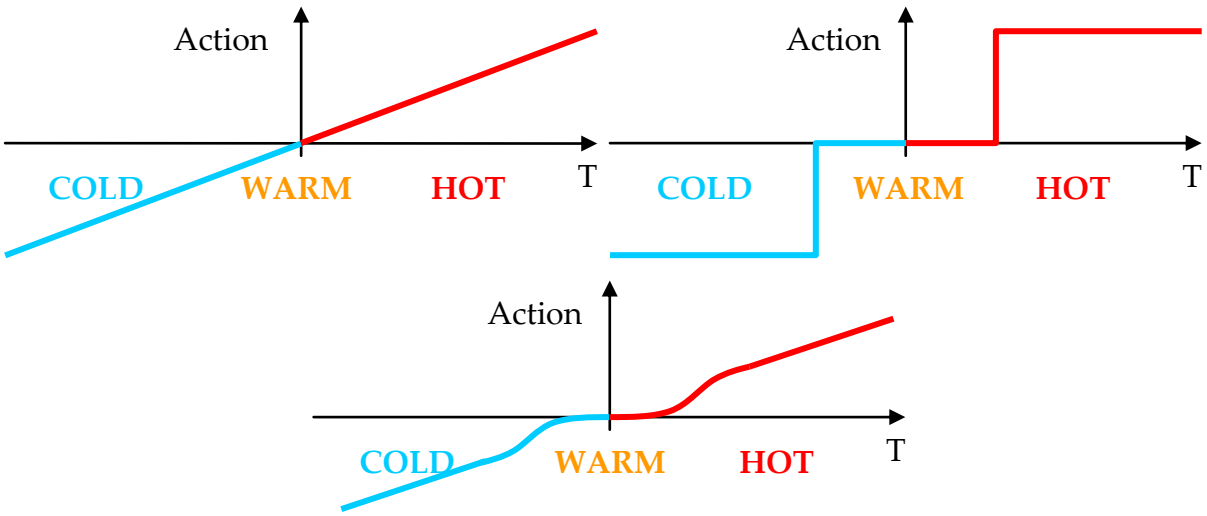

Figure 5. 9: Action of the different controllers

The interest of fuzzy logic can be understood with a simple introductive example. Consider temperature control of a room with two actuators: one heater and one air conditioner. Different controllers can be used in order to obtain a warm temperature:

- A linear controller: an ideal temperature is defined and the actuators are used quite constantly to follow this setting, with an action proportional to the gap between the measured and the set temperatures. In this case, during the same day the heater and the air conditioner can be used with an obvious waste of energy.
- A controller with Boolean logic: two thresholds are defined. If the measured temperature is inferior to the temperature defined as cold, the heater is fully on and respectively, for hot temperatures. The problem is the definition of thresholds, which temperature is cold, warm or hot? In addition, large oscillation of temperature can occur.
- A fuzzy controller: membership functions are defined for the temperatures cold, warm and hot. For warm temperature the actuators are set off. If the

temperature decreases, the heater is progressively set on. When the temperature becomes fully cold, the action of the heater is equivalent to that of the linear controller (it could be also equivalent to the Boolean controller). Of course, fuzzy logic leads to non-linear controllers.

The actions obtained with the three controllers are plotted in Figure 5. 9. The approach used to obtain the mathematic expression of a fuzzy controller is detailed in the following. In this work, the Takagi-Sugeno method is used for its effectiveness in real-time computations. Thus, this method is used in order to present fuzzy logic theory.

Fuzzy set theory

The main principles of the fuzzy approach are first the fuzzification of the inputs into linguistic quantities, e.g. high and low. Each input state is associated with a mathematic membership function. Second, the inference engine implements a set of linguistic rules based on the behaviour of the system. Finally, the control is obtained after defuzzification. This consists in transforming the linguistic conclusions of each rule in a command with a numerical value.

Considering, a space of elements X called *universe of discourse*. A *fuzzy set* A in X is characterized by a mathematic *membership function* $f_A(x)$ which associates with each element x in X a real number in the interval [0;1]. Generally, a linguistic name is associated to each fuzzy set. In the case described by Figure 5. 10, the universe of discourse is [0;40], and three fuzzy sets are defined (cold, warm and hot). Each fuzzy set is represented by a bell-shaped function, but it could be triangular, trapezoidal, etc.

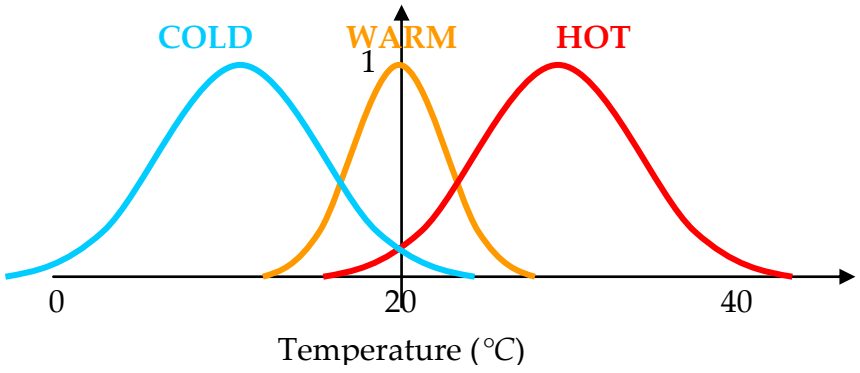

Figure 5. 10: Membership functions

The fuzzyfication enables to compute for each element of the universe of discourse its degree of belonging to each fuzzy set. This operation permits to conclude that

15°C is 70% cold 15% warm and 0% hot. The total is often different from 100%, it can be seen as a manner to take into account uncertainties.

There are a number of heuristic rules that permit to design a suitable fuzzy controller. For examples,

- The fuzzy sets must cover the entire universe of discourse,
- Only one membership function can equal 1 for a given element (a given temperature can not be considered fully cold and fully warm)…

The human reasoning is implemented in the inference engine. Rules are determined based on the behaviour of the system. The experience of the designer is used in order to define a set of rules that permits to have the best reaction to each event. These rules are conditional and should describe all the possible events that can occur. This evaluation requires solid knowledge of the system. A few simple rules can be sufficient to describe the system's behaviour, as a limited number of rules simplifies the design process and can lead to optimized performances.

In the case of our introductive example, the rules could be chosen as follows:

- If the temperature is cold then the heater is turned on,
- If the temperature is warm then no action, and
- If the temperature is hot then the air conditioner is turned on.

The control action is obtained after defuzzification. It consists in aggregating the conclusion of each rule. Each fuzzy method possesses its own defuzzification process. Only the Takagi-Sugeno defuzzification is presented hereafter.

Generally, each rule conclusion is a linear function of the inputs, but it can be more complex like quadratic or something else. The parameters of these functions are tuned according to the system and the desired behaviour.

For the introductive example, three actions are defined:

- Heater is turned on corresponds to $u_{heater} = a_1 T + b_1$,
- No action corresponds to $u_0 = 0$, and
- Air conditioner is turned on corresponds to $u_{air-conditioner} = a_2 T + b_2$.

The final action is the sum of the products of membership function values times the action of each rule. The result is weighted by the sum of the membership function values as indicated in Figure 5. 11.

$$A = \frac{\sum f_i u_i}{\sum f_i} \qquad \textbf{5. 7}$$

For our example:

$$A(T)=\frac{f_{COLD}(T)(a_1T+b_1)+f_{HOT}(T)(a_2T+b_2)}{f_{COLD}(T)+f_{WARM}(T)+f_{HOT}(T)} \qquad 5.8$$

As a function of the sign of the action A, the heater is used or the air conditioner. There are never both in the same time, as there is only one output to our simple controller. The method used in order to calculate the control command is illustrated with an example presented in Figure 5. 11.

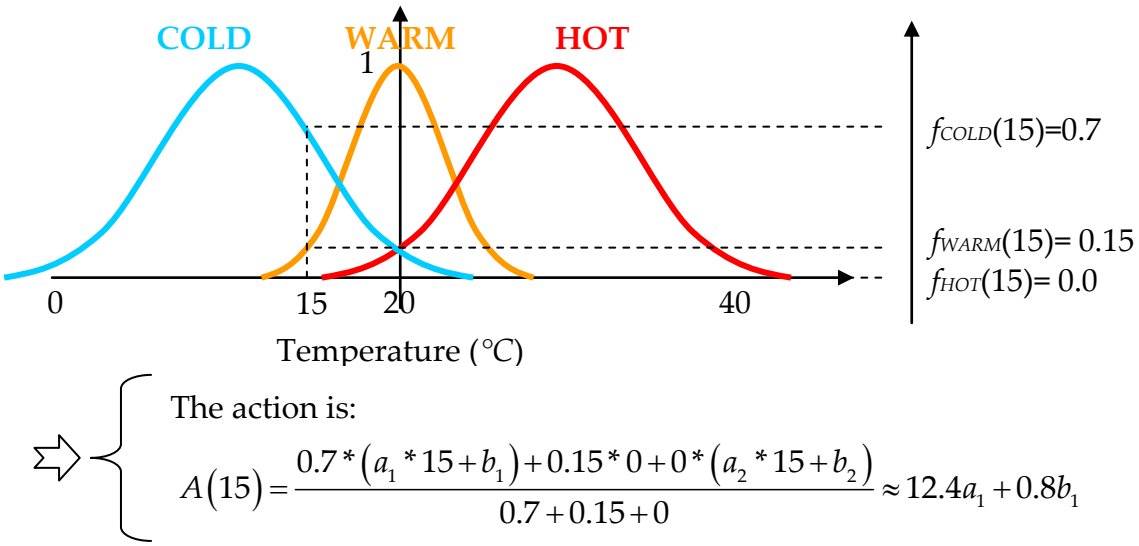

Figure 5. 11: Computation of the control command

The mathematical formulation of the fuzzy controller is a relatively simple expression whose complexity increases with the number of variables, the number of fuzzy sets and the number of rules.

SISO Fuzzy

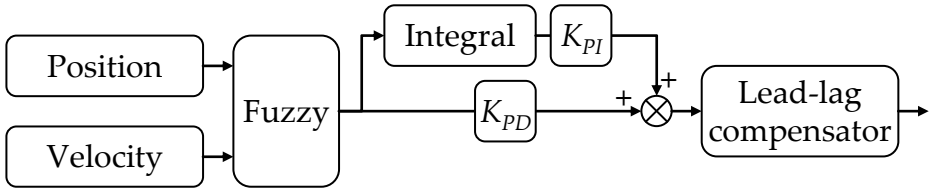

Figure 5. 12: Structure of the fuzzy controller

Fuzzy controllers can be designed from scratch but they have gained many industrial successes by upgrading an existing linear controller. Generally, industrial applications of AMBs make use of SISO controllers. Thus, it was convenient for a first

approach to base the fuzzy controller on an existing strategy. The non-linearity of fuzzy controller offers several possibilities for the control of disturbances. It is possible to increase the performance of the controller with the same level of robustness and the reduction of control forces.

The SISO fuzzy PID designed has the general structure described by Qiao and Mizumoto [1996]. It is the sum of a fuzzy PI with a fuzzy PD controller as described by Figure 5. 12. In addition, as for the polar fuzzy controller, a lead-lag compensator is used in order to ensure stability of high frequency flexible modes of the rotor and robustness of the system. The displacement is measured and the velocity is calculated by numerical differentiation. The two data (position and velocity) are used as inputs for the fuzzy controller.

Four generalized bell shape membership functions were utilized, since this type of membership function offers smooth transitions as shown in Figure 5. 13. Smooth transitions are preferred in order to avoid high frequency contents in the control forces.

Nondimension inputs are used in order to obtain a flexible fuzzy controller. It is easier to handle the relative displacement with respect to auxiliary bearing clearance than the displacement itself. This is the way that universe of discourse was normalized. For velocity membership functions, several case studies were realized, and analysed in order to quantify the maximum possible velocity, and then a safety factor was applied.

The design of the membership function should take into account the noise of measurement. The noise of measurement can be evaluated either by the sensor resolution, or by measurement when the rotor is levitated in steady state conditions. For this second case, the displacements and velocities are measured, and their respective amplitude gives directly the measurement uncertainty. These amplitudes of displacements and velocities should be insufficient to change of prevalent membership function. On the other hand, in order to be efficient small amplitude of displacement and velocity should belong to one of the two fuzzy sets (positive or negative). Finally, as nominal behaviour is considered and, the displacements and velocities are relatively small compared to noise of measurement, only two membership functions were utilized for each input of the fuzzy controller.

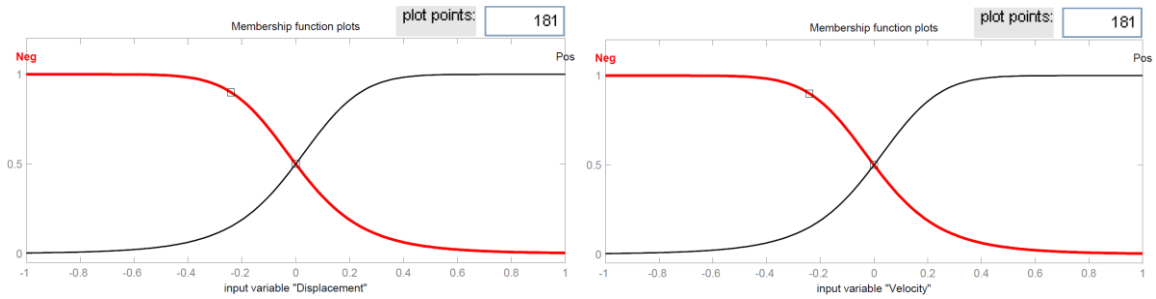

Figure 5. 13: SISO Membership functions

The rules are chosen in order to optimize the energy dissipation and to minimize the kinetic energy of the rotor (the force is always opposite to the velocity as illustrated in Figure 5. 14). The rules selected were:

- When position and velocity have the same sign, then the proportional gain is activated. Note that the other gains are always activated.
- When the displacement and velocity have opposite signs, the damping gain is conserved but the stiffness is set to zero.

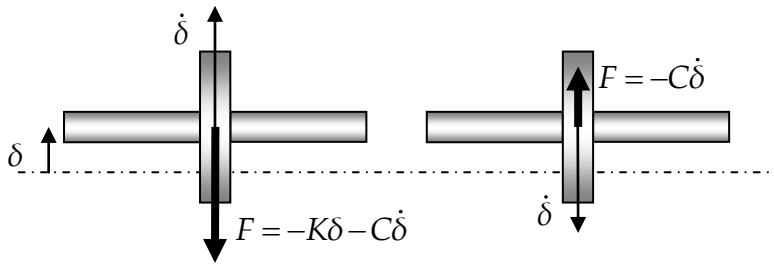

Figure 5. 14: Control strategy

Different sets of rules were assessed by numerical computations. Particularly, the case where the action force is completely set off when position and velocity have opposite signs. This configuration was not retained because the damping was not optimized. For the controller developed, the dimensionless resulting action surface is shown in Figure 5. 15.

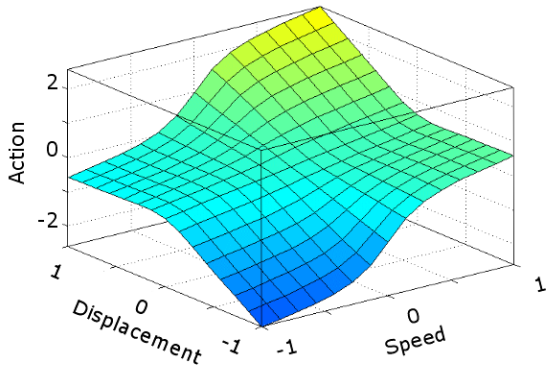

Figure 5. 15: SISO Fuzzy surface

This type of controller can offer good performances. Nevertheless, their non-linearity can involve undesirably anisotropic behaviours, especially when it is applied as a SISO controller. Thus, a number of disadvantages appear:

- The bearing characteristics depend on the direction. Thus, there are infinity of directions to analyse in order to characterize the robustness, the stability and the performances of the controller.

- The response to a harmonic excitation has a large spectrum, which can excite modes of the structure. Thus, since there is always at least an unbalance, the controller excites constantly the structure.
- The bearing generates cyclic bending of the rotor, with an obvious reduction of the rotor lifetime.

The anisotropy induced by non-linear SISO controllers can be illustrated with two simple examples.

- Let us consider a controller with two rectangular membership functions. If the displacement is between $-x_0$ and x_0, the stiffness K_1 is applied, otherwise the stiffness K_2 (different from K_1) is applied. For this case, there is at least one circular trajectory for which the rotor sees both stiffness as indicated in Figure 5. 16.
- Second, if the damping C is non-linear, and is a cubic function of the velocity. When the velocity equals 1 and has the same direction as a control axis, the damping force equals C. However, for the same velocity, if the direction is exactly between the two axis, the damping force equals:

$$F = \sqrt{\left(C\left(\frac{1}{\sqrt{2}}\right)^3\right)^2 + \left(C\left(\frac{1}{\sqrt{2}}\right)^3\right)^2} = \frac{C}{2} \qquad \textbf{5. 9}$$

Thus, for the same velocity the damping force is halved.

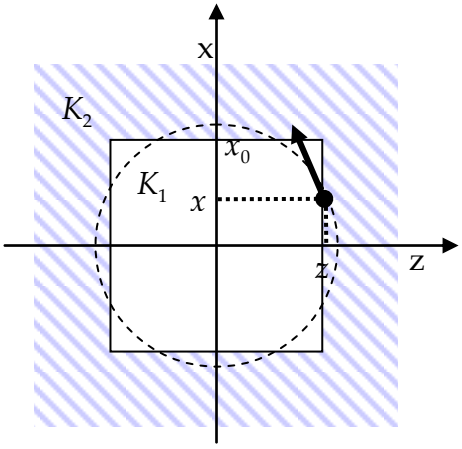

Figure 5. 16: Example of anisotropic behaviour

This study considers only the case of nominal behaviour with low displacements. Consequently, if the membership functions are tuned too smoothly, a linear controller can approximate the non-linear one. And, if the membership functions are tuned with too hard transitions, disturbances can appear, and lead to system

instability. Finally, for these operating conditions, there is a narrow range of membership functions that enable to make use of the unique capabilities of fuzzy controllers without disturbing the system.

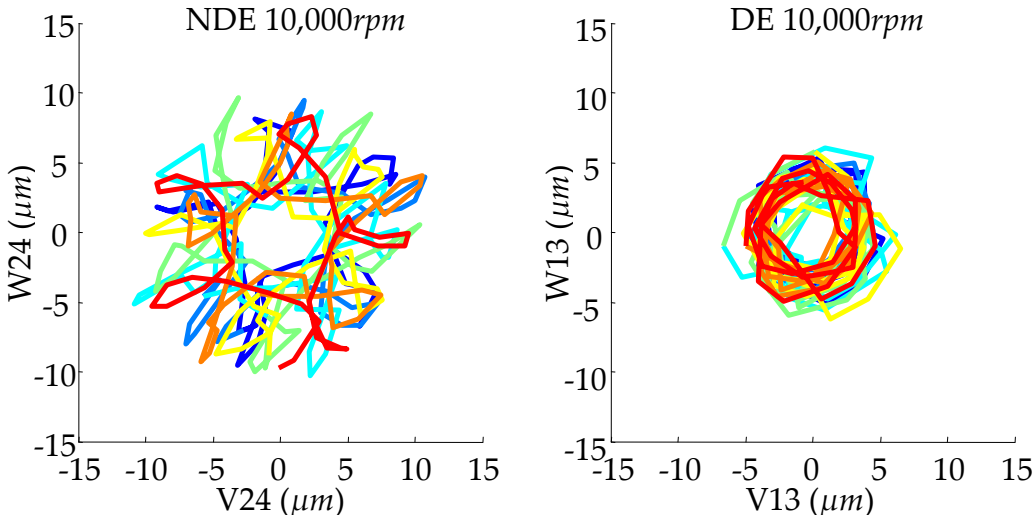

Figure 5. 17: Non-linear response 10,000rpm

An experimental result is shown in Figure 5. 17. The SISO fuzzy controller utilizes membership functions with a state transition from 0 to 1 on narrow ranges of displacements and velocities. The controller has almost a switching behaviour and is very non-linear. Each colour corresponds to one rotation of the rotor (spin). The rotor had a good behaviour with low vibrations. After few minutes at 10,000*rpm* a disturbance had appeared. It was the backward response of the third flexible mode.

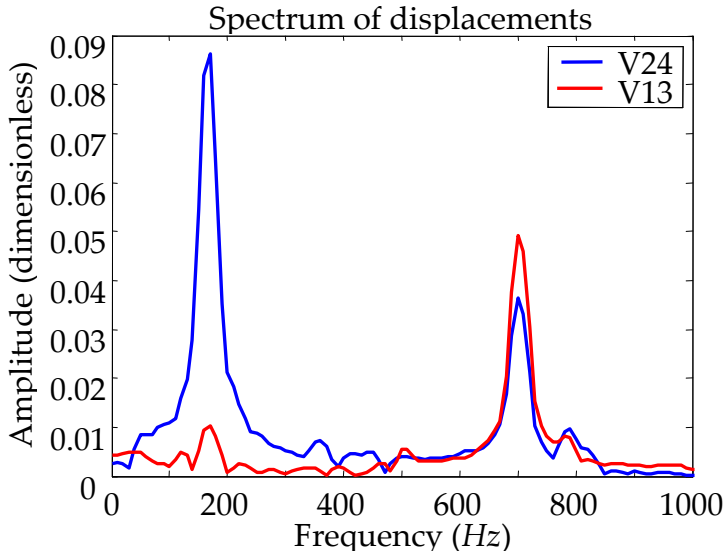

Figure 5. 18: Spectrum of the signals provided by the two bearings

Peeters et al. [2011] discuss the non-linear behaviour of structure and show that non-linear modes can exhibit coupling with several harmonics. Here, the behaviour could appear to be a non-linear mode with harmonics 1 and 5, but it is only the response of a higher frequency mode whose frequency is not a harmonic of the rotating speed as shown in Figure 5. 18. It is worth mentioning that for the DE bearing the whirling frequency is the one of the third flexible mode. Then, after a few minutes, the system became unstable and landed on its auxiliary bearings.

It is demonstrated that Cartesian coordinates are not well adapted to rotating machinery equipped with non-linear controller then, it is natural to consider the polar coordinates as an alternative.

Polar fuzzy control strategy

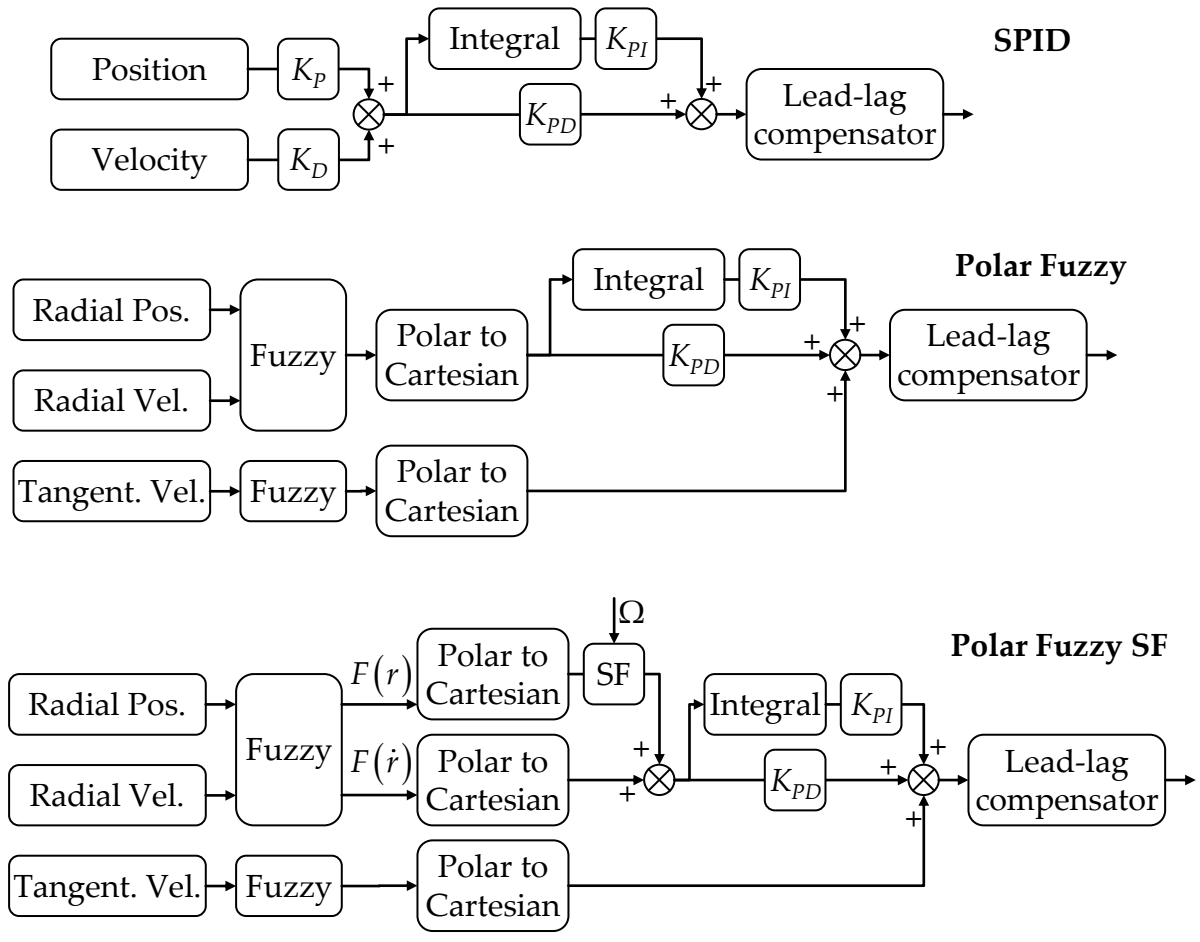

Figure 5. 19: Schemes of Controllers

The fuzzy approach is well adapted for controlling complex systems and is less sensitive to parameter variations. Unfortunately, this kind of controller cannot

prevent spillover effects. Two solutions can be considered: either the application of modal control or implementing a fuzzy controller based on a Standardized PID (SPID). The SPID control enables managing the stability of high frequencies by introducing lead-lag compensators as shown in Figure 5. 19. These filters guarantee stiffness and damping for high frequency modes. In this study, the latter solution was chosen. Then, fuzzy process is used to modulate the gains of the SPID determined previously. The controller could be enhanced by using a synchronous filter. In the following, the fuzzy and the polar approaches are introduced, then the SPID is presented and finally, the synchronous filter is described.

Fuzzy approach

The fuzzy logic controllers developed consider each bearing as a single MIMO system as presented in Figure 5. 19. The inputs are the radial position and velocity and the tangential velocity stemming from the displacements measured in the two directions. The outputs of the fuzzy controller are then used in order to modulate the gain of the SPID. The outputs are the forces computed in the polar coordinates and then converted into command currents.

The tangential damping could attenuate the low frequency performance of the system since it is sensitive to low frequency noise. Thus, it is interesting to apply it only when it is necessary. In the polar coordinates system, a critical speed can be detected by a high tangential velocity. In addition, it is very common that a critical speed is seen with two different levels of amplitude on the two bearings. Consequently, one bearing could damp the synchronous vibrations and the other has its best performance in the low frequency range by avoiding to apply unnecessary tangential damping.

Usually, there is a trade-off between the stiffness and the damping of the bearing. Thus, the bearing stiffness cannot be increased infinitely. An abnormal behaviour can be detected with polar coordinates (e.g. dissymmetry, subsynchronous vibration…). Then, an increase of stiffness during a short time enables to restore the steady state behaviour without reducing the damping of the system.

Fuzzy controllers with trapezoidal membership functions were utilized. These simple membership functions seem sufficient for this study. The rules are:

- For permanent behaviour, when tangential velocity is high tangential damping increases by 50%.
- For transient behaviour, when radial velocity is positive, radial stiffness increases by 50%.

This set of rules seems adapted to the system, an optimization could improve it or complete them for particular operating conditions (large displacements, faults…).

SPID

The polar fuzzy controller permits to obtain performance margins not achievable by linear controllers. Here, we have chosen to distribute equitably these margins in order to reach three objectives: first to simplify the controller design, second to satisfy standards requirements without synchronous filters and finally to improve the low frequency performances. It is worth mentioning that it is not the only choice possible.

Usually, the characteristics of an augmented PID are determined as a function of the dynamic behaviour, the number of modes included in the operating speed range and the operating conditions (gas flow and pressure ratio). Also, the stiffness is chosen low and the damping is concentrated around system natural frequencies.

The first step of the fuzzy approach was the definition of the specifications of the SPID. The controller bandwidth is divided into low and high frequency domains with a transition around the second flexible mode. The idea is to standardize the design in the low frequency bandwidth, which corresponds to the operating speeds range that includes three vibration modes (cylindrical, conical and the first flexible). The consequence of this standardization is the reduction of the performance of the first flexible mode response since the damping is not concentrated on the bending frequency. The high frequency stability and robustness depend on the mode shapes and frequencies. The parameters that provide a suitable behaviour are specific to each bearing. Lead-lag filters tuned for each bearing manage these properties.

The controller must overcome the principal sources of instability, such as the negative stiffness and the seals dynamic coefficients. A high stiffness enables to counteract AMB and seals negative stiffness. SPID have naturally its minimum stiffness around the first rigid body mode. Consequently, if the designed stiffness is "sufficient" to control the first mode, this will be the case for the higher ones. Since the stiffness is high, the possibilities to introduce damping are limited. In addition, the seals effects introduce negative effective damping especially in low frequency. Thus, the damping of this domain becomes a priority. Finally, the damping is made constant for the remaining operating speeds. Consequently, the controller became less efficient but more multifunctional. Moreover, the bearing characteristics are almost independent of rotor geometry in the operating frequency range. It can be supposed that the modification of the global gain can be sufficient to adapt the controller to different sizes of bearings and rotor for a given application.

Synchronous Filter

The fuzzy controller developed provides performance close to the requested specifications. However, we have developed a strategy that improves the performance of the system by using additional forces. So, the energy consumption of

the system is not optimized. It could be the topic of future researches. Nevertheless, if the bearing has not the required capabilities and if it is impossible to change it, we propose a simple solution, which uses synchronous filters.

A simple notch filter enables the reduction of vibration and control forces when passing through critical speeds. Among the different existing methods, the notch filter implemented in this study rejects the synchronous bearing stiffness only. This choice was motivated by the fact that generally, filters used to cross bending mode critical speeds reduce the synchronous stiffness and add synchronous damping. As the fuzzy controller generates damping, only the first effect was necessary. The filter has a gain of *-6dB* at the synchronous frequency. It was activated at speeds beyond the rigid modes and before the flexible one and it is maintained until the maximum speed. Finally, this filter has the advantage to be independent of rotor characteristics.

$$N(s) = \frac{\Omega^2 + K_\Omega \Delta_\omega \Omega s + s^2}{\Omega^2 + \Delta_\omega \Omega s + s^2} \qquad \textbf{5. 10}$$

Where:

- Ω is the rotational speed of the rotor,
- K_Ω is the gain for the rotational speed frequency, and
- Δ_ω is the width of the stop-band.

Conclusions

The requirements for centrifugal compressors and the limitations of PID controllers have encouraged us to develop a new control strategy. The strategy chosen enables to enhance the machinery dynamic behaviour and to simplify the design and the design process. The approach is destined to operate without synchronous filters. In this way, a simpler and more robust system is expected. In addition, the bearings have almost standardized characteristics. These could improve the design process of turbomachinery as mechanical engineers would have a precise idea of bearing characteristics during the design of the rotor. Finally, only the high frequency parameters must be tuned and this should lead to a shorter design time.

The strategy was assessed numerically and experimentally. In the following, only the major results are reported.

Chapter 6 – TEST RIG

This test rig was ordered for the needs of this thesis. During the first year, the specifications for this one were established based on an acceptable size for safety reasons and a dynamic behaviour as close as possible to the one of centrifugal compressors. Thus, the main specifications were a supercritical rotor with a maximum speed around 10,000*rpm*. The rotor would have low gyroscopic effects but at least one disk. It would be supported by two radial AMBs. The objectives were to have a flexible rotor in complete levitation since a classic bearing could damp high frequency modes, whose stability we wished to study. Finally, it must have a flexible coupling with the motor in order to avoid to modelling this one.

Based on these specifications, the manufacturing of a test rig was considered. However, an existing design was available commercially. Finally, it was purchased as it satisfied our specifications and allowed us to save time.

The first objectives of this test rig were to assess the performances, the stability and the robustness of different control strategies. Then, the limits of the different control strategy were assessed. Finally, it was used in order to show that numerical predictions are representative of experimental results.

The aim of the test rig was to assess control approach developed numerically. Also, if the approach was sufficiently robust, it could be implemented experimentally without any additional tuning. As we apprehended, a tuning was necessary mainly due to our inexperience. The tuning was made in the same time on the test rig and on the numerical model in order to understand the phenomena and to adjust the approach. At the end, the controller was running well on both. However, there were discrepancies between numerical results and experimental ones. The results were analysed in order to understand the different sources of deviations. Besides, the different phenomena that could explain them will be discussed.

Some system characteristics are difficult to measure experimentally. Consequently, it is important to validate the numerical model in order to ensure that the numerical predictions are in accordance with the real system. A comparative study of numerical results and measurements is presented. To do so, the model needs a calibration. It is not identification since a global parameter (the current stiffness) is used to compensate both modelling parameters errors and phenomena not taken into account in the model. In addition, this calibration can be implemented in the controller in order to obtain experimentally results with the same trend as the numerical predictions.

In the following, the experimental test rig and the associated numerical model are presented. The characteristics chosen to perform numerical simulations are reported, and the controller tuned for this test rig is presented. Then, the sources of deviation between numerical and experimental results are studied. The numerical model is calibrated in order to match the experimental system. Finally, a design approach is used, and the numerical model is validated according to the method recommended by API 617 [2002].

Remark: In the following, only the controller supplied with the test rig is considered.

Experimental apparatus

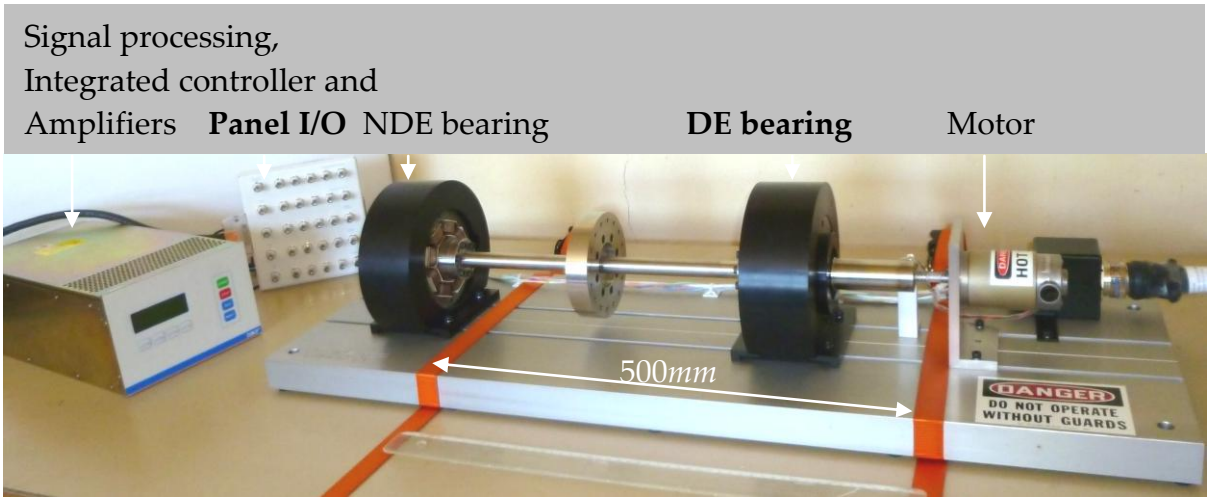

Figure 6. 1: Test rig

The experiments were performed using an academic test rig presented in Figure 6. 1. It is a commercial product manufactured by SKF® and was delivered with a dedicated PID controller. The test rig is equipped with two identical AMB called NDE (Non Drive End) and DE (Drive End) bearings. Each bearing has a maximum static capability of 280N with air gaps of 0.375mm. The action lines are positioned in the configuration load between axes. They are powered in differential driving mode with a bias current of 1A. Current are provided in the range of 0-3A using PWM amplifiers. Two displacement sensors (variable reluctance probes) are integrated in the housing of each bearing and are non-collocated with actuators, as shown in Figure 6. 3. The Input/Output panel gives access to the displacements measured and enables setting currents for the amplifiers. Each AMB has one auxiliary bearing with a clearance radius of 0.1mm.

The shaft is composed of three parts bolted together. A central part (diameter: 19.05mm; length 344mm) with a disc 120mm in diameter and 25mm long placed at

mid-span, together with two shaft ends (35*mm* of main diameter). The stack of laminated steel sheets is shrunk on each of these two shafts. Due to the different lengths of the latter (190.5*mm* at DE and 110.5*mm* at NDE), the rotor is not symmetric in relation to the central disk. The total rotor length is 645*mm*. The rotor mass is 5.89*kg*. Three balancing planes are available: one at the central disc and one at each bolted plane. The rotor is driven by a 500*W* electric motor with a maximum speed of 12,600*rpm*. Power transmission is provided through a flexible coupling. The operating speed range used in this work is up to 10,000*rpm*, which includes three critical speeds (two forward rigid modes and the first forward flexible mode). The speed of the rotor is monitored by using a speed sensor placed close to the motor.

As suggested by the third part of ISO 14839 [2006], the frequency bandwidth considered in this study is 0-2*kHz*. The test rig can be controlled either by using the dedicated device or externally via the input/output panel. The new controller is implemented under Simulink® and dSpace® environments, with a sampling frequency of 20*kHz*. The four control axes available on the test rig are shown in Figure 6. 2. Actuators and sensors are represented by red circles and balancing planes by green ones.

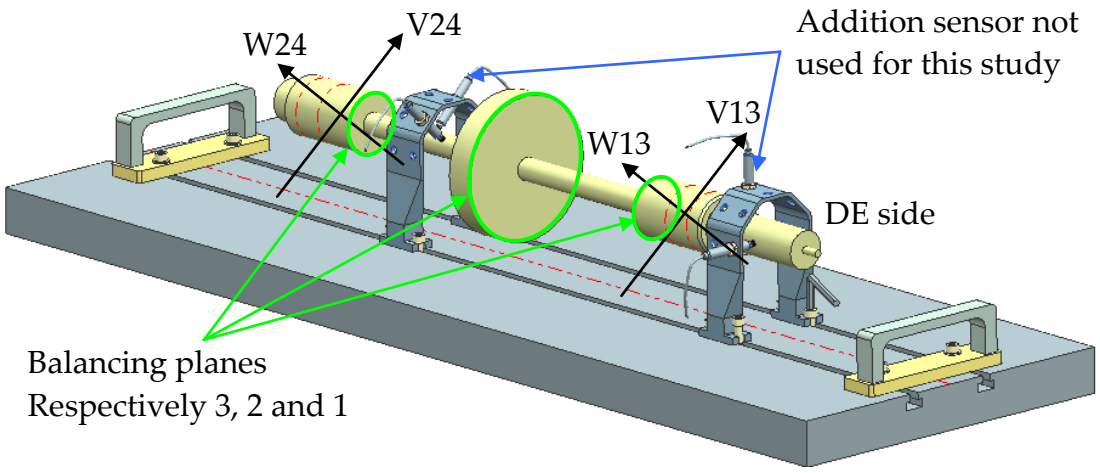

Figure 6. 2: Definition of the control axes

Numerical model

Two fuzzy controllers were developed with numerical simulations and then applied to the academic test rig. The first one is a SISO fuzzy controller. It exhibits good performances but its non-linear behaviour generates anisotropy and leads to a complex system difficult to analyze. Defoy et al. [2012] have presented the experimental results. The second one is the polar fuzzy controller studied in this thesis.

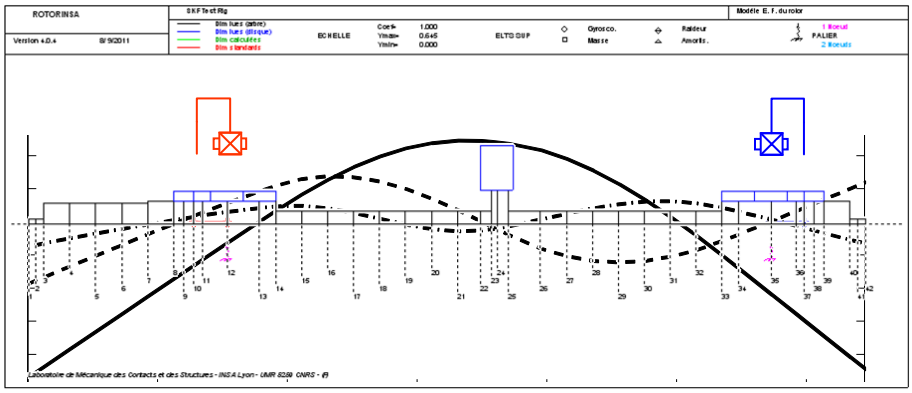

Figure 6. 3: Finite Element model of the rotor (Red DE, Blue NDE)

The numerical model was necessary in order to establish the design methodology and tune the controller parameters. The numerical model of the rotor was formulated with the finite element method, without experimental identification. The radial AMBs are presented in Figure 6. 3, as suggested in the standard ISO 14839 [2002]. The rotor model is composed of the following elements: rigid discs, flexible shafts and bearings. The shaft model is composed of 41 Timoshenko beam elements. The calculations of the natural frequencies and the mode shapes were performed with direct stiffness (no cross stiffness and no damping). For a preliminary dynamic behaviour assessment, the stiffness value ($8.10^5 N.m^{-1}$) is chosen in the order of magnitude of the AMBs final stiffness. The natural frequencies of the rotor computed for the frequency bandwidth studied are summarized in Table 6. 1. For the sake of clarity, only the shapes of the first flexible modes are plotted in Figure 6. 3. Then, the free-free modes of the rotor are computed and introduced in the complete model with AMBs. The pseudo modal method is used in order to keep only the first 14 free-free modes (to conform to the bandwidth of frequency).

Modes	0*rpm* (*Hz*)	15,000*rpm* Backward (*Hz*)	15,000*rpm* Forward (*Hz*)
Rigid 1	70	69	70
Rigid 2	90	88	92
Flexible 1	134	130	138
Flexible 2	413	345	476
Flexible 3	766	719	822
Flexible 4	1,139	1,043	1,287
Flexible 5	2,643	2,627	2,663

Table 6. 1: Rotor natural frequencies

As the AMB is powered in differential driving mode, it can be considered as linear in the range of nominal displacements. Thus, it is taken into account with a current

stiffness of -138$N.A^{-1}$ and a negative stiffness of -0.34$N.\mu m^{-1}$. These values were estimated with respect to the bearing geometry. The electronic part of AMB is represented with a first order low pass filter with a cut-off frequency of 2kHz.

Polar fuzzy controller

The SPID coefficients chosen for the academic test rig were intentionally simple in the low frequency range. In order to generalize the design process, the coefficients were chosen such that the damping was almost constant and with a low constant slope for the stiffness for the operating range considered as shown in Figure 6. 4. The stiffness is plotted on the critical speed map. Strictly speaking, they are the natural frequencies and not the critical speeds, i.e. the analysis was done without considering gyroscopic effects. The gyroscopic effect was very low on the three first modes and the fourth critical speed was about 100Hz higher than its related natural frequency.

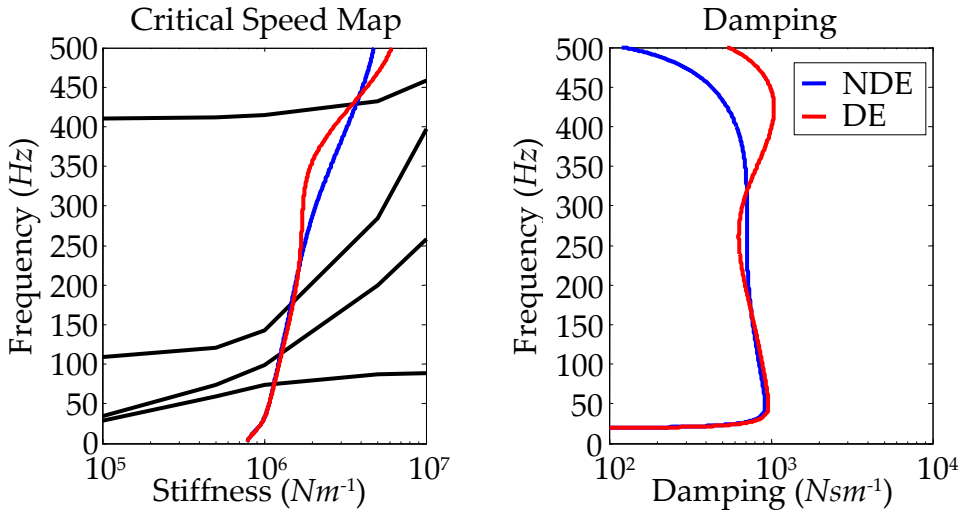

Figure 6. 4: Standardized stiffness and damping (Red DE, Blue NDE)

Finally, the fuzzy controller and the synchronous filter have the characteristics discussed in the previous chapter.

Misalignments

In this section, the positions of the bearings are studied since the misalignments could explain some differences between experimental and numerical results in the next sections. The static control currents that enable to support the weight of the rotor give a good idea of the degree of misalignment of magnetic bearings. They are

represented in Figure 6. 5 and compared to numerical prediction in Table 6. 2. The static currents were measured also with the motor coupling removed, and the coupling effect was revealed negligible.

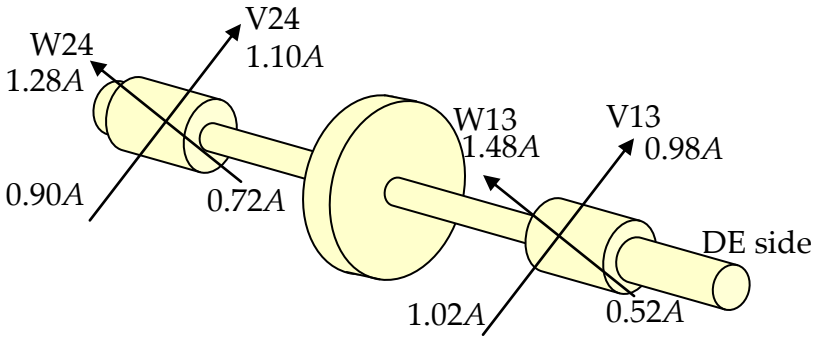

Figure 6. 5: Static currents

Regarding experimental results, it is clear that there are assembly errors. Only the V24 static current matches numerical predictions. As the rotor is centred relatively to the auxiliary bearing, it is very common that the two bearings are not perfectly concentric and consequently current and negative stiffness are slightly modified.

	DE		NDE	
	V13	W13	V24	W24
Load (*N*)	34.2		25.0	
Numerically (*A*)	-0.175		-0.128	
Experimentally (*A*)	0.016	-0.484	-0.102	-0.281

Table 6. 2: Static control currents

Let us consider that the relation (3.15) between force, current and position is suitable. Hence, it is possible to determine the position of the rotor inside the magnetic bearing (see Table 6. 3).

	DE		NDE	
	V13	W13	V24	W24
Rotor position (μm)	75.5	-132.3	10.8	-64.1

Table 6. 3: Position inside the magnetic bearing

It seems that there is important errors mainly on DE bearing. The estimated position of the rotor on the DE side bearing is presented in Figure 6. 6. Prins et al. [2007] present a second method to identify the centre of the magnetic bearing using bias current perturbation. The current in the upper electromagnet i_{up} and the current in the lower i_{low} are used in order to estimate the rotor position.

$$\Delta x = \frac{2g_0 + \frac{L_S + L_R}{\mu_r}}{2\cos(\alpha)} \frac{i_{up1}^2 + i_{low1}^2 - i_{up2}^2 - i_{low2}^2 \pm 2\sqrt{\left(i_{up1}^2 - i_{up2}^2\right)\left(i_{low1}^2 - i_{low2}^2\right)}}{i_{up2}^2 - i_{low2}^2 - i_{up1}^2 + i_{low1}^2} \quad \textbf{6. 1}$$

This method is interesting since it minimized the number of parameter supposed known. The method needs iteration to be efficient and then cannot converge if the centre is not in the range of auxiliary bearing clearance. Applying these methods, the centre of NDE magnetic bearing seems 10μm lower on V24 and 50μm upper on W24 than the actual position. On the other hand, the centre of DE magnetic bearing seems slightly out of auxiliary bearing clearance. Thus, these results confirm the results of the first method.

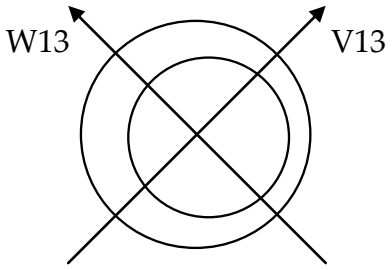

Figure 6. 6: Estimated position of the rotor

However, the two methods suppose that the bearing is known and there is only parallel offset misalignment error. Modelling parallel offset misalignment is quite easy, but it is much more difficult to study angular offset misalignments. On real systems, there are both and it is difficult to differentiate the contribution of each one (Figure 6. 7).

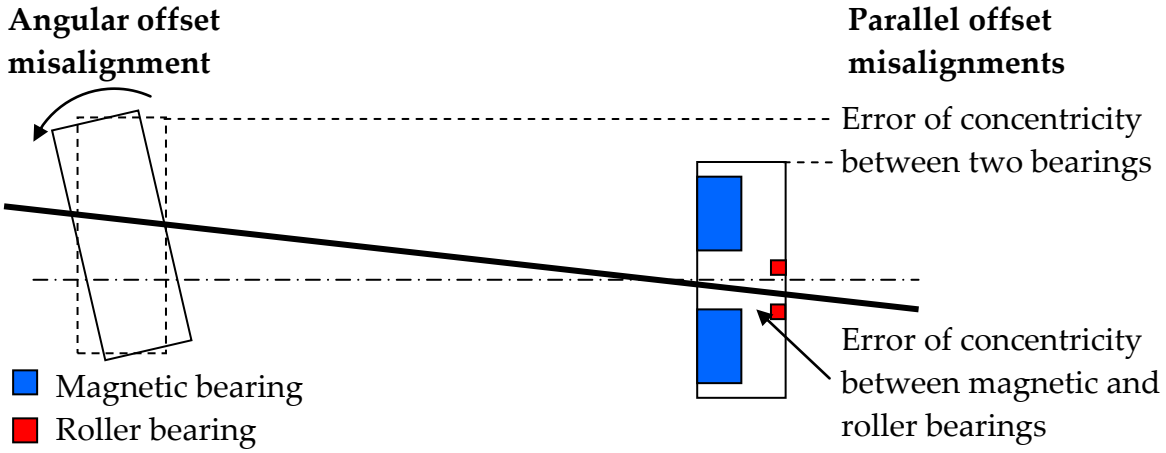

Figure 6. 7: Three misalignment errors

Finally, based on these results and our observations of the test rig, the estimated positions of the two bearings are shown in Figure 6. 8.

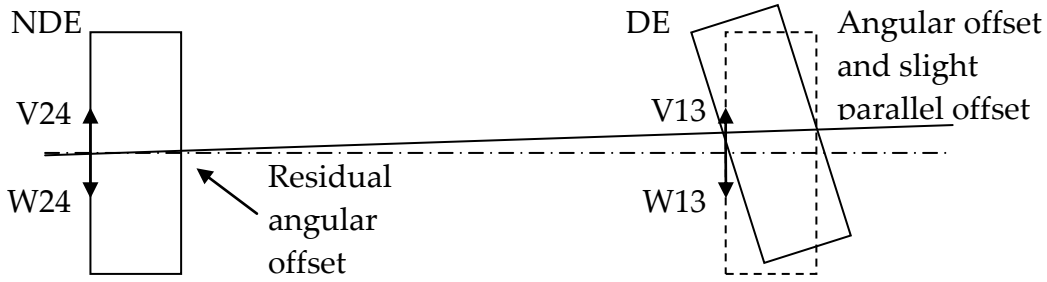

Figure 6. 8: Estimated real position (Top view)

As we are unable neither to measure angular misalignments nor to modelling them, no misalignment is considered in the numerical model.

Calibration of current stiffness

The negative and current stiffness of the bearings are investigated. In mechanics, the general approach is to identify the experimental system in order to adjust the numerical model. Here, the prevalent parameter is the current stiffness. Thus, it could be interesting to consider this parameter unknown, to measure it and to modify the controller accordingly. This method can be considered as a calibration as it is currently done for sensor sensitivity.

The calibration was performed on unbalance responses. The main sources of deviations between numerical and experimental results were studied: time delay, bearing asymmetry, negative stiffness and current stiffness. Time delay acts more on high frequency stability than on performances. Asymmetry can explain the differences between the measurement obtained in the two orthogonal directions (V and W), but even for our case with an important asymmetry, this effect is not responsible for the global trend of unbalance responses. Finally, unbalance response is less sensitive to negative stiffness than current one. Consequently, it appears that the current stiffness is the main parameter.

A heuristic method has enabled to identify that experimental current stiffness was 30% below estimation. The error is huge and only a complete identification of the bearing could explain it, as the values stemming from measured currents and estimated positions are somewhat different (Table 6. 4).

	DE		NDE	
	V13	W13	V24	W24
Current Stiffness (NA^{-1})	-151.5	-135.3	-139.1	-135.7
Negative Stiffness ($daN\mu m^{-1}$)	-0.394	-0.297	-0.340	-0.317

Table 6. 4: Current stiffness & negative stiffness

Where:

$$K_x = -16\cos^2(\alpha)\mu_0 SN^2\left[\frac{(I_0 - I_W)^2}{\left(\frac{L_S+L_R}{\mu_r}+2g_0-2\cos(\alpha)x_0\right)^3}+\frac{(I_0+I_W)^2}{\left(\frac{L_S+L_R}{\mu_r}+2g_0+2\cos(\alpha)x_0\right)^3}\right], \text{ and}$$

$$K_i = -8\cos(\alpha)\mu_0 SN^2\left[\frac{I_0 - I_W}{\left(\frac{L_S+L_R}{\mu_r}+2g_0-2\cos(\alpha)x_0\right)^2}+\frac{I_0+I_W}{\left(\frac{L_S+L_R}{\mu_r}+2g_0+2\cos(\alpha)x_0\right)^2}\right]$$

If x_0 negligible, then

$$\frac{K_x}{K_i} = \frac{2\cos(\alpha)}{I_0}\frac{I_0^2+I_W^2}{\frac{L_S+L_R}{\mu_r}+2g_0} \qquad \textbf{6. 2}$$

Schweitzer and Maslen [2009] show that by applying a position offset, it is possible and simple to measure the ratio of negative stiffness over current stiffness.

$$K_i i_1 - K_x x_1 = K_i i_2 - K_x x_2 \Leftrightarrow K_x = K_i\frac{i_1 - i_2}{x_1 - x_2} \qquad \textbf{6. 3}$$

This relation is used to compare the "analytical results" with the experimental results. The measurements were performed with ±50μm of position offset. The results are presented in the Table 6. 5.

$\frac{K_x}{K_i}$ ($A.m^{-1}$)	DE		NDE	
	V13	W13	V24	W24
Analytically	2,601	2,194	2,446	2,337
Experimentally	2,300	1,950	2,650	2,500
Error (%)	-13	-13	8	7

Table 6. 5: Negative over current stiffness

The results are convenient. Thus, considering only the model there are four possibilities:

- A modelling error cannot be completely excluded, even if the probability is supposed low in our case.
- The error comes from one of these parameters: the pole surface, the number of turn in coils or magnetic permeability of vacuum space. The probability for that seems still lower.

- The error comes from one or more phenomenon not taken into account in the model. It could be angular misalignment, eddy currents, magnetic hysteresis or the relative permeability of the iron depends on the frequency.
- The error stems from the high parallel offset measured and manufacturing tolerances. This hypothesis is the most likely; indeed the error on the ratio K_x over K_i could be squared. For the axis V24, where the misalignment can be neglected the ratio is proportional to the inverse of the complete equivalent air gap (see equation 6.2), whereas the current stiffness is proportional to the inverse of the square of this value. In addition, the high misalignment could lead to more non-linear effects and important errors stemming from actuator linearization. Therefore, an important part of the error is stemming from the misalignment.

A particular attention has been paid to the high frequency gain of the SPID controller in order to be sure that both controllers (PID and SPID) have equivalent high frequency robustness and tuning difficulty. Thus, the two controllers have almost the same gain for high frequencies. Consequently, all the controllers have been tuned for the test rig current stiffness, obviously the delivered PID but also the SPID and the polar fuzzy controller.

In the following, the numerical model was modified to correspond to the test rig behaviour. A negative stiffness of $-0.34 N.\mu m^{-1}$ with a current stiffness of $-97 N.A^{-1}$ are considered for numerical computations.

Comparison of numerical and experimental results

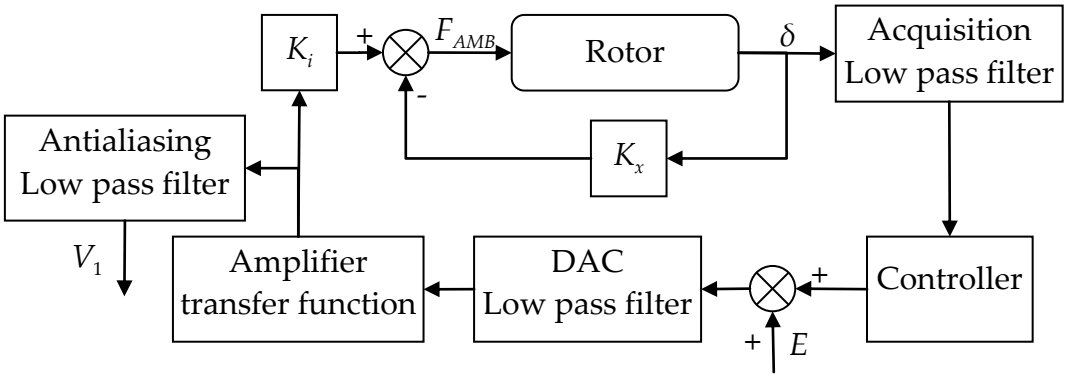

Figure 6. 9: Measurement of sensitivity function

Experimental and numerical results are compared. The sensitivity function, the natural frequencies and unbalance responses are studied. On the other hand, the characteristics of the system controlled with the supplied controller are studied. These characteristics will be compared with the results obtained with the new

controller in Chapter 7. In addition, as the same modelling approach is used for the compressor, this study makes it possible to quantify the differences between numerical simulations and experimental results and to extrapolate the results that we could obtain on a real compressor.

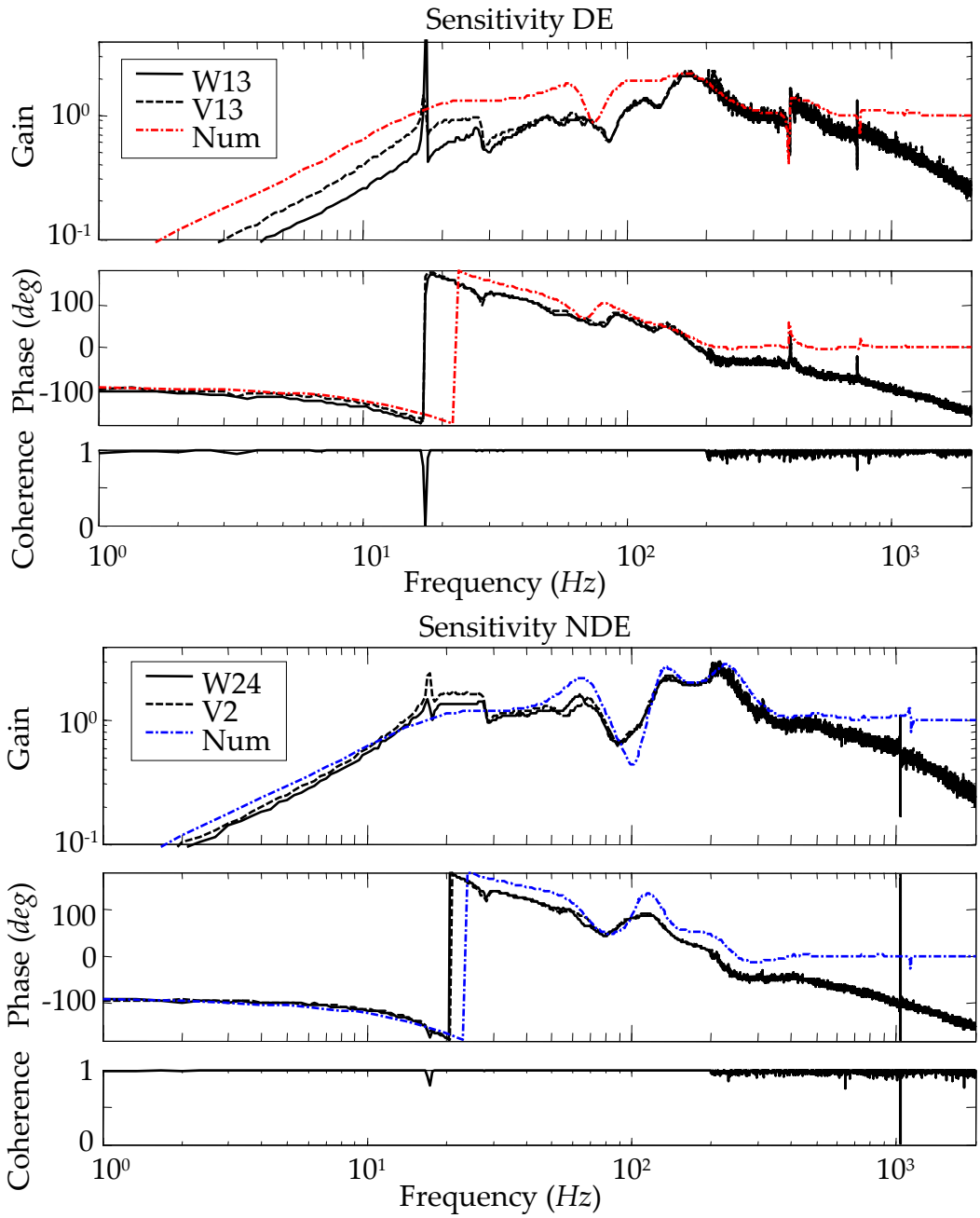

Figure 6. 10: Comparison of sensitivity functions

Remark 1: The phase curves are wrapped.

Remark 2: The bearings are considered symmetric for numerical computations, therefore for each bearing there are one numerical result and two experimental results

Theoretically, the respective limits of the sensitivity gain and phase for high frequencies are one and zero. In experimental results, the gain and phase decrease due to amplifier transfer function and antialiasing filters, as shown in Figure 6. 9. This protocol was used because the controller output signal was not available for the supplied controller. Thus, the experimental method used for sensitivity function measurement differs slightly from the one recommended by ISO 14 839. The curve must be rectified by mind to be compared with numerical results (Figure 6. 10).

Experimental results are far richer than numerical one. In the low frequency range, there are several peaks, whereas there is only one with numerical computations. Beyond 150*Hz* the results are close and the natural frequencies are quite the same as indicated in Table 6. 7. It is worth mentioning that the rigid body modes are mainly managed by bearings whereas flexible modes are managed by rotor itself. Thus, the rotor model seem appropriate but even with the calibration the bearing model is not satisfactory.

The calibration was done on the unbalance response. Hence, the model is mainly calibrated for the first bending mode and the NDE bearing, since bending mode is mainly visible on NDE side. In addition, the misalignment is more important on DE side. Thus, it is not surprising that the numerical and the experimental results matches better on NDE sensitivities.

The two modes at 17*Hz* and 27*Hz* present in experimental results of both controllers was identified as foundation modes. From our observations, the mode at 17*Hz* corresponds to the vertical vibration of the test rig frame on its rubber feet; the one at 27*Hz* corresponds to the bending mode of the table supporting the test rig. In addition, other peaks in the low frequency range could be also identified as stator modes of vibration.

The bad coherence at 17*Hz* indicates that there is a resonance, but its amplitude is over estimated. This was confirmed by a more precise measurement of the sensitivity function value around this frequency.

From these results, it is quite difficult to know if the damping of the high frequency modes was well estimated by numerical computations.

Finally, the most important thing to notice is that the maximum of the sensitivity was well estimated and experimental is inferior to the numerical one for both bearings as shown in Table 6. 6.

Maximum peak of sensitivity	Numerical	Experimental
DE	2.2	2.2
NDE	2.9	2.8

Table 6. 6: Stability margins

Natural frequencies	Numerical (*Hz*)	Experimental (*Hz*)
Flexible 2	414	414
Flexible 3	765	743
Flexible 4	1,140	1,040

Table 6. 7: Natural frequencies

The two rigid body modes and the first flexible mode are too damped to estimate their frequency with the sensitivity function. The high natural frequencies of the system (where the estimation is more reliable) are compared in Table 6. 7. The estimation of natural frequencies is satisfactory. Nevertheless, even for a quite simple rotor it is not so easy to obtain the good frequencies. Here the main difficulty was the bolted planes. The stiffness reduction, seen experimentally, was anticipated by considering a smaller shaft section than the actual around these planes as shown in Figure 6. 3. However, this correction seems insufficient.

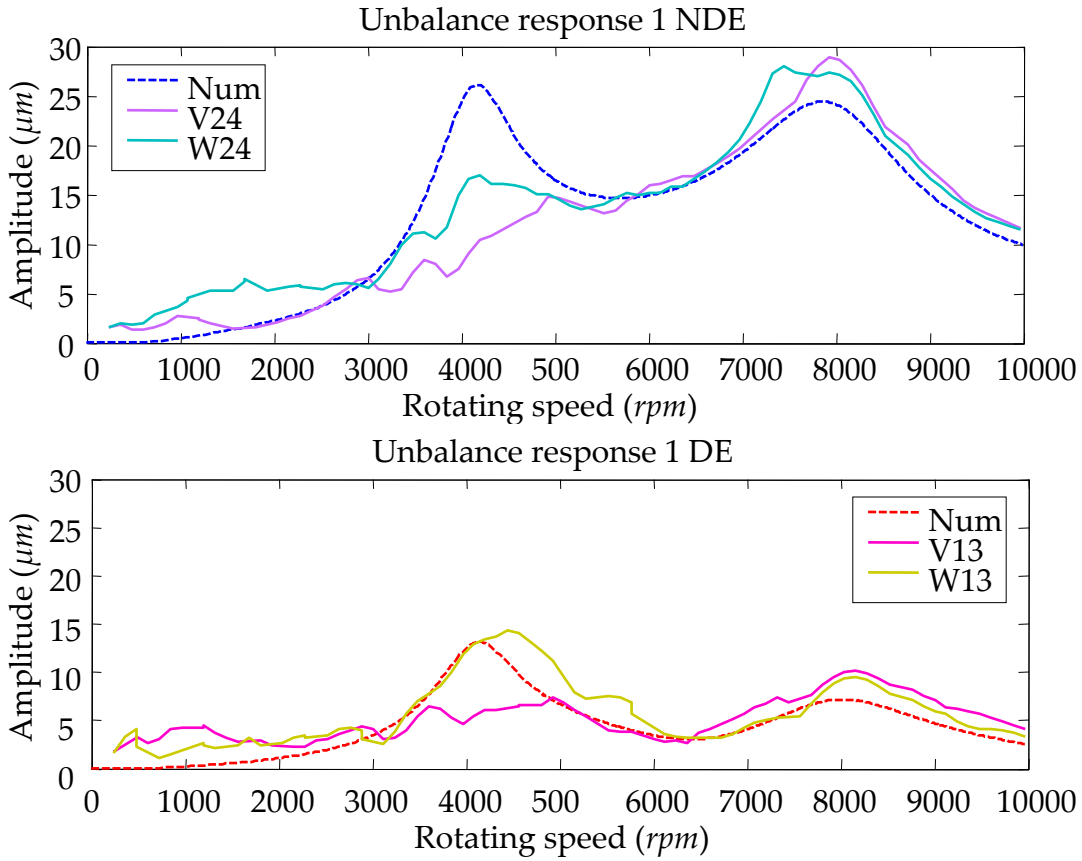

Figure 6. 11: Response with unbalance on plane 2

API 617 [2002] recommends carrying out the unbalance tests during coastdown, with fixed increment of speed. The tests performed are slightly different, since they are performed during run-up with low acceleration from 0-10,000*rpm* (50*rpm*/*s*). The sampling frequency equals 2*kHz*. Time windows of 0.5*s* are extracted from run-up

measurements. Fast Fourier Transforms (FFTs) computed on these signals have a resolution of 2*Hz*. Therefore, the rotational speed can be supposed constant.

This method was used because it was more convenient to obtain automatically the unbalance response on the overall range of speed with a small step of rotating speed.

The numerical and experimental results were compared for two unbalance distributions as presented in Figure 6. 11 and Figure 6. 12. First, with an unbalance of 25.35*g.mm* placed on the central disk (plane 2). Second, with two opposite unbalances of 11.82*g.mm* and 9.63*g.mm* respectively placed on planes 1 and 3. The unbalances are different in order to take into account the difference of load on the two bearings.

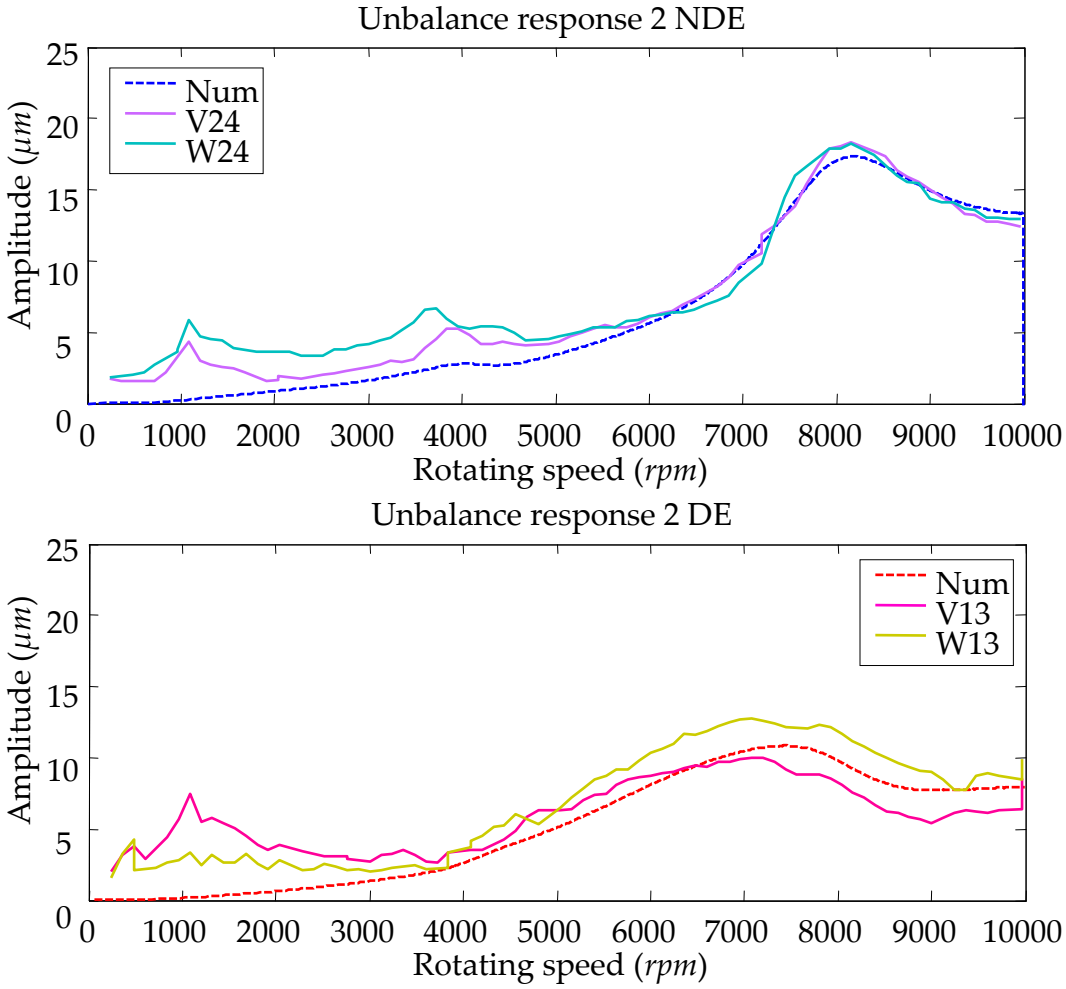

Figure 6. 12: Response with unbalances on plane 1 and 3

The bending critical speed responses were correctly estimated. As for sensitivity the rigid body critical speeds response is far from experimental results. Nevertheless, the difference between the two measurement axes is of the same order of magnitude as the difference between numerical and experimental. Consequently, the results obtained can be considered as satisfactory.

From the two resonances visible at low frequency on sensitivity transfer functions (17*Hz* and 27*Hz*) only the first is present on unbalance responses (1,020*rpm*). Although, it seems to be a backward cylindrical mode from orbits, it is interesting to see that it is mainly excited by the second unbalance distribution.

Finally, the main differences can be attributed to misalignment since there is not the same behaviour on the two axes of each bearing.

Validation of numerical predictions

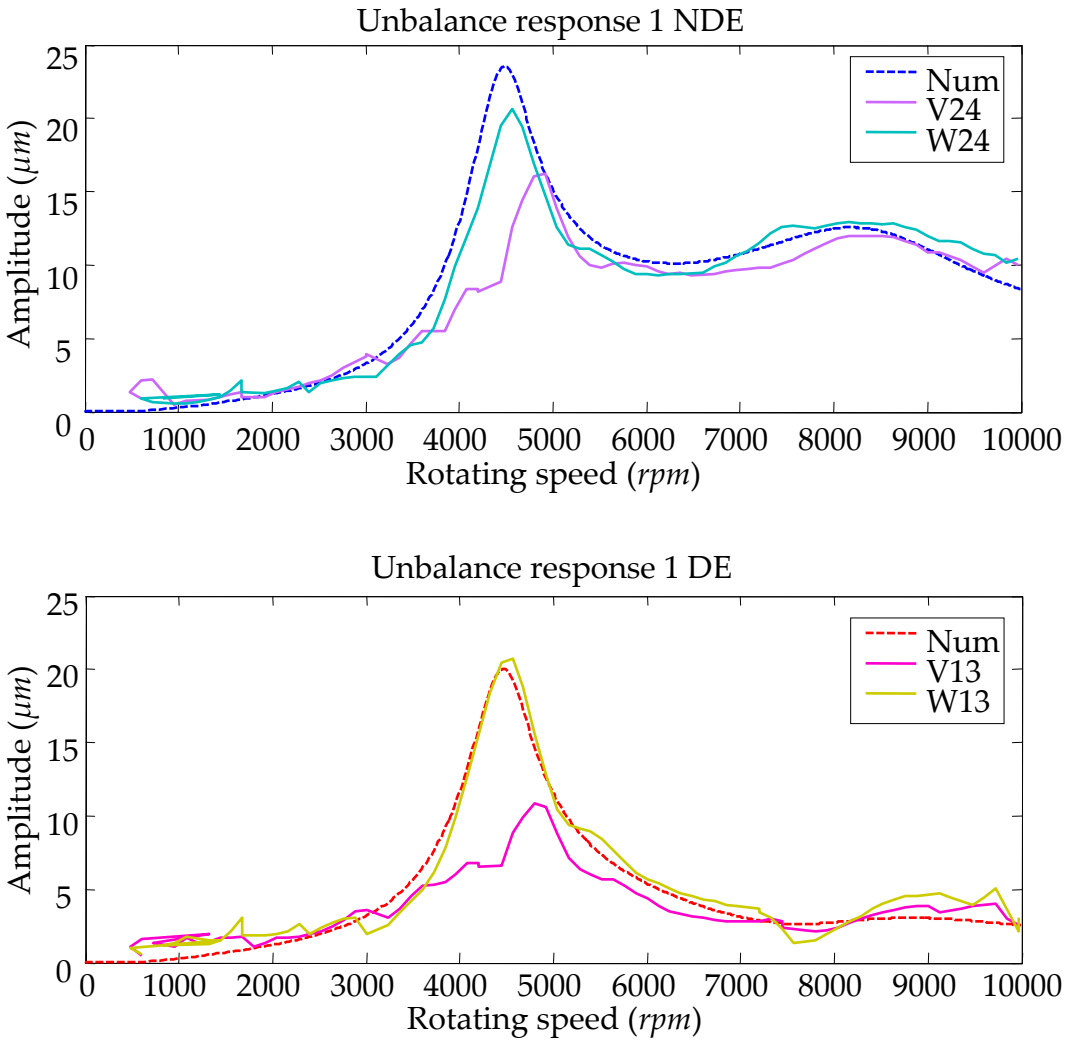

Figure 6. 13: Response with unbalance on plane 2

In the previous section, the controller has been calibrated in order to obtain numerical results with the same trend as experimental ones. For an industrial point of view, it is preferable to adjust the test rig parameters and not the numerical model. The controller should be calibrated in order to obtain the same electrical stiffness as the one used for numerical computation. Then, the machine exhibits the forecast

behaviour and there is no need for addition computations. A test was performed in order to show that this method is possible. The results are presented in Figure 6. 13. The controller gain was increased by 43% on the test rig, this induced a same gain for the overall action line as the one used during numerical predictions.

The experimental and numerical responses to an unbalance of 25.35$g.mm$ placed on the central disk are shown in Figure 6. 13. The error on the critical speed value is less than 2% for the main critical speed. In addition, the maximum experimental displacement is less than the numerical result. Thus, from an API 617 point of view the results are satisfying. Nevertheless, due to the asymmetry the first critical speed is split into two critical speeds. The second on the V axes is less important, but the critical speed value is 8% higher than the predicted value.

Conclusions

During this thesis, an important effort has been done in order to predict correctly the dynamic behaviour of rotors supported by AMBs.

A first source of errors is well identified. The misalignment leads to a rich dynamic behaviour in the low frequency range and it is impossible for the moment to explain all the visible phenomena. For example, it is worth mentioning that the misalignment errors seem higher on W axes, whereas the difference of behaviour between prediction and measurement are more important on V axes. Thus, it would be interesting to set up a model of magnetic bearing with an angle of misalignment. This model could permit a better understanding of these phenomena. Nevertheless, even with a perfect model it will be impossible to predict the behaviour, since misalignment is a random phenomenon. Consequently, there is more to do on the manufacturing quality than on modelling.

It could have a second source. It could be eddy currents, magnetic hysteresis or the relative permeability of the iron depends on the frequency. In all the cases, it was demonstrated that this phenomenon can be compensated by calibrating the controller. In addition, the results with the two values of current stiffness (action line gain) give the predicted results, and this confirms that it is the prevalent parameter.

In the future, an identification of the actuator behaviour and a precise modelling of all of the physical phenomena could permit to predict correctly the final behaviour. Nevertheless, this estimation of the actuator behaviour could be reasonably done only, if the whole characteristics of actuators are available. Although, we do not have such information for the moment, at least the materials, the geometry and the amplifier control should be known.

The comparison of numerical predictions with experimental results allows us to have a relative confidence in the numerical results obtained and exhibited in the Chapters 7 and 8.

Chapter 7 – POLAR FUZZY CONTROLLER ASSESSMENT

The aim of this study is to assess numerically and experimentally the control strategy developed. The stability, the robustness and the performances of the system equipped with the polar fuzzy controller are highlighted through different tests. In the following, experimental and numerical results are presented. Most of time only one of them is presented in function of the needs, the clarity or the technical possibilities. Only the more relevant characteristics have been measured.

The fuzzy controller was compared with the initial augmented PID controller delivered with the test rig. Five case studies were performed:

1. The sensitivity, that permits to quantify the system robustness.
2. The closed loop transfer function in order to assess the sensitivity of the system to noise of measurement.
3. The dynamic stiffness computation and amplification factors evaluation, which are related to the system performances and the severity of resonance frequencies.
4. The unbalance responses, for the assessment of the rotor dynamic behaviour.
5. The response to subsynchronous excitations is measured to estimate the capacity of the controller to manage disturbances as aerodynamics ones.

The polar fuzzy controller modulates the gain of the underlying SPID controller. As this controller is non-linear, the transfer functions are not defined. Moreover, the fuzzy controller applies targeted actions. Consequently, the transfer functions of the system controlled with the SPID appear sufficient for a first evaluation.

The polar fuzzy controller modifies mainly the synchronous characteristics of the system with tangential damping and the low frequency performances with the increase of the radial stiffness. Therefore, it can be considered that the differences between polar fuzzy controller and SPID are mainly in the operating frequency range.

Sensitivity

The sensitivity of the system controlled with the SPID controller was computed and measured. As for the PID controller, the NDE sensitivity function was correctly predicted, but the error on the DE side was important as shown in Figure 7. 1. Consequently, the maximum of sensitivity was over estimated and the test rig is

more robust than predicted. Once again, the error can be due to the misalignment of the DE bearing.

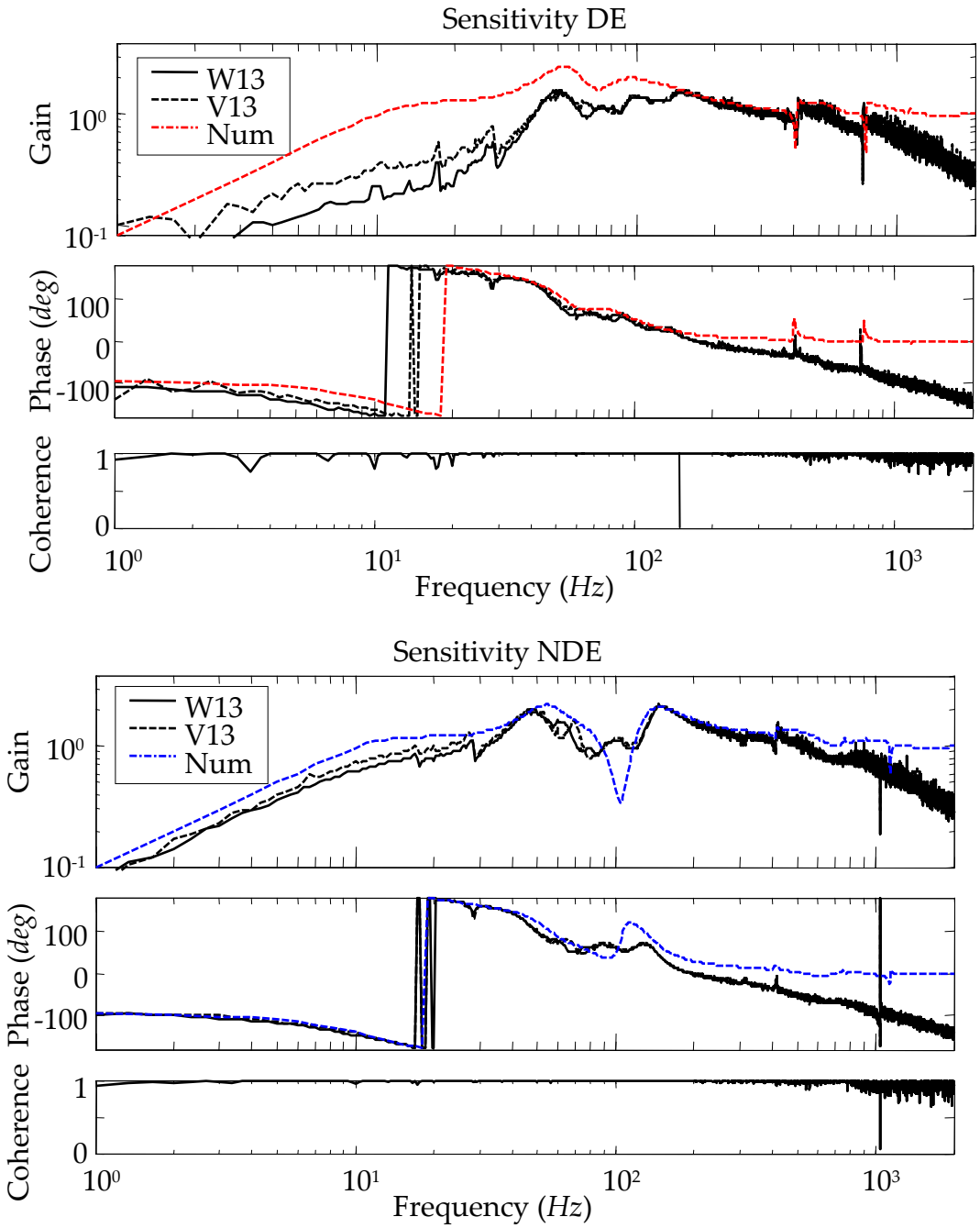

Figure 7. 1: Comparison of sensitivities for the SPID controller

The sensitivity of the SPID was measured with a maximum value of 2.2. The sensitivity stemming from the manufacturer controller (here called PID) reached 2.8, leading to 20% of improvement as indicated in Table 7. 1. Eventually, the sensitivity analysis shows that the system has satisfying stability margins.

Maximum peak of sensitivity	SPID Numerical		SPID Experimental	PID Experimental
	At rest	10000*rpm*	At rest	At rest
DE	2.5	2.5	1.6	2.2
NDE	2.2	2.2	2.2	2.8

Table 7. 1: Stability margins

Closed loop transfer function

The low frequency gain, of the Closed Loop Transfer Function (CLTF), must equal one in order to ensure that the system follows the setting point. For a levitated rotor, this enables to keep the rotor in the centre of the bearings. The high frequency gain must be low to ensure system robustness. Finally, the maximum gain must be as low as possible to avoid measurement noise amplification.

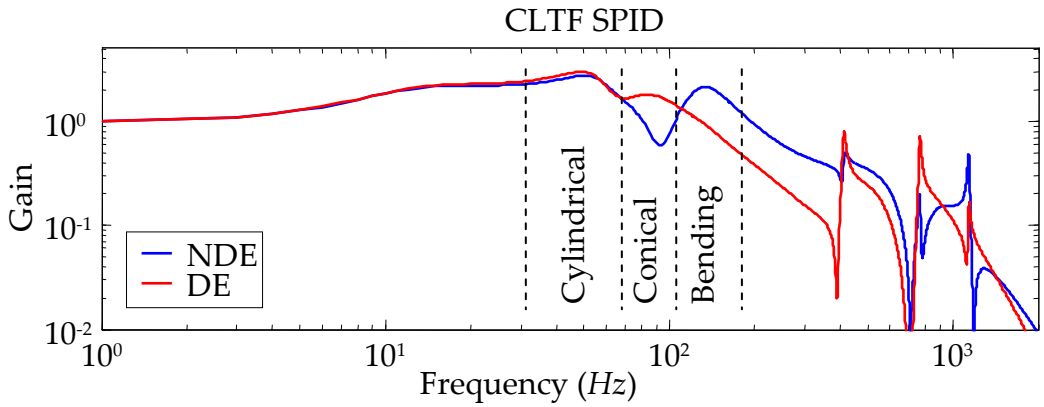

Figure 7. 2: Numerical CLTFs

The CLTFs are shown in Figure 7. 2. The CLTFs are much more difficult to measure than the sensitivity, because the gain is lower and consequently the measurement is more disturbed by noise. Nevertheless, there is a direct relationship between the two transfer functions as:

$$G_S + G_C = 1 \qquad \textbf{7. 1}$$

Thus, the experimental results can be deduced from sensitivity measurement in the low frequency range. On the NDE side the sensitivity is well estimated then the CLTF too. However, on the DE side the actual sensitivity gain is quite nil hence, the CLTF gain is closer to the value one than predicted.

Globally, the two controllers have the same CLTF characteristics, as indicated in Table 7. 2. Even more than predicted, because the two absolute maxima are likely to be on NDE bearing. Finally, the SPID is 3% more sensitive to noise of measurement, and both controllers are suitable.

Maximum peak of CLTF	Numerical SPID		Numerical PID	
	At rest	10000*rpm*	At rest	10000*rpm*
DE	3.0	3.0	2.3	2.3
NDE	2.7	2.8	2.9	2.9

Table 7. 2: Measurement noise sensitivity

Dynamic stiffness

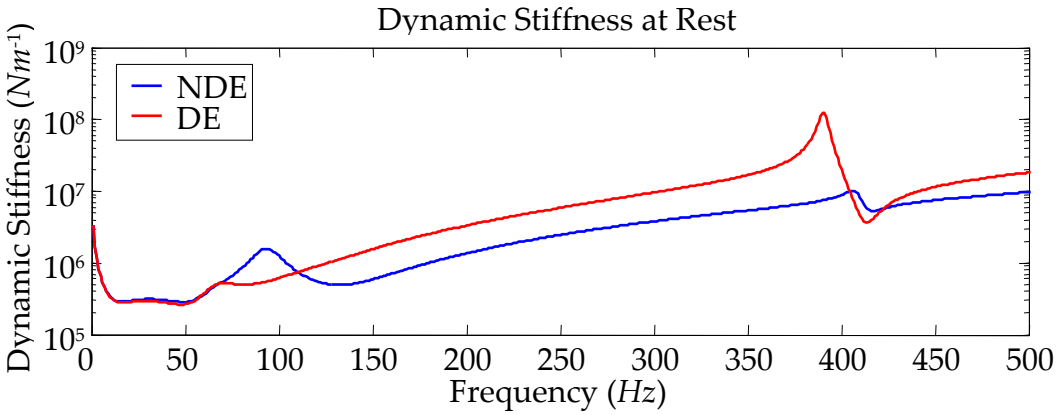

Figure 7. 3: Numerical Dynamic stiffness of the bearings

Usually, mechanical structures are identified by measuring the transfer function between an exciting force and the corresponding displacement (admittance). For magnetic bearings, the dynamic stiffness K_{Dyn} is preferred, it is the gain of the inverse of this transfer function, when the force is applied at actuator location and the displacement measured at bearing sensor location. Thus, the dynamic stiffness can be measured easily.

The dynamic stiffness of the system, when the rotor is levitated in standstill conditions is shown in Figure 7. 3. From a mechanical behaviour point of view, this curve is one of the most interesting. It gives a precise idea of the bearing capacity to reject disturbances. The dynamic stiffness is shown until 500*Hz*, as this curve is used essentially in order to analyse the dynamic behaviour in the operating frequency range. In addition, the high frequency characteristics can be deduced from CLTF as explained in the following.

The minimum of the dynamic stiffness function quantifies the performance of the bearing. This minimum should be specified according to the machine application. The results with the PID and SPID controllers are compared in Table 7. 3. The PID controller delivered with the test rig exhibits better performances than our SPID controller, as the minimum is decreased by 9.6%. Thus, for a same disturbance (in the low frequency range) the displacements level would be higher with the SPID.

Minimum of Dynamic Stiffness ($N/\mu m$)	Numerical SPID		Numerical PID	
	At rest	$10000 rpm$	At rest	$10000 rpm$
DE	0.264	0.263	0.292	0.292
NDE	0.285	0.285	0.313	0.313

Table 7. 3: Disturbance rejection

Generally, the first rigid body mode is split into two peaks as shown in Figure 7. 3. The first minimum, at $16Hz$ for our case, is not a mode of vibration, even if the shape is the one of the cylindrical mode (stator modes are not considered in the model). This peak is produced by the stiffness variation. Where, for a typical mechanical mass-spring system the stiffness is constant, here it has large variations. At very low frequencies, the stiffness can be considered infinite due to the integral part. It decreases with a minimum value around the minimum gain in the Bode diagram ($12Hz$) and then increases. Thus, the value and the frequency of this peak can be estimated from the bode diagram.

$$\min_1\left(K_{Dyn}\right) \approx \min\left(G_{AMB}\right) + K_x = 0.28 Nm^{-1} \qquad \textbf{7. 2}$$

The minimum value of this peak can be improved by increasing the integral gain, leading to an increase of stiffness but also to an attenuation of damping.

The second minimum at $49Hz$ is the first rigid body mode. It can be improved by increasing damping at this frequency. Consequently, the improvement of the first one leads to the deterioration of the second one. From a mechanical point of view, the second is more important since it quantifies the severity of a resonance frequency. The two peaks can be merged, in this case, it will be difficult to assess the first rigid body mode with the dynamic stiffness.

The amplification factor is valuable to estimate the severity of a mechanical resonance. The amplification factor is the ratio of the mechanical energy of the system over the energy provided by the external forces during one cycle at the resonance for permanent conditions. More the AF is high more the energy dissipated by the system is low. API 617 [2002] specifies that the log decrement shall be at least 0.1, which is equivalent to a maximum AF of 31.4 by using:

$$\log decrement = \frac{2\pi}{\sqrt{4AF^2 - 1}} \qquad \textbf{7. 3}$$

There is no direct method that enables to quantify the AF. The half power point method used in API 617 [2002] to assess unbalance responses must be seen as a definition. Since, this formula is suitable only for uncoupled oscillator with high AF and should be measured on velocity (with the mobility) and not on displacement. Alternative methods exist, Matsushita et al. [2005] proposed to compute a function that gives the AF for each mode. Here, as a first estimation half power point method is used, the results are summarized in Table 7. 4.

Natural frequencies (*Hz*)	AF DE	AF NDE
16	1	1
49	2	1.9
82	-	-
132	-	2.8
414	34.5	11
765	59	40
1140	48	63

Table 7. 4: Severity of resonance frequencies

As usual for mechanical system identification, the AF evaluations are calculated from the admittance (inverse of the dynamic stiffness G_{Dyn}). They can be also calculated from the CLTF, as in ISO 14839-3 [2006]. The difference is the bearing transfer function, which can be supposed to have small variations around a resonance frequency. In addition, the AF of the first rigid body mode is easier to assess.

$$G_C = \frac{G_{AMB}}{G_{Dyn}} \qquad \textbf{7. 4}$$

The modes belonging to the operating speed range have a small amplification factor. Sometimes, the AF is too small to be calculated with this method. In this case, the behaviour can be considered as acceptable. However, the AF increases with higher frequency modes. The AF of the free-free rotor modes has been chosen equal to 100. Thus, the controller applies damping to all the modes in its frequency bandwidth. There is no requirement for high frequency modes in the standards, because API 617 [2002] requirement is appropriate for fluid film bearings, and for the first rigid mode assessment. Finally, these values seem sufficient, since they are lower than 100 and the test rig is running well.

Unbalance responses

			Unbalance at 2 12.79$g.mm$			Opposite unbalances at 1&3 (1 - 7.39$g.mm$, 3 - 5.40$g.mm$)		
			AF	Disp. pp μm	Cur. A	AF	Disp. pp μm	Cur. A
DE	Cyl.	SPID	**2.6**	12.1	0.081	-	-	-
		Fuzzy	2.6	10.9	0.085	1.6	5.3	-
		PID	**4.8**	13.3	0.072	-	-	-
	Conic.	SPID	-	-	-	-	-	-
		Fuzzy	-	-	-	-	-	-
		PID	-	-	-	-	-	-
	Bend.	SPID	-	-	-	1.0	7.2	0.068
		Fuzzy	-	-	-	-	5.4	0.070
		PID	5.0	7.3	0.059	2.4	13.0	0.100
NDE	Cyl.	SPID	2.1	**13.7**	0.092	-	-	-
		Fuzzy	**3.0**	**13.3**	**0.104**	-	-	-
		PID	4.2	**26.5**	**0.141**	-	-	-
	Conic.	SPID	-	-	-	-	-	-
		Fuzzy	-	-	-	-	-	-
		PID	-	-	-	-	-	-
	Bend.	SPID	-	-	-	-	9.6	**0.095**
		Fuzzy	-	-	-	-	6.0	0.076
		PID	3.8	24.6	0.129	4.7	19.9	0.106

Table 7. 5: Table Unbalance response assessment

First numerical assessments were performed. The results obtained are summarized in Table 7. 5. The empty cells correspond to non-measurable values. The unbalances were applied according to API 607 [2002] requirements. Considering the controller developed, the AFs are slightly higher than the recommended values, but we consider it acceptable since calculations were performed without SF in the control loop. The displacements have a limited amplitude and the forces are within the capacities of the bearings. Thus, this controller can be applied experimentally. It is worth mentioning that the fuzzy controller improve mainly the bending critical speed response, as the worst behaviour is exhibits for the first critical speed, there is no global improvement between SPID and fuzzy controllers for this specific case. In addition, the performances of the SPID for these case studies are already satisfying. Thus, the fuzzy controller is partially set on leading to particular behaviour, where the AF is increased. In this case, the AF value is no more representative of the damping.

In addition, fuzzy controller exhibits better unbalance responses than the PID. The maximum AF is reduced by 37%, the displacement by 50% and the control current by 26%. Thus, the fuzzy controller enables notable improvements.

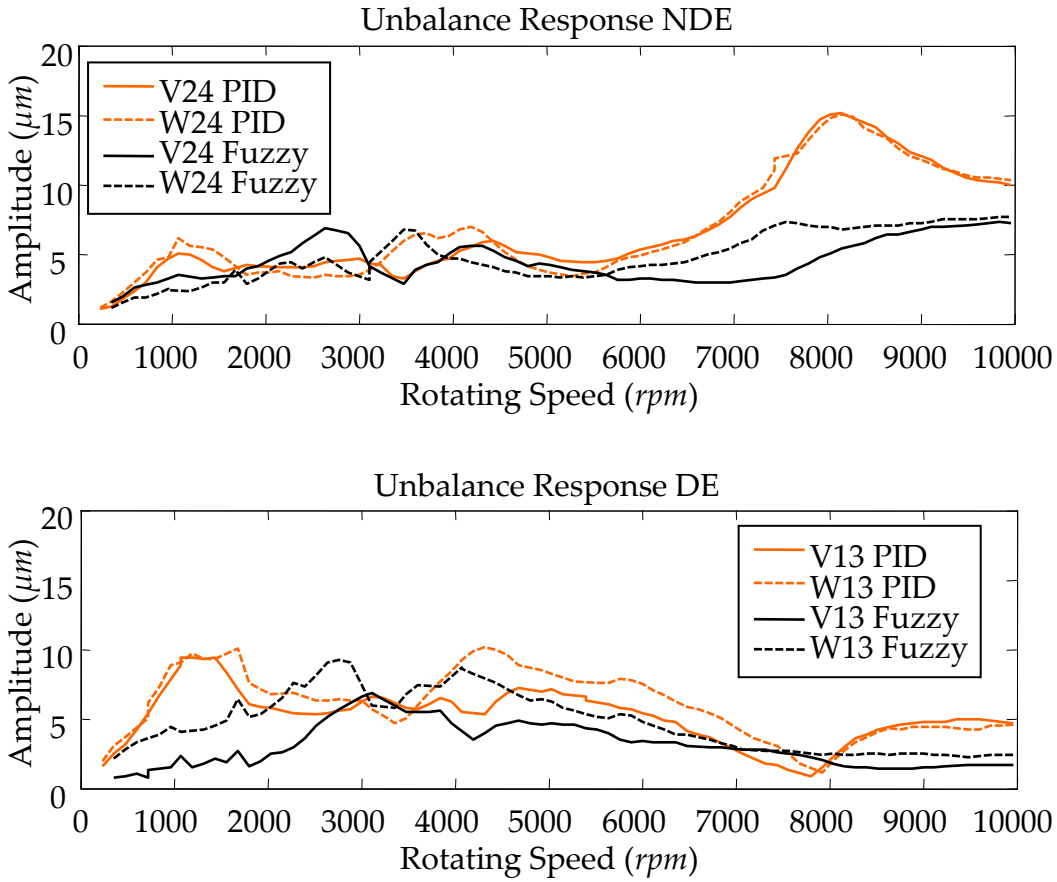

Figure 7. 4: Synchronous responses

For experimental evaluation, the unknown initial unbalance was considered. The synchronous vibrations were measured, in the conditions explained in Chapter 6, for the initial PID controller and for the polar fuzzy controller alone as shown in Figure 7. 4. The results emphasise the asymmetry of the bearings and the complexity of the dynamic response at low rotational speed. The modes at 17*Hz* and 27*Hz* are visible (1020*rpm* and 1620*rpm*). The critical speeds due to the cylindrical mode at 4200*rpm* and the bending mode around 9000*rpm* are clearly identified. There is one or two additional critical speeds not identified around 3,000*rpm*. Finally, it seems that as for the response plotted in Figure 6. 11, there is on the axis W24 (for the fuzzy controller) a critical speed at 7500*rpm*. This critical speed could be the bending backward critical speed. The conical mode was damped too strongly to appear in the unbalance response as predicted by numerical simulations. Finally, the maximum synchronous displacement was reduced by 37% by using polar fuzzy controller, a reduction in the same order of magnitude than the predicted value.

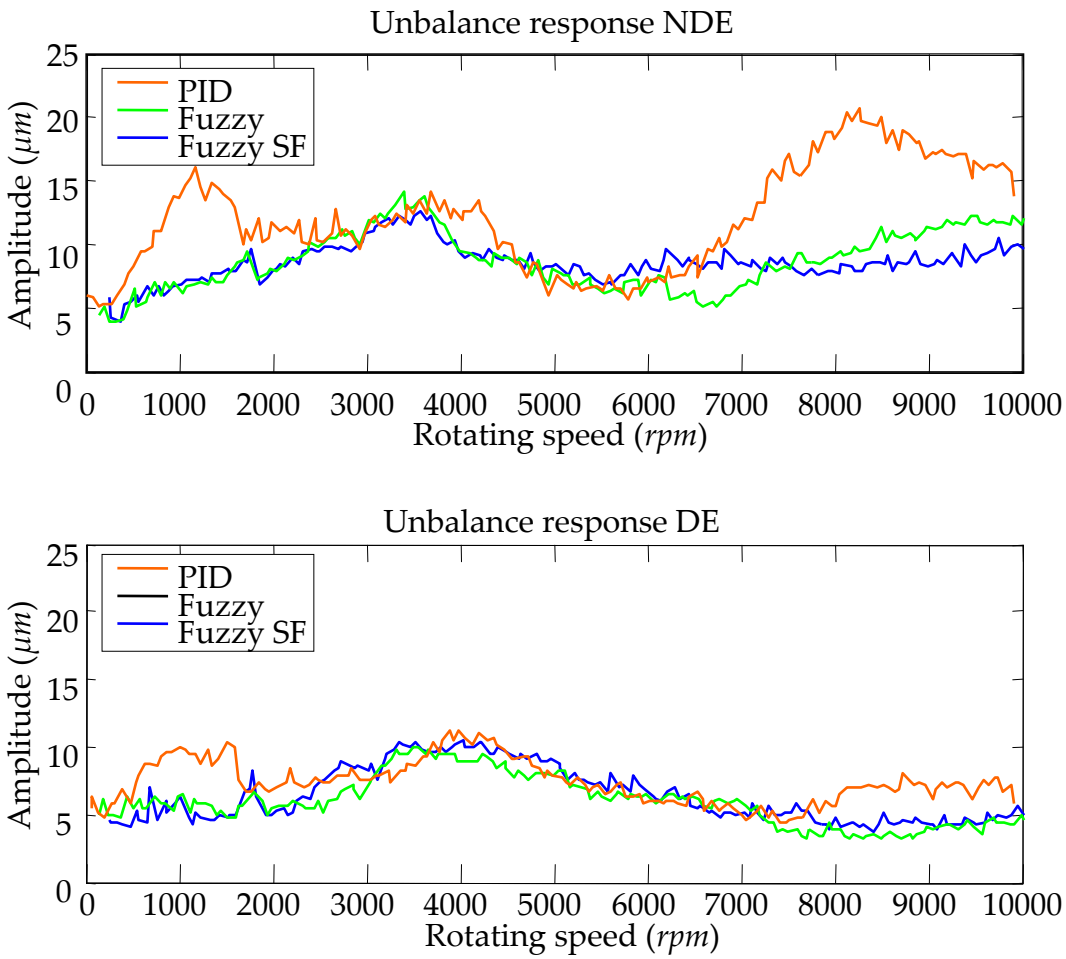

Figure 7. 5: Experimental unbalance responses

This study is completed by the assessment of the synchronous filter. The global level of vibration is considered as it is more representative of the system performances. The residual unbalance distribution is considered so the differences between Figure 7. 4,and Figure 7. 5 are only due to asynchronous vibrations and the different rotating acceleration. The measurements are realized with a constant acceleration $100 rpms^{-1}$. A low pass filter with a cut-off frequency at $1kHz$ is used in order to suppress the noise of measurement. The envelope of radial displacements, stemming from measurements in the two directions, was chosen as a representative value of vibrations. The results are presented in Figure 7. 5. The synchronous filter is set on from $6000rpm$ ($60s$) to the maximum speed.

Three critical speeds are sufficiently excited to be visible: the first around $1000rpm$ that occurred only when using the initial PID controller; the second around $4000rpm$ that corresponds to the cylindrical mode; and the last, around $9000rpm$, was identified as the first flexible critical speed. The mode around $1000rpm$ with the initial PID controller has a backward precession, the other are forward critical speeds. As the mode near $1000rpm$ was identified as one of the foundation modes, the new controller minimizes the energy and the vibration transmitted to the ground.

From the results obtained, the polar fuzzy controller exhibit better behaviour. The maximum displacement decreased by more than 30%. In addition, the simple synchronous filter enables a significant reduction of 14.6% of the vibrations by comparison with the polar fuzzy controller alone. However, the synchronous filter is mainly used in order to reduce the control forces.

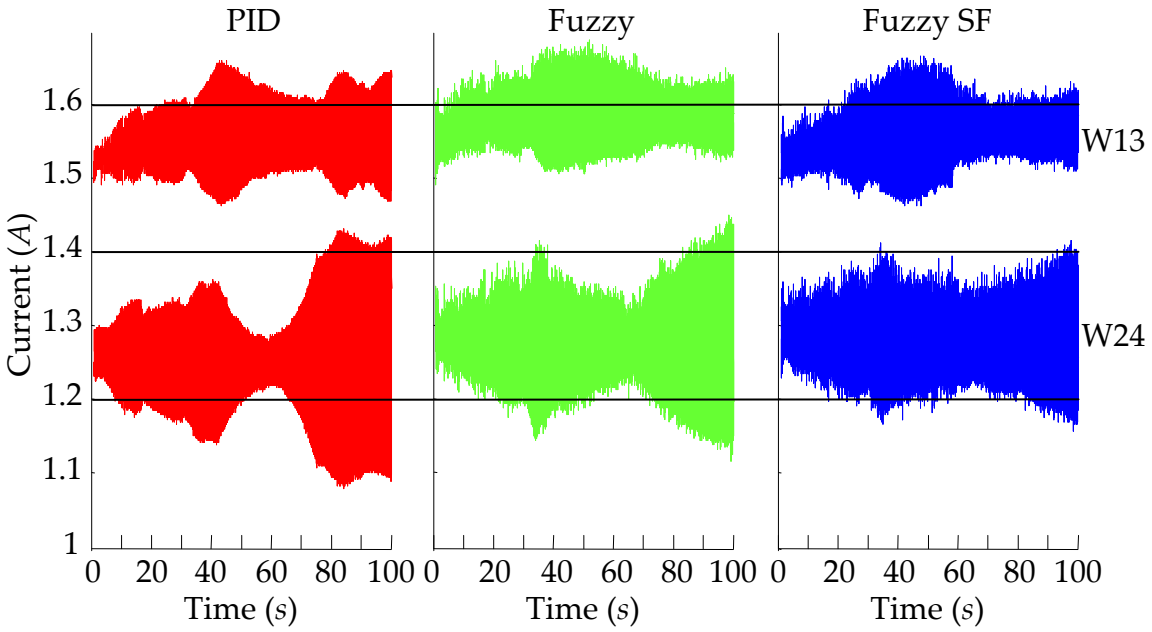

Figure 7. 6: Comparison of top currents

The standard deviations of the control current representative of the control energy is shown in Table 7. 6. The control energy is reduced by 31% compared to polar fuzzy controller alone and by 58% compared to the PID controller.

The currents in the top electromagnets are shown in Figure 7. 6. The same conclusions are done, but it can be added that for the DE bearing, the mean currents (static currents) evolve during the 20 first seconds. This can be attributed to the misalignment and could modify the bearing characteristics.

Standard deviations (A)		Bearing axes V13	W13	V24	W24
0 – 60s	PID	0.0272	0.0383	0.0205	0.0432
	Fuzzy	0.0247	0.0297	0.0253	0.0354
	Fuzzy SF	0.0255	0.0337	0.0263	0.0336
60 - 100s	PID	0.0260	0.0406	0.0577	0.0901
	Fuzzy	0.0168	0.0180	0.0424	0.0548
	Fuzzy SF	0.0136	0.0132	0.0331	0.0376

Table 7. 6: Control energy

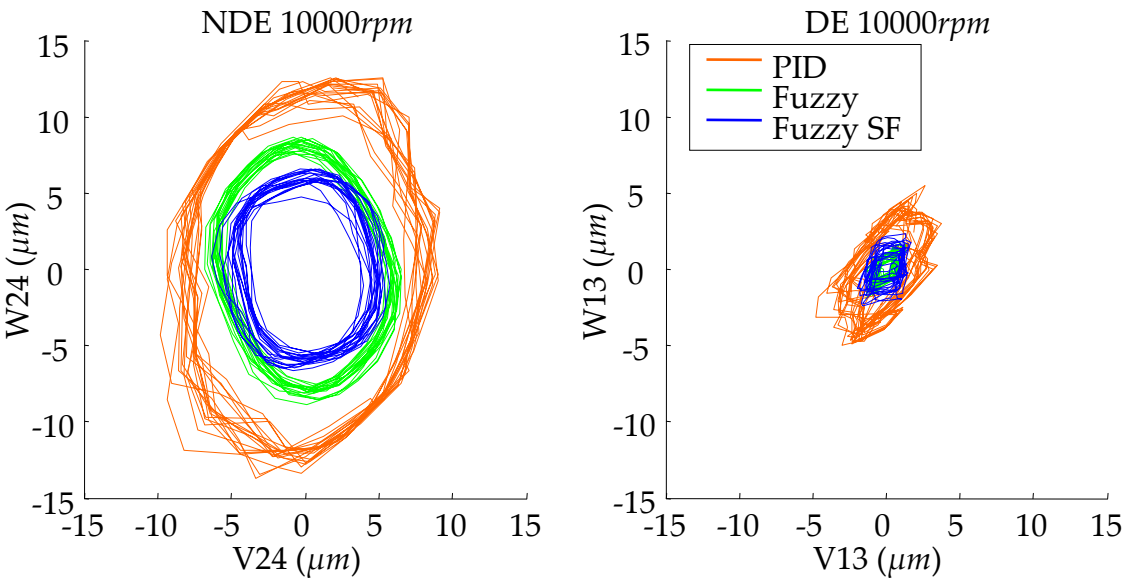

Figure 7. 7: Rotor orbit at 10000rpm

The rotor orbits measured for the stabilized speed of 10,000*rpm* are presented in Figure 7. 7. It can be seen that the displacements, stemming from the three controllers, are lower than those measured for the run-up configuration. This is due to the additional excitation introduced by the motor during run-up.

The Polar fuzzy controller provided a more circular response. Indeed, the controller defined this trajectory as natural and imposed corrective action on bearing misalignment.

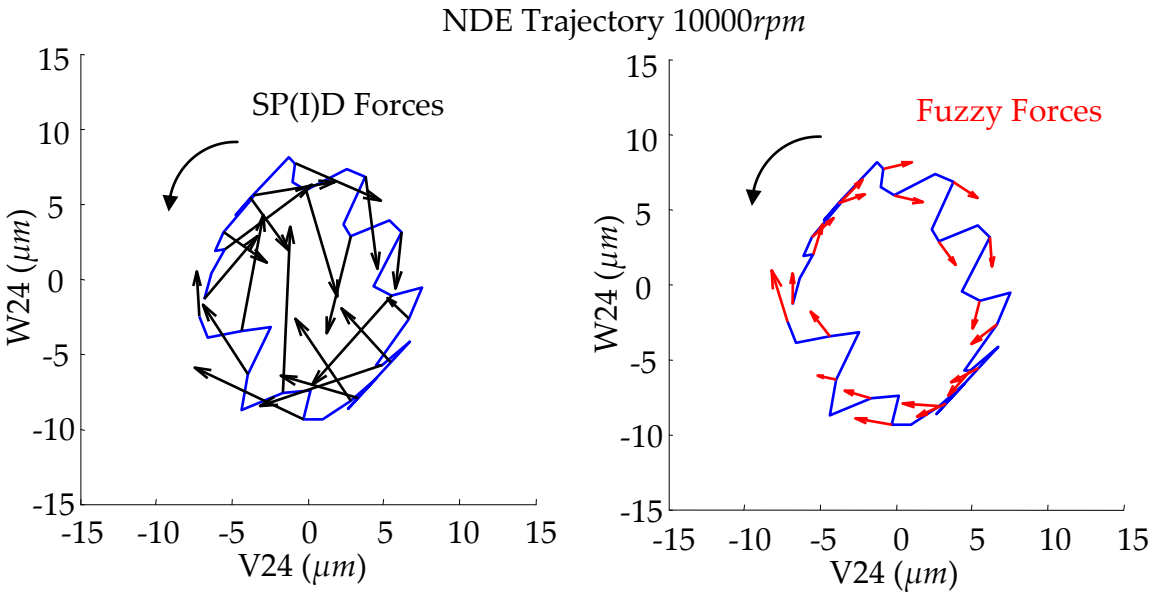

Figure 7. 8: Noise sensitivity of fuzzy forces

Finally, the forces applied by the fuzzy controller at 10,000*rpm* are revealed by Figure 7. 8. The first plot presents the proportional and derivative forces computed by the SPID. For the sake of clarity, the integral forces are removed because they introduced a constant force in the vertical direction, which counteracts the weights. It can be noted that the amplitude and the direction of the forces change constantly and the controller is sensitive to the measurement noise. On the other hand, the force applied by the fuzzy controller has almost constant amplitude and a same tangential direction. As expected, the utilisation of polar quantities with fuzzy logic permits to apply targeted forces.

Subsynchronous excitations

In this section, the dynamic behaviour in the presence of subsynchronous excitations is experimentally evaluated when operating at nominal speed (10,000*rpm*). This configuration corresponds to the aerodynamic disturbances common in turbomachinery applications. The disturbance was introduced by using the DE side bearing as an actuator. Two independent band-limited white noise are used. The signal is limited to 0-30*Hz* and has maximum amplitude of about 0.5*A*.

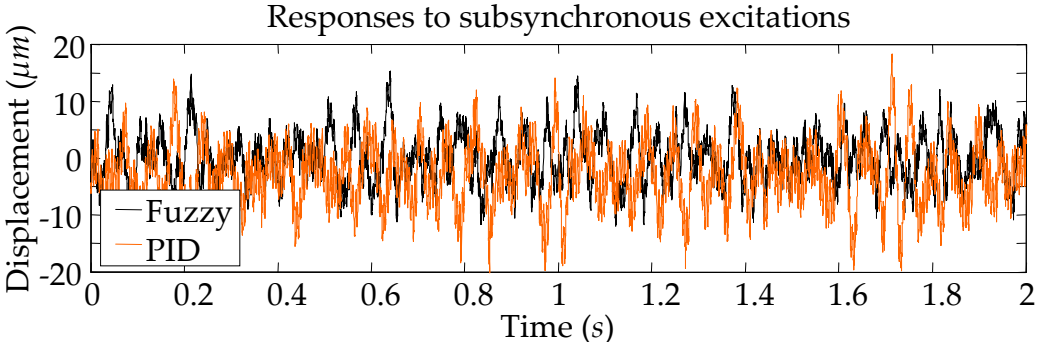

Figure 7. 9: Response to subsynchronous excitations

The control strategy developed is compared to the initial PID controller. The displacements measured during two seconds are presented in Figure 7. 9. The maximum peak-to-peak amplitude is reduced from 37.6μm to 27.2μm with the polar fuzzy controller. This reduction of 28% takes into account both the synchronous and the subsynchronous attenuation of vibration. However, the synchronous vibration is negligible. The Root-Mean-Square (RMS) value was computed for the two controllers over 20*s* of measurements. Respectively on the axes V13 and W13, 6.29µm and 6.16µm were obtained with PID controller, and 4.19μm and 4.77μm with the polar fuzzy controller leading to an attenuation of 24%.

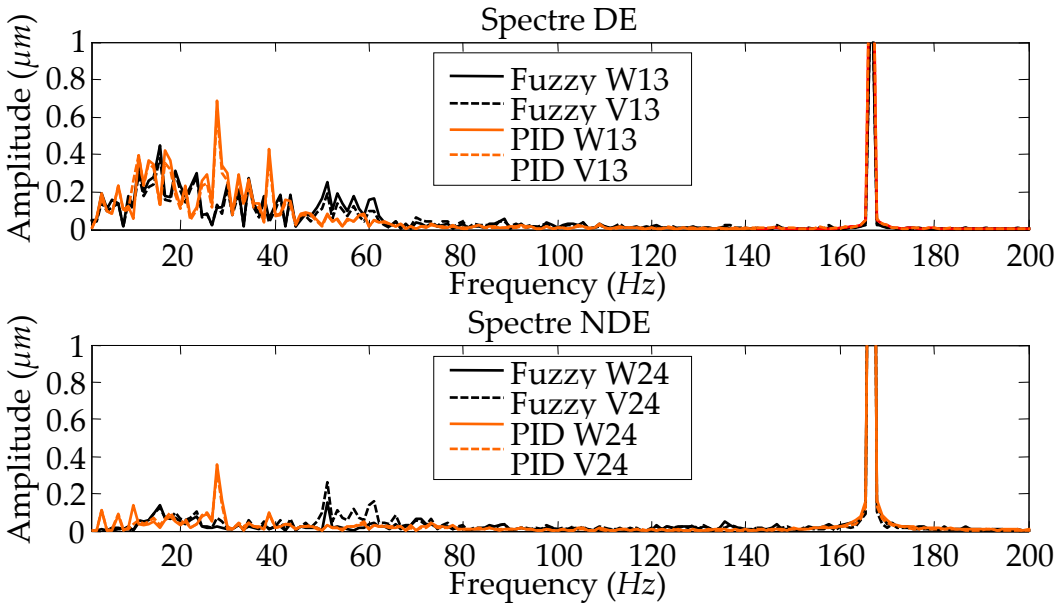

Figure 7. 10: FFT of the measured displacements

When observing in frequency domain, the polar fuzzy controller enables to reduce the subsynchronous excitation as shown in Figure 7. 10. Nevertheless, due to its non-linear properties, the fuzzy controller excites a narrow range of frequencies around $60Hz$. It is a drawback of non-linear control. The non-linear response of the controller contains more frequencies than the initial disturbance and then excites modes of the system.

Conclusions

The results show that it is possible to define a simple underlying controller with satisfying stability and robustness. Then, by using fuzzy logic with polar quantities as inputs, it is possible to have better performances than an augmented PID controller. The gains are first, a simpler design method and second, a better dynamic behaviour.

The simplicity of the SPID comes from several interconnected effects. First, the number of filters included in the operating speed range is reduced. The filters non-used are the ones specific to each rotor that enable to concentrate the damping properties of the bearing around the natural frequencies. For example, usually a phase lag filter is used in order to reduce the bearing damping on the range of frequency between the rigid body modes and the bending mode, and a phase lead filter to obtain more damping on the first bending mode. Consequently, these filters are highly dependent on the frequency of each mode. As, the performance of the system depends on these filters, a heuristic optimization process is necessary. The method developed enables the avoidance of this phase. Finally, the standardization

of the design process enables to obtain readily the resulting dynamic behaviour during the preliminary design of the machine.

It is worth mentioning, that the SPID could seem better than the PID, but the two controllers are not optimized for the same functions. In experiment, the SPID exhibited a higher sensitivity to DE bearing misalignment. This can be seen on experimental sensitivity function, where the errors between numerical and experimental results are higher with SPID. This result was confirmed when examining the unbalance response with SPID. Excessive displacements were observed on DE bearing. Thus, an unintended advantage, of polar fuzzy controller, was found. Indeed, it has exhibited no particular sensitivity to misalignment.

There is a trade-off between the three transfer functions studied: the SPID has better stability margin, but higher sensitivity to measurement noise and less disturbance rejection capability. As expected, since the gyroscopic effects are small, the transfer functions are almost identical at rest and for the maximum speed at 10,000rpm.

The polar fuzzy controller enables to improve the performances of the system for the whole range of operating frequencies. This can be seen on both the unbalance response and the response to subsynchronous excitations.

The study of the dynamic stiffness has shown that the SPID alone has worse performance than the augmented PID at least for low frequencies. Here, the results of subsynchronous excitations demonstrate that the polar fuzzy controller enables to improve significantly the performances of the underlying SPID controller, since the polar fuzzy controller exhibits better performances than the PID controller.

Finally, the synchronous filter permits to reduce significantly the control energy, giving the possibility for smaller actuators.

Chapter 8 – INDUSTRIAL APPLICATION – NUMERICAL ASSESSMENT

After the successful application of the strategy developed for the control of an academic test rig (Chapter 7), it is adapted here for the control of an industrial compressor whose flexible rotor is supported by Active Magnetic Bearings (AMB). For this industrial application, only numerical investigations were performed.

The aim is to show the easiness of design, and the efficiency and the robustness of the approach developed. In addition, the main steps of the evaluation of a compressor supported by AMBs are presented.

The methodology to assess the dynamic behaviour of an industrial compressor supported by magnetic bearing can be found in the literature. Masala et al. [2010] evaluate the rotordynamic behaviour of a vertical high speed compressor equipped with AMBs for subsea application. As the compressor is vertical, they introduce the flexible characteristics of the stator in the model. Then, they present an overview of the system assessment method. In addition, they compare experimental and numerical results giving an idea of the deviation.

First, the model of the compressor used for numerical computation is described. The main differences with the test rig are the rotor mechanical properties and the effects of gas seals. The bearings and the controller are simply adapted. The controller is assessed for different configurations that correspond to the standards and the compressor final user specifications. The polar fuzzy controller is compared to the SPID controller. Six case studies were performed:

1. The sensitivity, that permits to quantify the system robustness.
2. The closed loop transfer function in order to assess the sensitivity of the system to noise of measurement.
3. The dynamic stiffness computation and amplification factors evaluation, which are related to the system performances and the severity of resonance frequencies.
4. The unbalance responses, for the assessment of the rotor dynamic behaviour. Three unbalance distributions are examined for run-up conditions up to 125% of trip speed.
5. The response to subsynchronous excitations is computed in order to estimate the capacity of the controller to manage disturbances as aerodynamics ones.
6. The impulse response at nominal speed is analyzed in order to highlight the performances of the polar fuzzy controller.

As for the test rig, the transfer functions of the system controlled with the SPID appear sufficient for a first evaluation.

Detailed model

For this study, the prototype of the ICL was used in order to be able to validate experimentally the results on an existing machine. The experimental tests have not been realized due to cost and time delay. This machine has typical characteristics of a midstream machine used for gas storage. It is presented in Figure 8. 1.

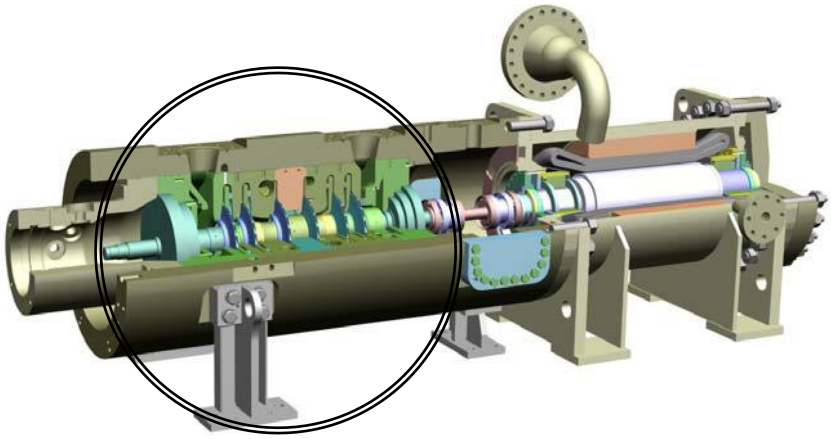

Figure 8. 1: Integrated Compressor Line

The centrifugal compressor is equipped with a magnetic thrust bearing and two identical radial AMBs called NDE (Non Drive End) and DE (Drive End) bearings.

The rotor is composed of a shaft of 2m length, six impellers and two stacks of laminated steel sheets shrunken on each bearing location. The total rotor mass is 370kg. The compressor delivers 5.5MW. The operating speed range used in this work includes three critical speeds (two forward rigid modes and the first forward flexible mode), that makes the machine supercritical.

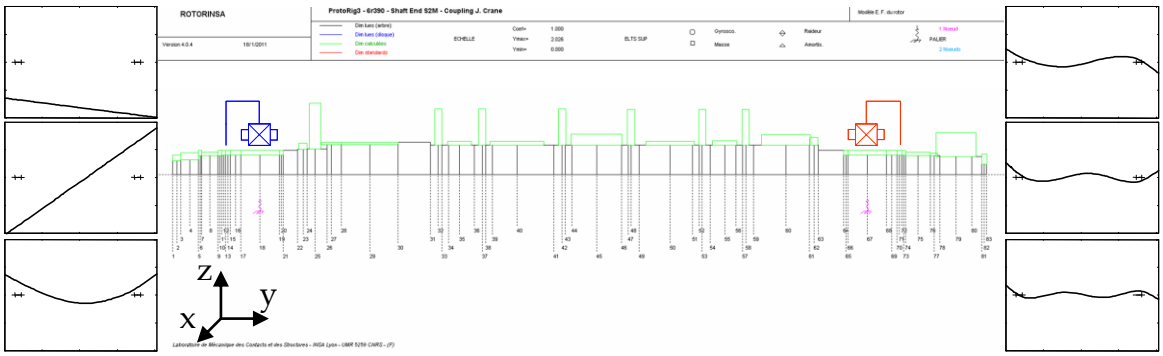

Figure 8. 2: Finite Element model of the rotor (Red DE, Blue NDE)

The action lines are positioned in the configuration load between axes. They are powered in differential driving mode. Two displacement sensors are integrated in the housing of each bearing and are non-collocated with actuators, as shown in

Figure 8. 2. A flexible coupling is positioned between the compressor rotor and the electrical motor. Thus, the lateral analysis of the two rotors is uncoupled and the study is focused on the compressor. The frequency bandwidth considered in this study is 0-2kHz.

For the sake of clarity, only the shapes of the first six modes are plotted in Figure 8. 2. The rotor model is composed of the following elements: the flexible shaft and rigid discs (for the impellers and the two stacks of laminations). Regarding the shaft model, it is set up with 82 Timoshenko beam elements. The calculations of the natural frequencies and the mode shapes were performed with direct stiffness (no cross stiffness and no damping), which equal $2.10^7 N.m^{-1}$ (as for test rig this stiffness is used only for preliminary assessment then free-free modes are used). The pseudo modal method is used to keep only the first 20 modes (to conform to the bandwidth frequency). The natural frequencies of the rotor are presented in Table 8. 1. Globally, the gyroscopic effects are negligible.

Modes	At rest (Hz)	125% of trip speed	
		Backward (Hz)	Forward (Hz)
Rigid 1	48	48	48
Rigid 2	74	72	77
Flexible 1	152	144	160
Flexible 2	324	306	341
Flexible 3	554	528	579
Flexible 4	835	799	871
Flexible 5	1171	1114	1231
Flexible 6	1564	1478	1658
Flexible 7	1920	1840	2012
Flexible 8	2382	2313	2462

Table 8. 1: Rotor natural frequencies

As the AMBs are powered in differential driving mode, they can be considered as linear in the range of nominal displacements. Thus, they are taken into account with a current stiffness and a negative stiffness of $-6.3 N.\mu m^{-1}$. These values were estimated with respect to the bearing geometry and load. The electronic part of each AMB is taken into account with a low pass filter with a cut-off frequency below 2kHz.

The study was carried out with dynamic coefficients of seals as defined by Childs and Scharrer [1986]. The effects of gas seals were taken into account for all the study except the response to unbalances and impacts. They are not considered for unbalance responses, as the effect of gas seal depends on operating conditions and consequently on the rotating speed. The impact was to illustration of fuzzy controller performances, it is not a case study for compressors assessment as this type of excitation is rare. Thus, without gas seal coefficient the system is simplified. The

coefficients are summarized in the Table 8. 2. The shaft is oriented along the y axis and the direction of rotation is defined from the axis z to the axis x. The position is measured from the NDE side.

Position (mm)	K_{zz}=K_{xx} ($N/\mu m$)	K_{zx}=-K_{xz} ($N/\mu m$)	C_{zz}=C_{xx} (Ns/m)	C_{zx}=-C_{xz} (Ns/m)
635.1	0.89	0.84	550	-265
744.1	0.87	0.95	629	-281
943.1	1.05	1.06	711	-295
1049.1	-8.23	-0.24	2717	5252
1155.1	1.28	1.38	963	-332
1332.1	1.19	1.27	875	-319
1440.1	1.19	1.27	875	-319
1520.3	-6.08	0.64	2037	3955

Table 8. 2: Seals dynamic coefficients at 100% speed

The characteristics of the SPID are those described in Chapter 5. They are evolved along the study in order to take into account the particular disturbances existing on compressors. The main difference with the version applied on the academic test rig is the increase of damping at low frequency in order to consider seals dynamic coefficients. In addition, the general gain is increased in order to take into account the "scale effect", as shown in Figure 8. 3.

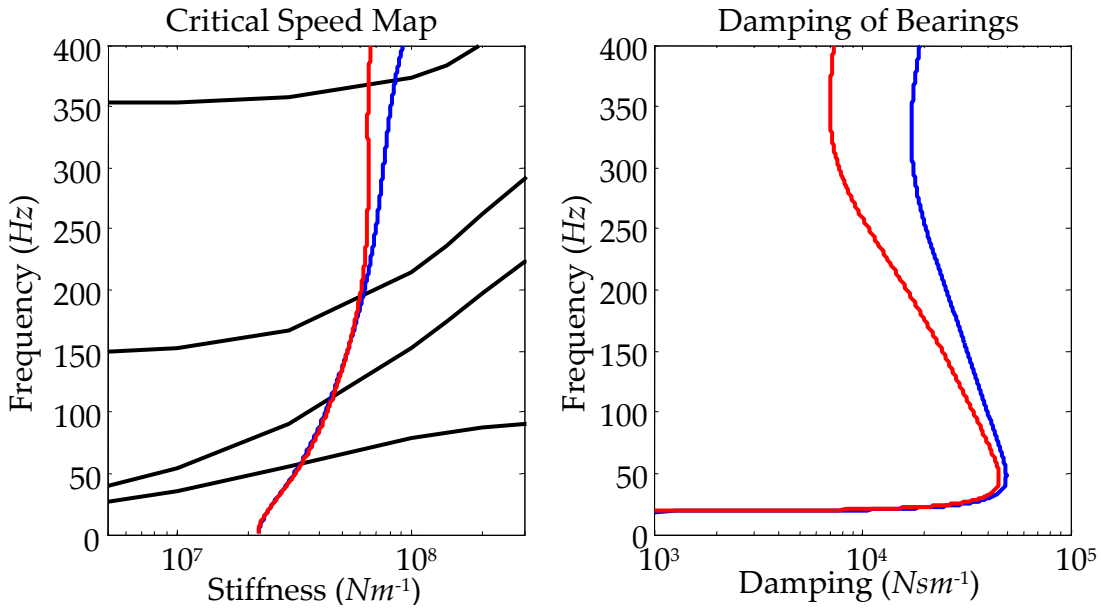

Figure 8. 3: Standardized stiffness and damping (Red DE, Blue NDE)

The Bode diagram of the bearings is presented in Figure 8. 4. On the phase graph, black squares are issued from the Campbell diagram. The width represents the

variation of natural frequencies due to gyroscopic effect (from the second flexible mode) for the whole range of rotating speed considered. Green squares take into account modelling uncertainties. They are not centred in order to consider that the compressors natural frequencies are generally under estimated for compressors. Blue and red squares represent a node between sensor and actuator with respect to the associated bearings (NDE and DE respectively).

It can be noted that the high frequency gain is much higher than the one in operating speed range due to the necessity of a high Q-factor.

The controllers have been tuned by considering an internal dissipation. In addition, according to mode shape, the bearings were considered to have low effect on the 6th flexible mode. Thus, the controller can reduce the modal damping of the 6th flexible mode without producing any instability.

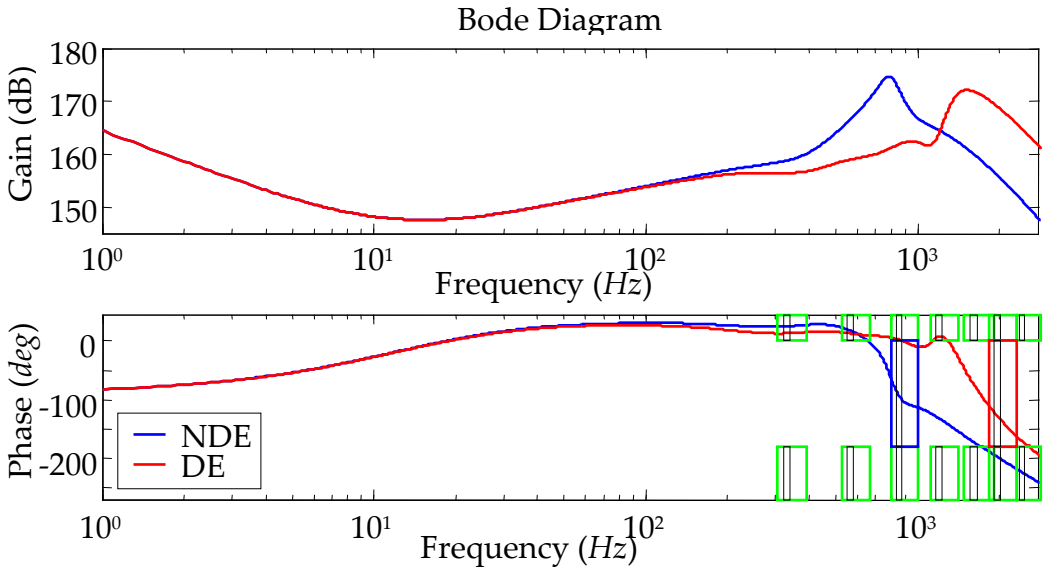

Figure 8. 4: Transfer function of controllers

For almost each high frequency mode, we have designed a low damping, but on a quite large range of frequency, in order to consider modelling uncertainties. If this damping value was found insufficient by experimental results, it would be easy to concentrate the damping on each mode.

Results

Sensitivity

The compressor has a "modal density" greater than that of the test rig (we mean by modal density, the number of natural frequencies within a defined frequency range). Consequently, the cut-off of the controller gain is more difficult and the sensitivity exhibit maximum peaks at high frequencies (300-1,500*Hz*) as shown in Figure 8. 5,

where the gain of the controller is maximum, whereas it was for first bending mode frequency on the test rig.

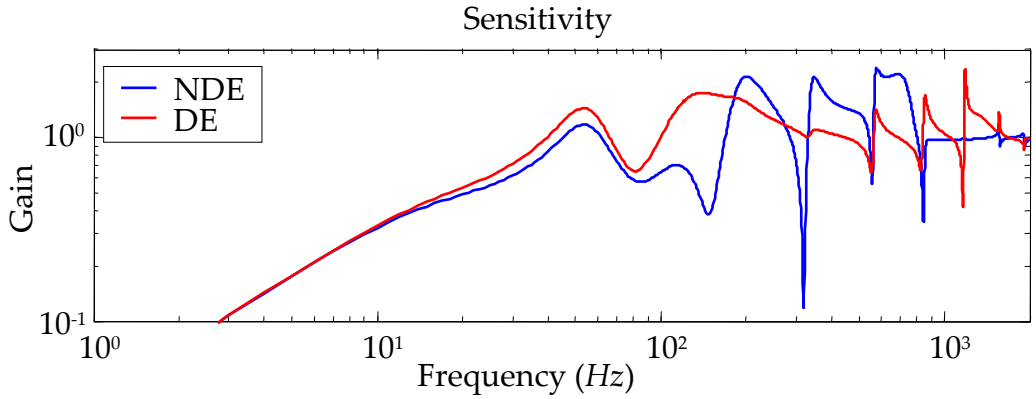

Figure 8. 5: Sensitivities at rest

The sensitivity of the SPID was measured with a maximum value of 2.4 as shown in Table 8. 3. It is 0.6 below the zone A limit.

Maximum peak of sensitivity	At rest	At MCS	At MCS with seals
DE	2.34	2.12	1.80
NDE	2.39	2.29	2.25

Table 8. 3: Stability margins

Natural frequencies are functions of the rotating speed due to gyroscopic effects. As narrow lead-lag filters are used to ensure damping for high frequency modes, the modification of natural frequencies changes the damping of the bearing (for the considered mode). Then, the sensitivity maximum value changes too. Consequently, when the maximum of sensitivity is found for high frequency modes, the sensitivity should be verified for different rotating speeds, even with low gyroscopic effects.

It can be noted that seals dynamic coefficients provide damping for high frequencies. Thus, the sensitivity of the system is attenuated, when they are taken into account.

Closed loop transfer function

The CLTF at rest is provided in Figure 8. 6. The influence of measurement noise is quite independent of operating conditions as shown in Table 8. 4.

The results on the CLTF show that the system has an acceptable sensitivity to noise of measurement since the maximum gain has a limited value.

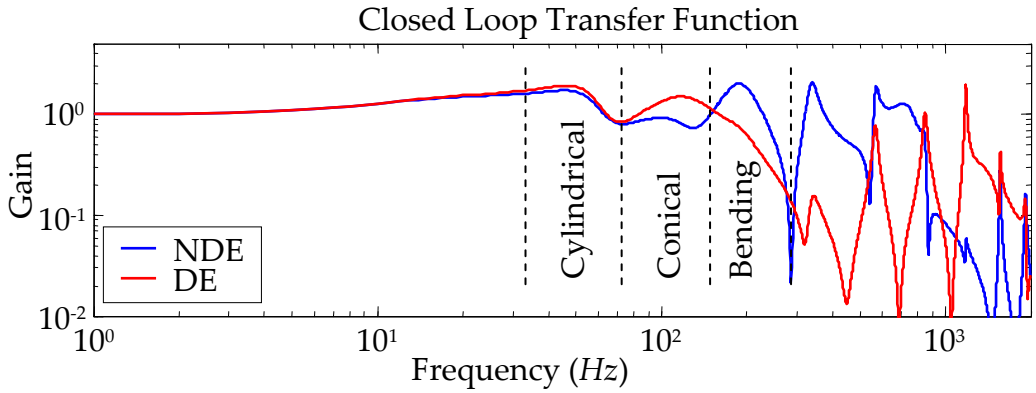

Figure 8. 6: CLTF at rest

As shown in the following the AF of the first mode is difficult to obtain from dynamic stiffness. The CLTF permits a better evaluation. At rest the AFs equal 2.0 and 1.8, and at MCS with seals, 2.1 and 1.6 respectively on DE and NDE sides. Thus, the damping of the first mode is satisfying.

Maximum peak of CLTF	At rest	At MCS	At MCS with seals
DE	1.95	1.92	2.21
NDE	2.05	1.90	1.85

Table 8. 4: Measurement noise sensitivity

Dynamic stiffness

The seals dynamic coefficients induce negative stiffness and negative damping at low frequencies. In addition, there are a series of seals on the two balance drums. One is positioned at middle span and the second on the drive end side. Consequently, the effect of gas seals appears mainly on DE side as shown in Figure 8. 7, where the dynamic stiffness is reduced by 20% as indicated in Table 8. 5.

Minimum of Dynamic Stiffness ($N/\mu m$)	At rest	At MCS	At MCS with seals
DE	16.0	16.0	12.8
NDE	16.4	16.4	16.7

Table 8. 5: Disturbance rejection

The damping is not identical for the two bearings, thus the tilting mode appears at a lower frequency (91Hz) on the NDE side than on the DE side (112Hz). The undamped natural frequencies are the same, but as the action is applied at bearing location, the

effect of the other bearing on damping should be negligible. Consequently, the frequencies of the maximum amplitude are different.

The bending mode does not appear on the DE side, because the bearing has relative high stiffness and damping, and one node is relatively close to the bearing actuator. Consequently, the DE bearing has less impact on the bending mode than the NDE one.

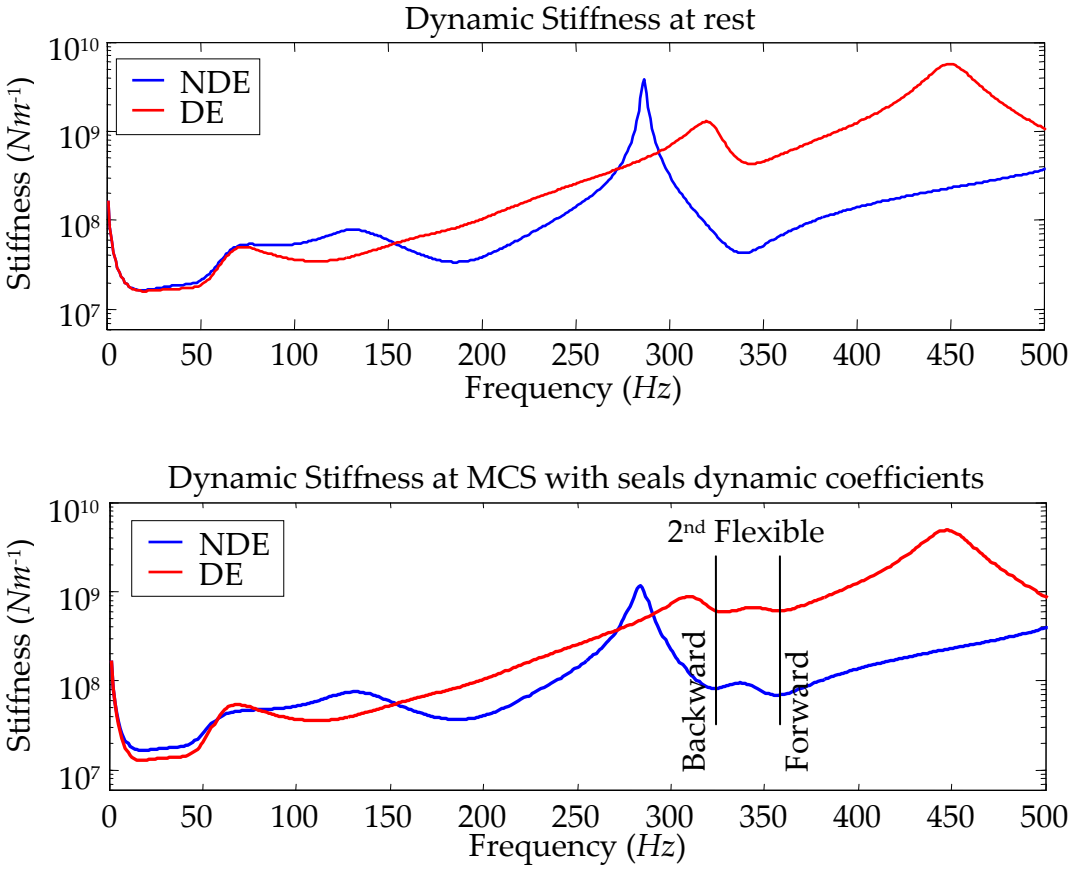

Figure 8. 7: Dynamic stiffness at rest

With this SPID the damping is increased for low frequencies, then the minimum of the dynamic stiffness function is not split into two small peaks as for the test rig as shown in Figure 8. 7. Here, the two peaks are merged, and a better robustness to variations of negative stiffness and seals dynamic coefficients is expected. However, the AF of the first mode cannot be calculated with the half power point method, as this will induce large errors (see Table 8. 6 and CLTF evaluation).

The AFs should be assessed for the different operating conditions. They are computed from the admittances as explained in chapter 7. Hereafter, only the AFs at rest are reported in Table 8. 6. The amplification factors permit to assess the severity of resonances. The first modes are well damped. It can be seen than the bending

mode (186*Hz*) has an amplification factor relatively high. Thus, it can be supposed that the study of unbalance response should not satisfy API 617 [2002] requirements.

The modes with higher frequency have an increasing AF, which reaches progressively the value corresponding to the utilized internal damping of the rotor (100). It is worth mentioning that it is visible that the controller affects the 6th flexible mode, since its AF is greater than 100. Therefore, it is essential to obtain a good estimation of internal dissipation in order to ensure the stability of the closed loop.

Natural frequencies (*Hz*)	AF DE	AF NDE
20	0.43	0.42
91	-	1.4
112	1.6	-
186	-	3.7
340	10.8	11.7
570	28.4	22.8
845	33.9	35.0
1,185	78.7	20.8
1,560	97.8	**134.6**
1,915	56.3	83.4

Table 8. 6: Severity of resonance frequencies

It should be unnecessary to observe modes beyond 2*kHz* since the controller gain has already largely decreased, and the phase is adapted in order to ensure damping for the very next modes.

Unbalance responses

Three different unbalance distributions were studied which correspond to the standards specifications as indicated in Table 8. 7.

Configurations	Position of unbalances
1	Unbalance at middle span
2	Two opposite unbalances at rotor ends
3	Two unbalances at rotor ends coupled with an opposite unbalance at middle

Table 8. 7: Unbalance configurations

The envelope of the radial displacement was chosen as a representative value of the system response. The unbalance responses exhibited three critical speeds: the cylindrical, the conical, and the last, the first flexible The system response and the

control force for configuration 1 are presented in Figure 8. 8. This configuration was chosen for its relative simplicity of interpretation and demonstration. It could be noticed that the conical mode does not appear in this unbalance response. In addition, the Synchronous Filters (SF) introduces a slight softening effect (the bending critical speed is shifted toward a lower value) and reduces the bearing dynamic forces.

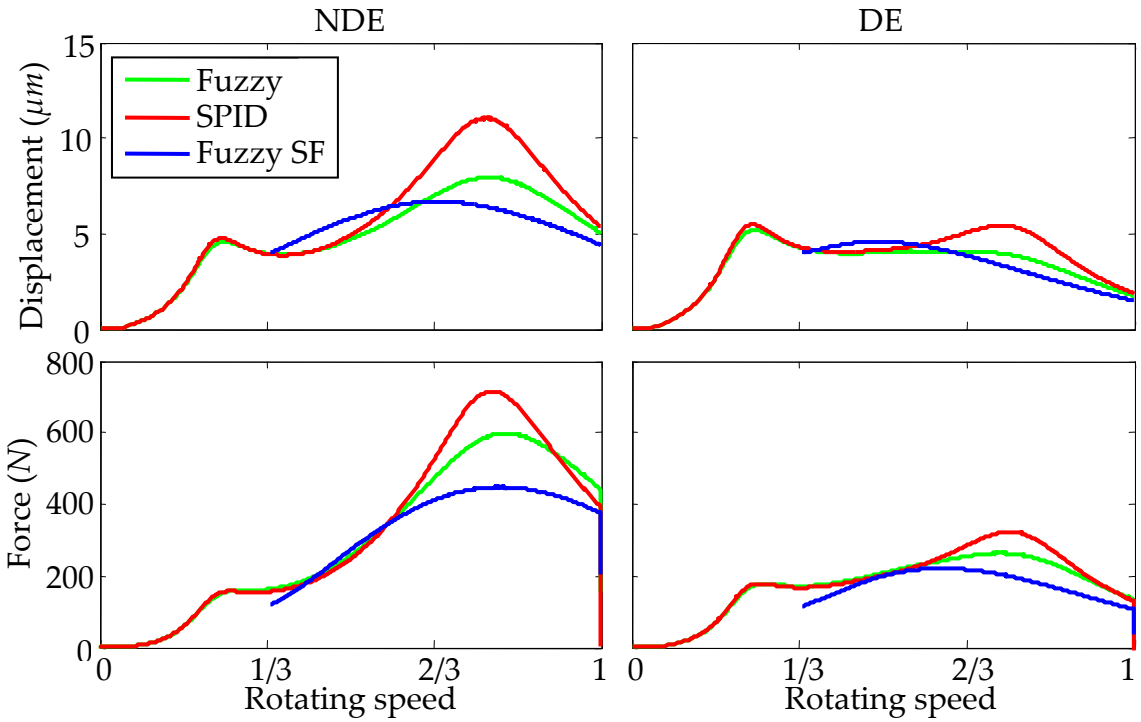

Figure 8. 8: System response due to unbalance at middle span

As shown in Table 8. 8, the unbalance responses demonstrate the better efficiency of the fuzzy controller. The maximum displacement decreases by 27% and by more than 40% with the activation of the synchronous filters. The amplification factors (AF) were also assessed. As expected, making use of fuzzy approaches enhances the dynamic behaviour. The initial maximum AF (2.9) was reduced by 20% and almost halved for the bending critical speed when using synchronous filters. Finally, the maximum force necessary was reduced by 12% and by 28% with synchronous filters.

The SPID enables to fulfil the requirement of the annexe (4F) of API 617 [2002] in terms of maximum displacement (90μmpp), but not the specifications for compressors on classic bearings (25μmpp). In addition, the AF is higher than 2.5 for the bending critical speed. Consequently, the machine could not operate at this speed and separation margins should be considered API 617 [2002]. It is worth mentioning that the AF of the bending mode is essentially identical on the two bearings and averaged compared to the values at rest. This makes it possible to obtain satisfactory AFs compared to the expected values.

With the fuzzy controller, the AF value is always under this limit, and the maximum displacement is close to the specifications for classic bearings. Finally, the association of the fuzzy controller and the synchronous filter enables to satisfy the totality of standards requirements.

			Configuration 1			Configuration 2			Configuration 3		
			AF	Disp. pp μm	For. N	AF	Disp. pp μm	For. N	AF	Disp. pp μm	For. N
DE	Cyl.	SPID	2.5	11	179	-	-	-	-	-	-
		Fuzzy	2.2	10.4	177	-	-	-	-	-	-
		Fuzzy SF	2.2	10.4	177	-	-	-	-	-	-
	Conic.	SPID	-	-	-	1.8	**27.4**	-	-	-	-
		Fuzzy	-	-	-	-	-	-	-	-	-
		Fuzzy SF	-	-	-	-	-	-	-	-	-
	Bend.	SPID	**2.9**	10.8	323	-	**26**	801	2.4	20.6	632
		Fuzzy	-	8.2	263	1.4	**25.5**	847	1.8	16	569
		Fuzzy SF	1	9.2	221	1.4	21.5	732	1.5	13.6	455
NDE	Cyl.	SPID	2.4	9.5	157	-	-	-	-	-	-
		Fuzzy	2.2	9.1	-	-	-	-	-	-	-
		Fuzzy SF	2.2	9.1	-	-	-	-	-	-	-
	Conic.	SPID	-	-	-	1.6	16.4	446	-	-	-
		Fuzzy	-	-	-	1.5	12.2	371	-	-	-
		Fuzzy SF	-	-	-	1.3	11.3	271	-	-	-
	Bend.	SPID	**2.8**	22.1	715	-	-	-	**2.6**	**36.2**	1,190
		Fuzzy	2	15.8	598	-	-	-	2.3	**26.5**	1,049
		Fuzzy SF	1.2	13.4	448	-	-	-	1.5	20.8	855

Table 8. 8: Unbalance responses

Subsynchronous excitations

This configuration corresponds to the aerodynamic disturbances applied on the coupling between compressor and motor. There is no standard specification. The main source is the gas inside the coupling cavity. These disturbances are visible around the first natural frequency because AMBs have a low dynamic stiffness at this frequency. In addition, dynamic coefficients of seals, shown in Table 8. 2, create a negative effective damping and an additional negative stiffness.

These disturbances can lead to relatively high vibration levels but without particular consequences. Nevertheless, this range of frequency is usually monitored, because a high displacement indicates that the stability of the first mode is too low with machine supported by fluid film bearing. Thus, there are two disadvantages of

these low frequency vibrations: the first mode cannot be monitored and an untrained staff could misunderstand these vibrations.

The SPID was designed in order to provide stability and robustness in the low frequency range, and particularly to improve the dynamic behaviour of the rotor excited by aerodynamic disturbances. A comparison of the response of the rotor with the SPID alone and with the fuzzy controller is presented in Figure 8. 9. Calculations were performed with the third unbalance distribution at operating speed (2/3 of the maximum speed). Due to confidentiality constraints, the synchronous response was dissociated (the vertical scale was conserved). The excitation was a white noise limited to 0-30Hz, with an amplitude of 15N in frequency domain. This value can seem low but, as it was applied on a given frequency range, in temporal domain this signal exhibit peaks close to 750N. That corresponds to an estimation of the maximum load present on compressors.

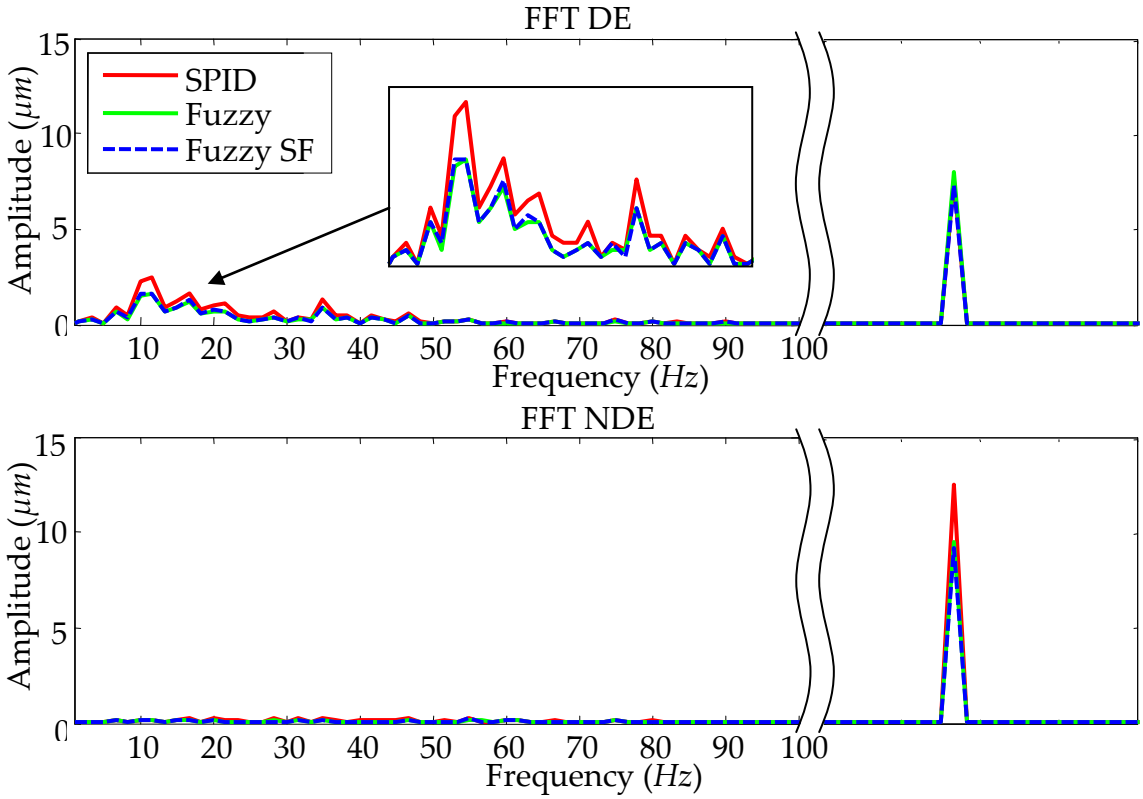

Figure 8. 9: Subsynchronous response

As expected, the results are very similar with or without synchronous filter. The fuzzy controller permits a reduction of 25% on low frequency vibration levels. On the other hand, and as the synchronous responses on DE side are almost identical, it is possible to compare also the displacement obtained in time domain. Whereas, the SPID exhibits a maximum displacement of 58μm, the fuzzy controller limits the displacement to 40μm, leading to an attenuation of more than 30% of the vibration

level. This difference is important since the maximum of displacement when using the fuzzy controller falls inside class A as defined by ISO 14839 [2004], while it was between class B and C with the SPID. It is worth mentioning, that class C is considered unsatisfactory for long term continual operation.

Impact response

The rotor orbit evolution at the NDE bearing due to an impact at a stabilized speed (operating speed) with the third unbalance distribution is presented in Figure 8. 10. The impact is defined by a triangular impulse applied at the NDE bearing. The base length of this isosceles triangle equals 0.01 second and the length of its altitude $500N$. The red arrow in Figure 8. 10 shows the direction of the impact and the black arrow the direction of rotation. It can be seen that the displacements, stemming from the fuzzy controller, are lower than those obtain for the SPID alone. The non-dimensional vectors on Figure 8. 10 show the additional radial forces applied by fuzzy controller relatively to SPID. The time is represented by the curve colour, the oldest position in dark blue and the newest in red.

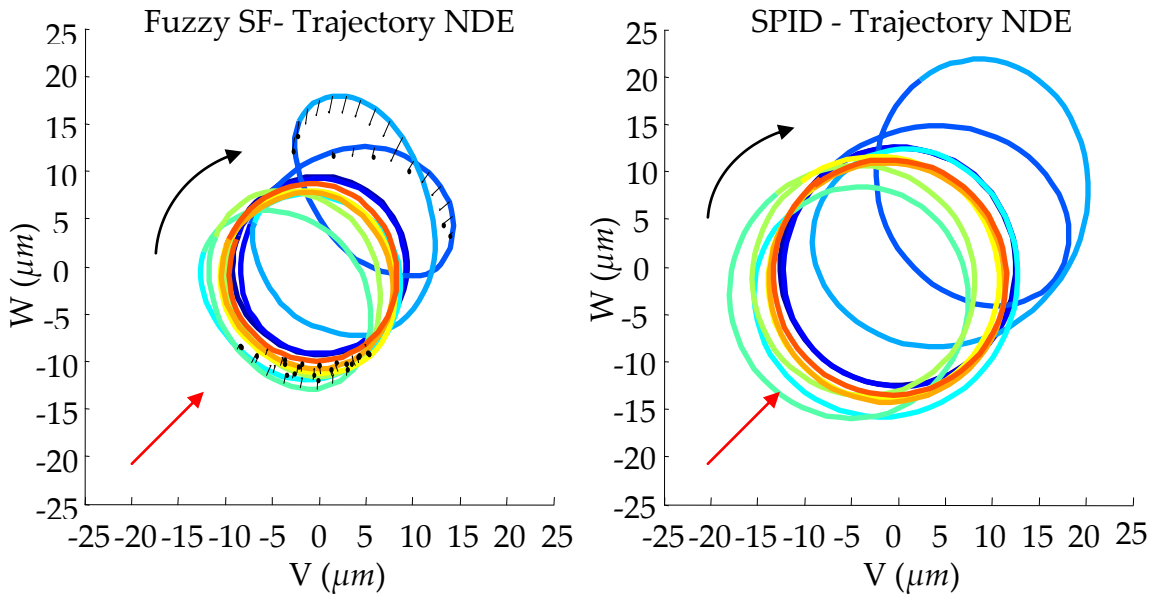

Figure 8. 10: Rotor trajectories

When the fuzzy controller detects a positive radial velocity, it applies additional radial forces (compare to SPID) that permit to reduce the maximum displacement achieved. This shows that the utilisation of polar quantities and fuzzy logic enables to apply targeted correction forces.

The fuzzy controller exhibits a more interesting behaviour with a maximum displacement of $19.1\mu m$ ($18.1\mu m$ when synchronous filters are activated), while SPID exhibits $24.7\mu m$. Obviously, a part of this attenuation stems from synchronous

responses which have an amplitude of $9.8\mu m$ without SF, $9.2\mu m$ with SF and $12.7\mu m$ when using SPID.

The fuzzy controller applies additional stiffness thus compared to SPID the same potential energy is obtained with less displacement. However, there is no additional damping (except tangential), thus the settling time is equivalent.

Conclusions

The new control approach is assessed numerically for the control of the dynamic behaviour of an industrial supercritical compressor. The system is assessed through the classical transfer functions, and acceptable properties are obtained for the SPID. The dynamic behaviour is compared for several configurations of excitations. Results obtained when using the polar fuzzy controller were compared to standards specifications. Results were also compared to those obtained when using a SPID, which exhibits a similar behaviour than an augmented PID. The controller developed exhibits stable and robust behaviour. All standards specifications were respected in associating the fuzzy controller to a SF. With respect to the SPID behaviour, better performances were obtained for the same level of robustness. Regarding the subsynchronous excitation, the fuzzy controller enables a reduction of 25% of vibrations level in low frequency.

It is worth mentioning, that the results obtained with the fuzzy controller without synchronous filter are very close to the standards requirements, even if, these ones are not fully adapted to compressors supported by AMBs. A study regrouping several machines could certainly permit to determine the adapted fuzzy controller, as we cannot reasonably design the definitive SPID and fuzzy characteristics, with only one machine. In this way, two advantages would be obtained: the standardization of the controller and the suppression of the speed sensor. Thus, the hardware of the bearing would be simpler and more robust.

Chapter 9 – CONCLUSIONS AND PROSPECTS

Summary and Conclusions

In this thesis, the dynamic behaviour of supercritical centrifugal compressors supported by active magnetic bearings is investigated. The unbalance distribution, the gas seals and the aerodynamic subsynchronous excitations are the main disturbances that affect the dynamic behaviour. They should be considered in order to assess the machine performances. In addition, the dynamic behaviour should satisfy stringent requirements dictated by international standards and final users. These requirements aim to the safety and the reliability of the system.

The potential of AMBs is not fully exploited by the usual industrial control strategy (PID controller). A new control strategy is developed. This strategy takes into account the possibilities and the limitations of the magnetic bearing technology.

As their structural damping is low, flexible rotors are very sensitive to spillover effect. Thus, the controller bandwidth is divided into two ranges of frequencies. For low frequencies, the controller characteristics are standardized for a given range of product. The characteristics of the controller are those of the developed polar fuzzy controller. For high frequencies, the underlying PID controller is tuned in order to ensure stability and robustness for each machine.

The controller developed consists of three elements: the underlying Standardized PID controller that we called SPID, the fuzzy logic controller and the polar quantities computation. The SPID controller is tuned in order to simplify the controller transfer function, while the complete controller is designed in order to achieve the standards requirements and improve the subsynchronous behaviour. With the use of polar quantities, each bearing is considered as one entity by coupling its two axes of action. The introduction of polar quantities permits a better observation of the rotor dynamic behaviour. In addition, as the polar quantities make use of the two sensors of the bearing, it is possible to calculate control forces less sensitive to measurement noise. Finally, fuzzy logic enables to apply corrective actions based on the global dynamic behaviour. As the polar quantities permit the observation and the separation of this behaviour, the coupling of the two methods is an efficient way to apply targeted corrective actions.

We have shown that this controller can attenuate the unbalance response by using damping forces that do not affect significantly the system robustness. In addition, it is also able to increase the bearing stiffness during transient or

asynchronous excitations in order to limit the maximum displacement reached. If necessary, the control forces can be reduced by using a simple synchronous filter. This SF aims to allow the use of smaller bearing sizes.

The control strategy is assessed numerically and experimentally. The numerical model of the system takes into account all the components of the action lines (the sensors, the electromagnets, the amplifiers, the electric cables, the digital controller and the rotor). The numerical results are compared with those obtained experimentally by using an academic test rig. The calibration of the current stiffness value has permitted to obtain satisfying results and the same trends are observed. The polar fuzzy controller exhibits a good robustness, a good stability and performances superior to the augmented PID supplied with the test rig for both unbalance responses and responses to subsynchronous excitations at operating speed. Then, the SF is assessed. It enables a reduction in control forces of 30% and an attenuation of the unbalance response of 14.6%.

Finally, the approach is applied for the control of an industrial compressor. The numerical assessments are very promising. When making use of SF, all the requirements are satisfied. It is worth mentioning that the results obtained with the polar fuzzy controller without SF are very close of the standards requirements used for classical hydrodynamic bearings. In the latter, the hardware is simpler and more reliable.

In conclusion, the design of the controller and the machine are easier, and the dynamic behaviour is improved. The optimization of the approach and the utilization of an automatic tuning algorithm for high frequency characteristics could lead to the standardization of Active Magnetic Bearings.

Comments

The standards requirements have not yet been fully adapted to centrifugal compressors supported by AMBs. We have attempted to do several propositions aiming at the adaptation of standards requirements to the particularities of both centrifugal compressors and AMBs.

The validation of the numerical model is realized as specified by API 617 [2002]. In this thesis, the verification was done with the augmented PID supplied with the test rig. This method is based on the hypothesis of a linear system. Consequently, this method is not suitable for the polar fuzzy controller developed. Nevertheless, as the underlying SPID exhibits satisfactory performances for short term operation, it can be used for the model validation during machinery commissioning.

Considering permanent behaviour, the controller developed should be classified in the range of adaptive control and not in the range of non-linear control. The unbalance responses are proportional to the unbalance value, as for linear controllers (at least around the critical speeds).

The polar fuzzy controller developed enables to obtain performance margins. Then, it is easier to respect the requirements. These margins can be used of different manners. For example, the dynamic behaviour could be optimized by using a classical augmented PID as underlying controller, and additional synchronous filters.

A study regrouping several machines could certainly permit to design the definitive SPID characteristics, which would satisfy the standards requirements without SF for every new machine.

The test rig has an important misalignment due to mounting errors. This misalignment disturbs the rotor dynamic behaviour and reduces the quality of numerical predictions. Nevertheless, it can be expected that the mounting tolerances for centrifugal compressors are considerably smaller.

The prediction of the bearing current stiffness was not satisfying. It is expected that the main source of errors are the assembly tolerances. A deeper identification of the test rig could definitely exclude the other potential sources.

Other possibilities of improvement were identified and could be developed in future work.

Future work

The main problems encountered on supercritical centrifugal compressors with classical controllers should be solved with the approach developed. However, several important issues need to be clarified:

- How the internal damping of an industrial rotor could be predicted?
- What is the maximum "reasonable" AF for high frequency modes?
- How manufacturing tolerances affect the system?

Finally, this thesis could be completed by several studies:

- The optimization of the approach,
- The systematic assessment of non-linear controllers,
- The development of a systematic tuning approach for the high frequency characteristics,
- The experimental application on a compressor, and
- The study of the system in the presence of fault.

The internal damping of a flexible rotor is a property essential for the design of the controller. The non-conservative forces stabilize the modes above the rotating speed but destabilize the modes below (Schweitzer and Maslen [2009]).

An industrial rotor is a complex structure mainly made of steel. The shaft has mechanical properties quite easy to predict (natural frequencies and mode shapes). Moreover, based on the experimental assessment of one shaft, the internal damping could be also predicted. However, the mounting of the impellers and the other disks have a large influence on the results. The manufacturing process and tolerances cannot be neglected. For example, the contact between a shrink fitted disk and the shaft is a complex mechanical system, which provide additional stiffness and damping to the whole rotor.

The amplification factor of the different modes is difficult to handle since its acceptable value depends on the mode considered.

For modes included in the operating speed range, there is no clear requirement from standards, but a value below 3.5 seems clearly suitable. If the value is greater than 3.5, separation margins could be considered. However, the maximum acceptable amplification factor for modes below the maximum speed is difficult to evaluate. The minimum log decrement required by API 617 [2002] for hydrodynamic bearings (0.1) seems low for AMBs.

For very high frequency modes, beyond the controller bandwidth, it is normal to achieve the AF equivalent to the internal damping.

Nevertheless, the modes between the two categories are embarrassing. Theoretically, they should be affected as little as possible by the controller in order to ensure the system robustness. However, these modes could be disturbed either by the bearing (the switching of the amplifier) or the process. Thus, a small damping decreasing with the frequency of the considered mode could be interesting. We think that the specifications need to be defined.

The test rig has an important misalignment that was both an opportunity and a disadvantage. The effects of misalignment are important, and they were not fully investigated. The bearing characteristics should be investigated as a function of combined misalignment offset. Then, manufacturing tolerances could be defined accordingly to the manufacturing possibilities and the effects on the system.

The approach could be improved by the definition of new fuzzy rules. For example, the critical speeds are detected by the tangential velocity, thus the effect is mainly on bending critical speed. A coupling of tangential velocity and radial displacement could improve the unbalance response of rigid body modes.

The SPID characteristics have an important influence on the results. They could be optimized. The main performance objectives have to be discussed and classified.

For a complete assessment of the fuzzy logic controller, it would be necessary to measure the different transfer functions (sensitivity, CLTF and dynamic stiffness) for different case studies with different amplitudes of the excitation signal in order to assess the effect of tangential damping and radial stiffness increase. Moreover, the tools for a systematic analysis of non-linear controllers must be defined.

For the approach developed, the high frequency characteristics and the controller general gain are the only parameters that need to be tuned from one compressor to the other. The systematic tuning of the high frequency characteristics would permit to simplify the design process of machinery. This systematic tuning could be achieved by making use of μ-synthesis.

The approach required an experimental validation on a compressor in order to be used industrially. In addition, the study of dynamic behaviour in the presence of faults will permit to extend the approach in order to control these particular events.

References

Aenis, M., Knopf, E. & Nordmann, R., 2002. Active magnetic bearings for the identification and fault diagnosis in turbomachinery. Mechatronics, Vol. 12, Issue 8, pp. 1011-1021.

API 617, 7th ed. 2002. Axial and centrifugal compressors and expander-compressors for petroleum, chemical and gas industry service.

Blom, R. & Van den Hof, P., 2008. Estimating Cutting Forces in Micromilling by Input Estimation from Closed-loop. Proceedings of the 17th IFAC World Congress, The International Federation of Automatic Control, Seoul, Korea, pp. 468-473.

Bolusset, D. & Pugnet, J.M., 1989. Expérience acquise d'une mise en service industriel d'un compresseur centrifuge sur paliers magnétiques actifs. Revue Française de Mécanique, 5p.

Borne, P., Rozinoer, J., Dieulot J.-Y. & Dubois L., 1998. Introduction a la commande floue. Edition Technip, 102p.

Bornstein, K. R., 1991. Dynamic load capabilities of active electromagnetic bearings. ASME Journal of Tribologie, Vol. 113, No.3, pp.598-603.

Burdet, L., 2006. Active magnetic bearing design and characterization for high temperature applications. PhD thesis, Ecole Polytechnique Fédérale de Lausanne (Suisse).

Charron, J.-L., 2003. Mesures sans contact, Techniques de l'ingénieur, Mesures Analyses R1331.

Charron, J.-L., 2004. Mesures sans contact, Techniques de l'ingénieur, Mesures Analyses R1335.

Chen, K., Tung, P., Tsai, M. & Fan Y., 2009. A self-tuning fuzzy PID-type controller design for unbalance compensation in an active magnetic bearing. Expert Syst. Appl., pp. 8560-8570.

Childs, D. W. & Scharrer J.K., 1986. An Iwatsubo Based Solution for Labyrinth Seals: A Comparison to Experimental Results. ASME Journal of Engineering for Gas Turbines and Power, Vol. 108, pp. 325-331.

Cole, M. O. T., Keogh, P. S. & Burrows, C. R., 2002. The dynamic behaviour of a rolling element auxiliary bearing following rotor impact, ASME Journal of Tribology, Vol. 124, Issue 2, pp. 406-413.

Cole, M. O. T., Keogh, P. S., Burrows, C. R. & Sahinkaya, M. N., 2006. Adaptive control of rotor vibration using compact wavelets. Journal of Vibration and Acoustics, Vol. 128, Issue 5, pp. 653-665.

Couzon, P.-Y., 2003. Contrôle actif neuro-flou de structures, Application aux rotors supportés par paliers magnétiques actifs. PhD thesis, INSA de Lyon, 233p.

Defoy, B., Mahfoud, J. & Alban, T., 2010. Paliers Magnétiques Actifs : Application à une turbomachine industrielle en régime transitoire. Compte rendu d'avancement I Etude de la chaîne complète pour la mise en place d'un modèle de comportement dynamique. 109p.

Defoy, B., Alban, T. & Mahfoud, J., 2012. Experimental assessment of a new fuzzy controller applied to a flexible rotor supported by active magnetic bearings. Proceeding VIRM10, IMechE, London, 11p.

Durand, S., 2002. Capteurs de déplacement, Technique de l'ingénieur, Mesures Analyses R1800.

Earnshaws, S., 1842. On the nature of the molecular forces which regulate the constitution of the luminiferous ether. Trans. Camb. Phil. Soc., Vol. 7, part I: pp. 97-112.

Elder, N. & Maslen, E., 2008. Effect of long cables on AMB systems. Proceedings of 11th ISMB, pp. 280-286.

Ertas, B. H., Delgado, A. & Vannini, G., 2012. Rotordynamic force coefficients for three types of annular gas seals with inlet preswirl and high differential pressure ratio. J. of Eng. for Gas Turbines and Power, Vol. 134, 12p.

Ewins, D. J., 2000. Modal Testing : theory, practice and application. 2nd Edition, Research Studies Press, 562p.

Fittro, R., L. & Knospe, C., R., 2002. The μ approach to control of active magnetic bearings. ASME Journal of Engineering for Gas Turbines and Power, Vol. 124, Issue 3, pp. 566-570.

Font, S., Duc, G. & Carrere, F., 1997. Commande frequentielle robuste – Application aux paliers magnetiques. Techniques de l'ingenieur, Mesures Analyses R 7 432.

Fuh, C.-C. & Tung, P.-C., 1997. Robust stability analysis of fuzzy control systems. Elsevier Science B.V. Fuzzy Sets and Systems, Vol. 88, Issue 3, pp. 289-298.

Gähler, C., 1998. Rotor dynamic testing and control with active magnetic bearings. PhD thesis, ETH Zürich, 196p.

Gelin, A., 1990. Etude théorique et expérimentale des comportements dynamiques permanent et transitoire de rotors sur paliers magnétiques. PhD thesis, Institut National des Sciences Appliquées de Lyon (France).

Golob, M. & Tovornik, B., 2003. Modeling and control of a magnetic suspension system. Elsevier Ltd. ISA Trans., Vol. 42, Issue 1, pp. 89-100.

Habermann, H., 1984, Paliers magnétiques, Techniques de l'ingénieur, traité Génie mécanique B 5 345.

Hamilton, S. B., 1973. Development of a magnetically suspended momentum wheel, Final Report General Electric Co., Binghamton, NY. Aerospace Controls and Electrical Systems Dept.

Hawkins, L. A., Murphy, B. T. & Kajs, J., 2000. Analysis and testing of a magnetic bearing energy storage flywheel with gain scheduled. MIMO control, In Proc. of ASME TURBOEXPO, Germany.

ISO 14839-1, 2002. Mechanical Vibration – Vibration of rotating machinery equipped with active magnetic bearings – Part 1: Vocabulary.

ISO 14839-2, 2004. Mechanical Vibration – Vibration of rotating machinery equipped with active magnetic bearings – Part 2: Evaluation of vibration.

ISO 14839-3, 2006. Mechanical Vibration – Vibration of rotating machinery equipped with active magnetic bearings – Part 3: Evaluation of stability margin.

ISO 14839-4, 2012. Mechanical Vibration – Vibration of rotating machinery equipped with active magnetic bearings – Part 4: Technical guidelines.

Jufer, M., 1979. Traite d'électricité de l'Ecole polytechnique fédérale de Lausanne – Vol. IX Electromécanique, Dunod, 307p.

Keith, F., J., Maslen, E., H., Humphris, R.R. & Williams, R., D., 1990. Switching amplifier design for magnetic bearings. Presented at the 2nd International Symposium on Magnetic Bearings, Tokyo, Japan, July 12-14.

Keith, F. J., 1993. Implicit flux feedback control for magnetic bearings. PhD thesis, University of Virginia (USA), 219p

Keogh, P. S., Cole, M. O. T., Sahinkaya, M. N. & Burrows, C. R., 2004. On the control of synchronous vibration in rotor/magnetic bearing systems involving auxiliary bearing contact. ASME Journal of Engineering for Gas Turbines and Power, Vol. 126, Issue 2, pp. 366-372.

Keogh, P. S. & Woon, Y. Y., 2007. Thermal assessment of dynamic rotor/auxiliary bearing contact events, Journal of Tribology, Vol. 129, Issue 1, pp. 143-152.

Koskinen, H., 1993. Fuzzy control schemes for active magnetic bearings. Springer Berlin / Heidelberg, Fuzzy logic in artificial intelligence, Lecture notes in computer science, Vol. 695, pp. 137-145.

Kjølhede, K., 2007. Experimental contribution to the problem of model parameter identification in rotating machines via active magnetic bearings. PhD thesis, DCAMM Special Report No. S101, DTU Copenhagen (Denmark).

Kwak, M., K. & Sciulli, D., 1996. Fuzzy-logic based vibration suppression control experiments on active structures. Journal of Sound and Vibration, Vol. 191, Is. 1, pp. 15-28.

Lacroix, J., 1988. Comportement dynamique d'un rotor au passage des vitesses critiques, PhD thesis, Institut National des Sciences Appliquées de Lyon (France), 160p.

Lalanne, M., Berthier, P. & Der Hagopian, J., 1983. Mechanical vibrations for engineers. John Wiley & Sons, 264p.

Lalanne, M. & Ferraris, G., 1998. Rotordynamics Prediction in Engineering. 2nd Edition, John Wiley & Sons, 252p.

Larsonneur, R., 2006. Modeling and analysis of dynamic mechanical systems with a special focus on rotordynamics and Active Magnetic Bearing (AMB) systems, Short Lecture Course.

Lee, W.-L., Schumacher, W. & Canders W.-R., 2003. Unbalance Compensation on AMB system without a rotational sensor. JSME International Journal, Ser. C, Vol. 46, pp. 423-428.

Lei, S., Palazzolo, A., B., Uhnjoo, N. & Kascak, A. 2000, Non-linear fuzzy logic control for forced large motions of spinning shaft, Journal of Sound and Vibration, Vol. 235, Is. 3, pp.435-449.

Lei, S. & Palazzolo, A. B., 2008. Control of flexible rotor systems with active magnetic bearings. Journal of Sound and Vibration, Vol. 314, Issues 1-2, pp.19-38.

Li, G., Lin, Z., Allaire, P., E. & Luo, J., 2006. Modelling of a high speed rotor test rig with active magnetic bearings. ASME Journal of Vibration and Acoutics, Vol. 128, Issue 3, pp. 269-271.

Lin, Y.-H. & Yu, H.-C., 2004. Active modal control of a flexible rotor. Mechanical Systems and Signal Processing, Vol. 18, Is. 5, pp. 1117-1131.

Lösch, F., 2002. Identification and automated controller design for active magnetic bearing systems. PhD thesis, ETH Zürich, 254p.

Mahfoud, J. & Der Hagopian, J., 2011. Fuzzy Active Control Of Flexible Structures By Using Electromagnetic Actuators. ASCE's Journal of Aerospace Engineering, Vol. 24, No. 3, pp. 329-337.

Mahlis, M., 2002. Contrôle actif modal floue des rotors flexibles par plan d'action piézoélectrique. PhD thesis, INSA de Lyon, 131p.

Mani, G., Quinn, D.D. & Kasarda M., 2006. Active health monitoring in a rotating cracked shaft using active magnetic bearings as force actuators. Journal of Sound and Vibration, Vol. 294, Issue 3, pp. 454-465.

Masala, A., Vannini, G., Lacour, M, Tassel, F.-M. & Camatti, M., 2010. Lateral Rotordynamic Analysis and Testing of a Vertical High Speed 12.5MW Motorcompressor Levitated by Active Magnetic Bearings. Proceeding 12th ISMB, China.

Maslen, E., Hermann, P., Scott, M. & Humphris, R., 1989. Practical limits to the performance of magnetic bearings: peak force, slew rate and displacement sensitivity. ASME Journal of Tribology, Vol. 111, No. 2, pp. 331-336.

Maslen, E., 2000. Magnetic Bearings, University of Virginia Department of Mechanical, Aerospace, and Nuclear Engineering Charlottesville, Virginia.

Maslen, E. & Montie, D., 2001. Sliding mode control of magnetic bearings: a hardware perspective. ASME Journal of engineering for Gas Turbines and Power, Vol. 123, Issue 4, pp. 878-885.

Maslen, E. H., 2008. Smart Machine Advances in Rotating Machinery. IMechE, Exeter, UK, 8-10 September, pp. 3-14.

Matsushita, O., Takagi, M., Yoneyama, M., Yoshida, T. & Saitoh, I., 1990. Control of rotor vibration due to cross stiffness effect of active magnetic bearing. Proceedings of the 3rd International Conference on Rotordynamics (IFToMM), CNRS Lyon, France.

Matsushita, O., Fujiwara, H., Ito, M. & Saigo, M., 2005. A Q-value measurement for damping evaluation of AMB rotors. Proceedings of the 2005 IEEE/ASME International Conf. on Advanced Intelligent Mechatronics, California (USA), pp. 1083-1090.

Matlab seen in 01/2011. The MathWorks – Matlab and Simulink for Technical Computing, www.mathworks.com.

Mertens, R.P., Hameyer, K. & Belmans, R., 1996. Two dimensional analysis of an e-core inductor. Proceedings of 3rd East-West congress on engineering education, pp. 108-112.

Na, U. J. & Palazzolo, A. B., 2000. Optimized realization of fault-tolerant heteropolar magnetic bearings. Journal of Vibration and Acoustics, Vol. 122, Issue 3, pp. 209-222.

Na, U. J. & Palazzolo, A. B., 2001. The fault-tolerant control of magnetic bearings with reduced controller outputs. Journal of Dynamic Systems, Measurement, Control, Vol. 123, Issue 2, pp. 219-224.

Na, U. J., Palazzolo, A. B. & Provenza, A., 2002. Test and theory correlation study for a flexible rotor on fault-tolerant magnetic bearings. Journal of Vibration and Acoustics, Vol. 124, Issue 3, pp. 359-366.

Nonami, K. & Fleming, D. P., 1986. Quasi-modal vibration control by means of active control bearings. Proceedings of the International Conference on Rotordynamics (IFTOMM), Tokyo, pp. 429-436.

Nonami, K., 1995. Control performances based on control system design strategies for active structural control. JSME International Journal, Series C, Dynamics, control, robotics, design and manufacturing, Vol. 38, Issue 3, pp. 367-378.

Nonami, K., Ide, N. & Ueyama, H., 1997. Robust control of magnetic bearing systems using μ-synthesis with descriptor form. JSME International Journal, Serie C, Vol. 40, Is. 4, pp. 688-693.

Nonami, K., Fan, Q.-F. & Ueyama, H., 1998. Unbalance vibration control of magnetic bearing systems using adaptive algorithm with disturbance frequency estimation. JSME International Journal, Ser. C, Vol. 41, Is. 2, pp. 220-226.

Nordmann, R. & Aenis, M., 2004. Fault Diagnosis in a Centrifugal Pump Using Active Magnetic Bearings. Taylor & Francis International Journal of Rotating Machinery, Vol.10, Issue 3, pp. 183-191.

Park, J., Palazzolo, A. & Beach, R., 2008. MIMO Active vibration control of magnetically suspended flywheels for satellite IPAC service, J. of Dyn. Sys., Meas., and control, vol. 130, I. 4, 22p.

Peeters, M., Kerschen, G. & Golinval, J.C., 2011. Dynamic testing of nonlinear structures using nonlinear normal modes. Journal of Sound and Vibration, Vol. 330, pp. 486-509.

Pesch, A., H. & Sawicki, T., 2012. Application of Robust Control to Chatter Attenuation for a High-Speed Machining Spindle on Active Magnetic Bearings. Proceedings of 13th International Symposium on Magnetic Bearings, Arlington (USA), 11p.

Ponsart, J.-C., 1996. Asservissements numériques de paliers magnétiques. Application aux pompes à vide. PhD thesis, Université de Savoie, 145p.

Prins, R. J., Kasarda, M. E. F. & Bates Prins, S. C., 2007. A system identification technique using bias current perturbation for determining the effective rotor origin of active magnetic bearings. J. Vib. Acoust., Vol. 129, Iss. 3, pp. 317-322.

Pugnet, J.-M., 2010. Dynamique des Machines Tournantes pour la Conception des Turbines a Vapeur et des Compresseurs Centrifuges : de la Theorie a la Pratique. PhD thesis, Institut National des Sciences Appliquées de Lyon (France), 301p.

Qiao, W. Z. & Mizumoto, M., 1996. PID type fuzzy controller and parameters adaptive method. Fuzzy Sets and Systems, vol. 78, pp. 23–35.

Ransom, D., Masala, A., Moore, J., Vannini, G. & Camatti, M., 2009. Numerical and Experimental Simulation of a Vertical High Speed Motorcompressor Rotor Drop onto Catcher Bearings. J. of Sys. Des. And Dyn., Vol. 3, No. 4, pp.596-606.

Schweitzer, G., 2009. Applications and research topics for active magnetic bearings. Springer-Verlag Proc. IUTAM-Symp. On Emerging Trends in rotor Dynamics, Indian Institute of Technology, Delhi (India).

Schweitzer, G. & Maslen, E., H., 2009. Magnetic Bearings, Theory, Design, and Application to Rotating Machinery. Springer-Verlag, 535p.

Shi, J., Zmood, R. & Qin, L., 2004. Synchronous disturbance attenuation in magnetic bearing systems using adaptive compensating signals. Control Engineering Practice, Vol. 12, Is. 3, pp. 283-290.

Siegwart, R., 1992. Design and application of Active Magnetic Bearings (AMB) for vibration control. Lecture series - van Kareman Institute for fluid dynamics, Vol. 6, pp. 1-65.

Simões, R., C., Steffen Jr., V., Der Hagopian, J. & Mahfoud, J., 2007. Modal active vibration control of a rotor using piezoelectric stack actuators. Journal of Vibration and Control, Vol. 13, no. 1, pp. 45-64.

Spirig, M., Schmied, J., Jenckel, P. & Kanne, U., 2002. Three practical examples of magnetic bearing control design using a modern tool. ASME Journal of Engineering for Gas Turbines and Power, Vol. 124, Issue 4, pp. 1025-1031.

Swann, M. K., Sarichev, A. P. & Tsunoda, E., 2008. A diffusion model for active magnetic bearing systems in large turbomachinery. Proceeding 11th ISMB, Japan, pp. 380-384.

Tamisier, V., Font, S., Lacour, M., Carrère, F. & Dumur, D., 2001. Attenuation of vibrations due to unbalance of an active magnetic bearings milling elector-spindle. CIRP Annals – Manufacturing technology, Vol. 50, Is. 1, pp. 255-258.

Traxler, A., 1985. Eigenschaften und auslegung von berührungsfreien elektromagnetischen lagern. Diss ETH Zürich Nr. 7851.

Viorel, I.-A., Hameyer, K. & Strete, L., 2007. On the Carter's Factor calculation for slotted electric machines, Advances in Electrical and Computer Engineering, vol. 7, no. 2, pp. 55-58.

Weens, Y., 2006. Modélisation des câbles d'énergie soumis aux contraintes générées par les convertisseurs électroniques de puissance. PhD thesis, Université des Sciences et Technologies de Lille, 226p.

Yu, H.-C., Lin, Y.-H. & Chu, C.-L., 2007. Robust modal vibration suppression of a flexible rotor. Mechanical Systems and Signal Processing, Vol. 21, Is. 1, pp. 334-347.

Zadeh, L.A., 1965. Fuzzy sets. Information and Control, Vol. 8, Issue 3, pp. 338-353.

FOLIO ADMINISTRATIF

THESE SOUTENUE DEVANT L'INSTITUT NATIONAL DES SCIENCES APPLIQUEES DE LYON

NOM : DEFOY DATE de SOUTENANCE : 14 décembre 2012

Prénoms : Benjamin, David

TITRE : Recherches sur le Contrôle des Compresseurs Centrifuges Supercritiques supportés par des Paliers Magnétiques Actifs : Vers une nouvelle stratégie de contrôle ?

NATURE : Doctorat Numéro d'ordre : 2012ISAL0140

Ecole doctorale : MEGA

Spécialité : Mécanique

RESUME :

Le comportement dynamique des turbomachines industrielles doit respecter des critères émis par les normes internationales et les utilisateurs. Les rotors flexibles sont sensibles à la distribution de balourd, et sont soumis aux excitations aérodynamiques de leur environnement. Usuellement, les contrôleurs utilisés peinent à délivrer le niveau d'exigence demandé, par conséquent les propriétés mécaniques des paliers magnétiques sont fortement dépendantes de celles des rotors. L'objectif de ce mémoire est d'analyser le comportement dynamique des compresseurs centrifuges afin de proposer une stratégie de contrôle innovante.

D'abord, chaque palier est considéré comme une entité a part entière en couplant ses deux axes d'action. Le comportement dynamique du rotor est exprimé dans le repère polaire. Par ailleurs, la logique floue, qui utilise un modèle de pensée proche du raisonnement humain, applique des actions correctives en fonction du comportement dynamique global du rotor. Ainsi, l'utilisation couplée de ces deux approches créé une synergie permettant d'agir sur le système de manière ciblée. Le contrôleur dissipe l'énergie cinétique du rotor lors du franchissement de vitesses critiques afin d'atténuer la réponse au balourd, ou augmente la raideur du palier lors de vibrations transitoires ou asynchrones afin de réduire la trajectoire du rotor.

Le faible amortissement structurel du rotor le rend sensible au phénomène de « spillover » (l'énergie de contrôle affecte les modes de fréquence élevée). Or, la logique floue ne peut pas gérer ce phénomène. Ainsi, un contrôleur PID sous-jacent est utilisé pour maîtriser la stabilité des modes hautes fréquences. Au final, le contrôleur flou polaire permet d'obtenir des marges de performances entre les capacités de cet asservissement et le cahier des charges. Ces marges sont utilisées pour trois objectifs : le respect des spécifications, l'amélioration du comportement subsynchrone, et enfin la simplification et la standardisation du contrôleur sous-jacent nommé ici SPID. Ce contrôleur est tel que ses caractéristiques, dans la plage de fréquence utile, sont indépendantes du rotor pour une application donnée.

Enfin, la stratégie développée est évaluée avec des simulations numériques et des essais expérimentaux. D'abord, le modèle numérique est validé, puis le contrôleur est appliqué à un banc d'essais académique. Le comportement est stable et robuste. Il présente des performances supérieures au PID augmenté fourni avec le banc, que ce soit pour la réponse au balourd, ou pour la réponse à des excitations subsynchrones. Finalement, la démarche est appliquée à un compresseur industriel. Les simulations montrent que le comportement est proche de celui exigé pour des machines sur paliers classiques. L'optimisation de l'approche et l'automatisation de la conception pourraient conduire à la standardisation des paliers magnétiques actifs.

MOTS-CLES : Paliers Magnétiques Actifs, Compresseurs Centrifuges, Logique floue, Rotor flexible, Dynamique des machines tournantes, Contrôle, MIMO.

Laboratoire (s) de recherche : Laboratoire de Mécanique des Contacts et des Structures (LaMCoS)

Directeur de thèse : J. Mahfoud et T. Alban

Président de jury : F. Thouverez

Composition du jury : T. Alban, P. Keogh, J. Mahfoud, E. Maslen et F. Thouverez